Title

Low-Carbon Belitic Calcium Sulfoaluminate Concrete Using Industrial Waste Products as Supplementary Cementitious Materials

ISBN

9798189263736

Author

Carver Miller, Renee Elizabeth

Publication Date

2026-08-27

Peer reviewed|Thesis/dissertation

UNIVERSITY OF CALIFORNIA

Los Angeles

Low-Carbon Belitic Calcium Sulfoaluminate Concrete Using Industrial Waste Products as Supplementary Cementitious Materials

A thesis submitted in partial satisfaction

of the requirements for the degree Master of Science

in Materials Science and Engineering

by

Renee Elizabeth Carver Miller

2026

ABSTRACT OF THE THESIS

Low-Carbon Belitic Calcium Sulfoaluminate Concrete

Using Industrial Waste Products as Supplementary Cementitious Materials

by

Renee Elizabeth Carver Miller

Master of Science in Materials Science and Engineering

University of California, Los Angeles, 2026

Professor Jaime Marian, Chair

Belitic calcium sulfoaluminate cement (BCSA) can mitigate the environmental impact of cement manufacture. It has less embodied CO_2 than Portland cement, significant strength within four hours of mixing, and better durability versus calcium sulfoaluminate cement (CSA), functioning as a standalone binder. This study examined class C fly ash, unclassified lignite fly ash, flue gas desulfurization (FGD) waste ash, and paper recycling waste as alternative supplementary

cementitious materials (SCMs) in BCSA to reduce embodied CO_2 while maintaining mechanical performance by utilizing the unique chemistry of BCSA. Set time, flow, shrinkage, and compressive strength characterized SCMs in mortars, while pastes' hydration and microstructure were evaluated via Rietveld refinement, thermogravimetry, isothermal calorimetry, and electron microscopy. The compressive strength of concrete containing FGD waste ash, the best-performing SCM, was measured. Carbon intensity quantifies embodied CO_2 per unit strength: FGD waste ash consistently reduced carbon intensity versus control specimens.

Keywords: Belitic calcium sulfoaluminate cement, sustainable materials, global warming potential, coal ash, flue gas desulfurization, paper recycling waste

The thesis of Renee Elizabeth Carver Miller is approved.

Eric P. Bescher

Aaron J. Moment

Bruce S. Dunn

Jaime Marian, Committee Chair

University of California, Los Angeles

2026

Table of Contents

List of Figures

List of Tables

Glossary

Cement Chemist's Notation (CCN)

A – Al_2O_3 (Alumina)

C – CaO (Lime)

Č – CO_2 (Carbonate)

H – H_2O (Water)

S – SiO_2 (Silica)

Š – SO_3 (Sulfate)

AFm – Aluminoferrite monosulfate (e.g. $C_3A{\cdot}C\check{S}{\cdot}H_{12}$)

AFt – Aluminoferrite trisulfate (e.g. ettringite)

AH_3 – Aluminum hydroxide

C_3A – Tricalcium aluminate

C_4AF – Brownmillerite (tetracalcium aluminoferrite)

C_2ASH_8 – Stratlingite

$C_4A_3\check{S}$ – Ye'elimite (calcium sulfoaluminate, abbreviated as CSA)

$C_6A\check{S}_3H_{32}$ – Ettringite (hexacalcium aluminate trisulfate hydrate)

C$\check{C}$ – Calcite (calcium carbonate)

CH – Portlandite (calcium hydroxide)

C_2S – Belite (dicalcium silicate)

C-S-H – Tobermorite or amorphous calcium silicate hydrate

CŠ – Anhydrite (calcium sulfate)

$C\check{S}H_{½}$ – Bassanite (calcium sulfate hemihydrate)

$C\check{S}H_2$ – Gypsum (calcium sulfate dihydrate)

Acknowledgments

Funding provided by Linda Rice and her late husband Edward Rice made this work possible. This funding was very important to my success. Without it, performing this research would have been much more complicated.

I am extremely grateful for the assistance I received from the CTS Cement Manufacturing Corporation, with provisions including equipment, materials, and training. The benevolence, kindness, humor, and unique perspectives of those working there made my time as a researcher a truly memorable and enjoyable experience.

At UCLA, professors Sergey Prikhodko of the Department of Materials Science and Engineering and Ignacio Martini of the Department of Chemistry and Biochemistry donated their valuable time and resources toward my training for the use of their electron microscope and plasma sputterer, respectively—two valuable pieces of equipment used in this research. Without their assistance this work would not assume the same degree of rigor.

I reserve my utmost gratitude for the members of my committee: Eric Bescher, Aaron Moment, Bruce Dunn, and Jaime Marian. Their continual feedback and guidance were crucial to the success of this work.

I also want to thank all who provided their opinions as I revised this work. This helped create a document that was much more coherent and comprehensible, in a way that I could not have achieved on my own.

1. Introduction

In 2024, cement production emitted 1.47 billion metric tons of CO_2 worldwide [1], accounting for up to 8% of annual anthropogenic CO_2 emissions globally [2]. For this reason, the development of sustainable construction materials remains an active area of research [3]. The high carbon emissions associated with cement production arise primarily from the calcination of limestone (calcium carbonate), the main raw material used in the manufacture of cement clinker, and the substantial energy use required to achieve the necessary high kiln temperatures for clinker formation. The manufacture of belitic calcium sulfoaluminate (BCSA) cement clinker, designed as a low-carbon cement, requires a temperature of 1250°C [4]. Ordinary Portland cement (OPC) requires a higher temperature of 1450°C; BCSA thus demands less energy in its production [4]. Additionally, the production of BCSA uses less limestone, further minimizing its CO_2 emissions [4]. These differences have a quantifiable effect on the CO_2 output of BCSA in comparison to OPC. The global warming potential (GWP) characterizes the environmental impact of a bulk product by quantifying the amount of CO_2-equivalent released per unit of material. According to its environmental product declaration, BCSA has a GWP of 673 kg CO_2-equivalent per metric ton of cement [5]; OPC has a GWP of 919 kg CO_2-equivalent per metric ton of cement [6]. BCSA contains 50% belite and 30% ye'elimite (calcium sulfoaluminate or CSA) as its primary phases by weight [7]. CSA contributes to the rapid hardening and early strength of the cement, while belite contributes to the strength at later ages [7].

Strategies for cement decarbonization include carbon capture, improvement of energy efficiency, and the use of low-carbon cements [8]. Low-carbon additives can further reduce the GWP of cement products. Additive materials that replace part of the mass of cement, reducing the clinker

factor, are called supplementary cementitious materials (SCMs). These materials affect the characteristics of a cementitious mixture by chemically reacting through hydraulic activity, where the SCM reacts with water; or pozzolanic activity, where the SCM reacts with cement [9]. In OPC, portlandite (calcium hydroxide) is a hydration product that does not significantly contribute to strength. Pozzolanic SCM reactions consume portlandite to produce C-S-H in its place, improving concrete durability [9]. The most common SCMs are coal fly ash, slag cement, and silica fume [9]. SCMs are usually classified according to certain standards. For example, fly ash may be classified according to the ASTM C618 standard as class C, comprising 50% or more silica, alumina, and iron oxides; or class F, comprising 70% or more of these oxides. Standards such as ASTM C618 may also set limits on sulfate content [9]. All additives used in this study are waste products. Accordingly, they are treated as though they have zero or negligible GWP. Huntzinger and Eatmon [10] make the same assumption in their analysis of supplementary cementitious materials. Through the addition of such zero-GWP SCMs, the GWP of a cement mix decreases. For instance, if 30% of the cement mass in a mix is replaced with a zero-GWP SCM, then the GWP of the mix is 70% as large as it would have been without the use of an SCM.

Carbon intensity serves as a figure of merit that quantifies the balance between GWP and strength. The carbon intensity of a mortar or concrete specimen at any age is defined as its GWP (in mortars) or CO_2 emissions per unit volume (in concrete) divided by its strength, resulting in units of psi^{-1} in mortars, or lb CO_2-eq yd^{-3} psi^{-1} in concrete. The SI-equivalent measurement of carbon intensity uses units of MPa^{-1} in mortars and kg CO_2-eq m^{-3} MPa^{-1} in concrete. A specimen with low emissions and high strength will have low carbon intensity. This is useful for comparing SCMs to control specimens: if a BCSA-SCM specimen has 30% of its GWP removed

with the addition of its SCM, but it maintains 90% of its strength, then its carbon intensity will be 78% as large as that of the control BCSA specimen. An ideal SCM can be used in large quantities without significant detriment to strength, minimizing carbon intensity.

In this study, four industrial by-products were studied as SCMs in BCSA cement. These included ASTM C618 class C fly ash, waste from paper recycling, and two ashes not classified according to ASTM C618, one being fly ash and one being blended ash from flue gas desulfurization (FGD). Fly ash, an industrial waste product of coal power generation, offers a promising route to reduce the GWP of BCSA cement. Fly ash is produced as a waste product of pulverized coal combustion. Coal dust is ignited and the resultant mineral residue is cooled, forming ash [11]. Coarse ash that falls to the bottom is called bottom ash or slag, while the finer particles that stay suspended in air are called fly ash [11]. According to the American Coal Ash Association, coal power generation produced over 24 million tons of fly ash as waste in 2024, along with over six million tons of ash from FGD [12]. However, of this output, only 19 million tons of fly ash were utilized (79%), and six thousand tons of FGD waste ash were utilized (0.09%) [12]. There remain significant quantities of this waste product for use in cement. Fly ash can be designated as class C or class F according to the ASTM C618 standard or remain unclassified if it does not meet the requirements of either class. Per the standard, class C fly ash is pozzolanic and cementitious, and the sum of silica (SiO_2), alumina (Al_2O_3), and ferric oxides (Fe_2O_3) must exceed 50% by weight. Class F fly ash is pozzolanic but not cementitious, and silica, alumina, and ferric oxides must constitute at least 70% of its mass. Both class C and class F ashes have sulfur trioxide (SO_3) content not exceeding 5% and loss on ignition (LOI) not exceeding 6%. Loss on ignition is a thermogravimetric quantity that describes the mass loss upon heating to high temperature and mostly corresponds to H_2O and CO_2 content, where low LOI may indicate

higher reactivity [13]. The concept of using fly ash as an SCM in BCSA is not strictly novel. Microstructural studies showing the effects of fly ash on CSA and BCSA cements date back to 2012, with the discovery of radial ettringite structures forming off of coal ash particles [14]. Under current construction specifications, the California Department of Transportation, or Caltrans, does not permit the use of supplementary cementitious materials in rapid strength concrete [15]. Caltrans permits the addition of fly ash to OPC but has not yet approved it or other SCMs for use in rapid-setting cements (RSCs) such as BCSA [16]. For this reason, the continued study of SCMs in BCSA is important, as better access to information may permit widespread use of BCSA with SCMs, reducing greenhouse gas emissions in California.

Paper recycling waste is generated as a product of wastewater treatment at paper mills due to pulping, papermaking, and deinking [17, pp. 9-17]. The composition of this waste varies significantly based on the plant processing it, but the waste is often high in calcium [17, pp. 19-29]. In 2007, five million tons of paper and board were produced, and one million tons of paper recycling waste were produced [17, pp. 9-17]. Research has been conducted on paper recycling waste as an SCM in OPC systems, but not in BCSA. For example, Jang, et al studied pozzolanic activity in paper waste under varying calcination and cooling conditions [18].

Flue gas desulfurization is a process used to mitigate sulfur dioxide emissions by coal power plants. It is produced when an alkaline sorbent reacts in the exhaust system of a coal-fired boiler, emerging initially as a wet residue before it dries [19]. FGD waste often contains varying amounts of fly ash because FGD installations can also include systems to collect fly ash [19]. FGD waste is high in sulfur, with most sulfur content existing in the form of calcium sulfite or calcium sulfate [19]. FGD waste ash has been studied as an SCM in CSA but not BCSA. As an example, Gao, et al, found that the addition of FGD waste ash to CSA promoted hydration and

improved strength [20]. The study of FGD waste ash in BCSA will permit better understanding of its effects on the properties of BCSA.

This study explores the effects of SCMS on BCSA phase development, chemical activity, carbon emissions, and macroscopic mechanical properties. Experimental methods used in this study include X-ray fluorescence (XRF), thermogravimetric analysis (TGA) & differential thermal gravimetry (DTG), scanning electron microscopy (SEM), X-ray diffraction (XRD) & Rietveld refinement, isothermal calorimetry (ASTM C1702 and C1897), flow testing (ASTM C1437), set time measurement via Vicat needle apparatus (ASTM C191), length change measurement (ASTM C157), and compressive strength testing (ASTM C109 and C39). Compressive strength testing included both mortars and concrete.

1.1 Scope

Cement production is a major contributor worldwide to greenhouse gas emissions. BCSA presents an alternative to OPC with less embodied CO_2 and lower carbon intensity. It also compensates for shrinkage and features high early strength that makes it suitable for rapid repair settings. The use of SCMs with BCSA has not been studied extensively and is not permitted in highway pavement applications by Caltrans. This study aims to better understand the effects of typical and atypical SCMs in BCSA cement, including measuring their impact on early- and late-age strength development. The difference in chemistry between BCSA and OPC may make the use of high-sulfur waste products not classified according to the ASTM C618 standard viable. SCMs can reduce the GWP of cement, making BCSA, with a GWP already substantially lower than that of OPC, an attractive target for study with SCMs. Calorimetry that mimics the chemical

environment of OPC provides a broad overview of the compatibility of SCMs between Portland and BCSA cements. This study seeks a comprehensive understanding of the relationship between SCM chemical compositions and their microstructural, chemical, and macroscopic effects on BCSA cement's final properties.

2. Literature Review

2.1 Belitic Calcium Sulfoaluminate Cement

BCSA cement hydrates upon contact with water. The simplified hydration of the main minerals of BCSA includes two primary hydration reactions. The hydration of ye'elimite ($C_4A_3\check{S}$) in the presence of calcium sulfate ($C\check{S}$) takes place rapidly and produces ettringite, as written in Equation (1). In the absence of calcium sulfate, ye'elimite produces monosulfates (AFm), as written in Equation (2) [21].

$$\underset{\text{Ye'elimite}}{C_4A_3\check{S}} + 2C\check{S} + 38H \rightarrow \underset{\text{Ettringite}}{C_3A \cdot 3C\check{S} \cdot H_{32}} + 2AH_3 \quad (1)$$

$$\underset{\text{Ye'elimite}}{C_4A_3\check{S}} + 18H \rightarrow \underset{\text{AFm}}{C_3A \cdot C\check{S} \cdot H_{12}} + 2AH_3 \quad (2)$$

In the presence of AH_3, belite (C_2S) reacts with water producing stratlingite (C_2ASH_8) [21]. In the absence of AH_3, belite reacts with water on its own, producing C-S-H gel and portlandite (CH) [21]. These two reactions are written in Equations (3) and (4).

$$\underset{\text{Belite}}{C_2S} + AH_3 + 5H \rightarrow \underset{\text{Stratlingite}}{C_2ASH_8} \quad (3)$$

$$\underset{\text{Belite}}{C_2S} + n\,H \rightarrow \text{C-S-H} + \underset{\text{Portlandite}}{n\,CH} \quad (4)$$

Ettringite crystallization leads to shrinkage compensation and rapid strength development initially, while belite reacts more slowly than ye'elimite and contributes to strength at later ages [21].

Citric acid is commonly used as a retarder in BCSA, with less common retarders including boric acid, tartaric acid, and molasses [22]. Advantages of BCSA cement over OPC include reduced drying shrinkage [4], better early strength [4], and lower GWP [5]. Advantages of BCSA over CSA include improved later-age strength and durability [4].

The material cost of BCSA is higher than that of OPC due to the required higher quantities of aluminum-bearing minerals such as bauxite for its production, but BCSA production costs less than CSA due to its lower alumina content and higher silica content [23]. Additionally, unlike CSA, BCSA is suitable for use on its own, while CSA is more commonly used as an additive to OPC systems, like in shrinkage-compensating Type K cements [24]. Concrete made with BCSA cement is self-levelling [22]. A common application for BCSA that takes advantage of its high early strength is its use in time-sensitive rapid repair of highways or airport runways [21, 22].

2.2 Alternative Supplementary Cementitious Materials

OPC contains 50-60% alite (C_3S) [25], which produces C-S-H and portlandite as it hydrates [26]. Equation (5) describes this hydration reaction.

$$\underset{\text{Alite}}{2C_3S} + 6H \rightarrow \underset{\text{C-S-H}}{C_3S_2H_3} + \underset{\text{Portlandite}}{3CH} \quad (5)$$

In OPC, pozzolanic reactions consume portlandite produced by the initial hydration of alite and produce additional C-S-H, contributing to durability [9]. BCSA hydrates via significantly different chemical pathways from those of OPC, as it does not contain alite as a primary reactant. SCMs that exhibit pozzolanic behavior in OPC thus cannot participate in the same hydration reactions in BCSA because BCSA does not contain or form significant quantities of portlandite, a necessary pozzolanic reactant [21, 27]. Because of the low portlandite content in BCSA, pozzolanic SCMs that react favorably in OPC may not perform well in BCSA. Simultaneously, an SCM with high sulfate content interrupts the sulfate balance of OPC and, depending on the type of OPC, can reduce its strength at later ages as well as cause it to delay setting, or to flash-set and quickly lose workability [28]. These unfavorable results make high-sulfate SCMs

atypical in OPC systems. But the hydration of BCSA relies on the presence of these sulfates for the crystallization of ettringite [21], meaning an SCM unsuitable for OPC may perform well in BCSA. Hence derives the interest in alternative, high-sulfate SCMs for BCSA cement.

2.3 SCMs for Hazardous Waste Storage

Fly ash, FGD waste ash, and paper recycling waste are all types of environmentally harmful waste [29, 30, 17, pp. 1-7]. After disposal, wastes such as these can leach toxic chemicals into the environment. Due to its high surface area, powder waste is significantly more reactive than waste contained in cement. Solidification and stabilization of waste in cement can negate environmental damage from waste disposal by preventing harmful components from escaping [31]. Ettringite can incorporate toxic heavy metal ions into its structure, which reduces the degree of leaching into water beyond the extent possible with a simple reduction in surface area [31, 32]. Because OPC is used more widely than BCSA, more information is available on the storage of hazardous waste in OPC than in BCSA. The Environmental Protection Agency (EPA) categorizes waste as hazardous based on the content of toxic heavy metal ions and other hazardous chemicals [33] and the leaching mobility of these ions according to SW-846 Test Method 1311 [34]. Similar tests can be applied to cement products containing environmentally hazardous waste by crushing the product, soaking it in water, and measuring the content of contaminants within the water after a set period [31].

2.4 Strategies for Mitigating Carbon Emissions due to Cement Production

Carbon emissions from cement production primarily arise due to the use of fossil fuels, and the calcination of limestone, which chemically frees carbon dioxide [35]. Emerging strategies for reducing CO_2 emissions due to cement manufacture include the use of alternative cements such as BCSA in place of OPC [4], clinker substitution by SCMs, the use of alternative low-carbon fuels, modernizing production equipment, carbon capture and storage, and the recovery of waste heat [35]. Of all these approaches, only the first two, the use of alternative cements and the use of SCMs in cement blends, involve direct changes to the cement itself. SCMs reduce the energy requirement for cement production, which directly reduces the total emissions of the manufacturing process. The technological and economic viability of each of these strategies depends on many factors, including the availability of SCMs and local regulations, but they are all generally feasible. Unlike the other strategies mentioned for curbing emissions, SCMs present multiple environmental benefits. Because cement can immobilize toxic heavy metal ions in SCMs, and SCMs can reduce GWP in cement, employing SCMs in cement is crucial for reducing environmental harm of the cement production industry as well as other industries that produce toxic waste. Complications of this process include the detrimental effect of SCMs on cement strength, as well as the possibility of cement products made with SCMs becoming environmentally hazardous due to failure to meet regulations such as those governing leaching [36].

3. Materials and Methods

3.1 Materials

3.1.1 BCSA Cement

All BCSA cement mixes used commercially available Rapid Set cement made by the CTS Cement Manufacturing Corp. This includes all mortar, paste, and concrete mixes. XRD of anhydrous BCSA cement is shown in Figure 1, with key phases labelled. XRD data was obtained using the procedure discussed in the test methodology section.

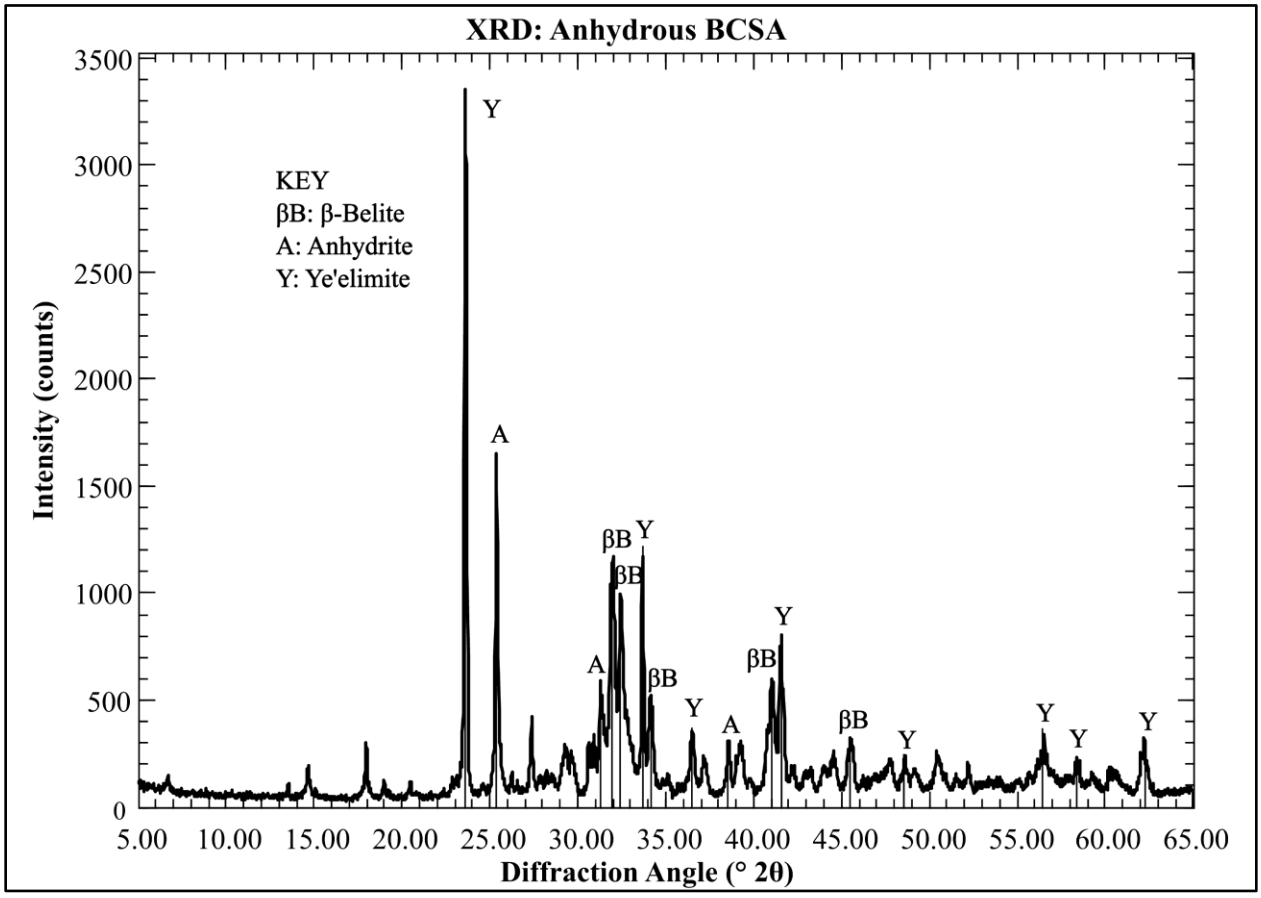

Figure 1: X-ray diffraction scan of BCSA cement. Some key phases, including β-belite (COD: 1535815), anhydrite (COD: 9017809), and ye'elimite (COD: 9009938), are highlighted.

Table 1 shows literature values [7] for the composition of BCSA cement obtained via XRF.

Table 1: Literature values for composition of BCSA cement [7]

Compound	Fraction in BCSA
CaO	49.4%
Al_2O_3	15.4%
SO_3	14.9%
SiO_2	14.3%
MgO	1.4%
Fe_2O_3	0.9%
Other	3.9%
Sum	100.2%

3.1.2 Sand and Concrete Aggregates

Sand used in mortars met the ASTM C778 standard. Concrete mixes used 1” gravel from Eagle Valley Aggregates as coarse aggregate, and sand from Irwindale Aggregates as fine aggregate.

3.1.3 Supplementary Cementitious Materials

Four SCMs are included in this study: fly ash from the Rush Island, Missouri coal power plant, designated as class C by the ASTM C618 standard; non-pulp waste from paper recycling, obtained from Epic Minerals, LLC; FGD waste ash from the Wyoming test reactor; and fly ash

from the North Dakota Coyote lignite power plant, not designated as class C or class F by the ASTM C618 standard. These SCMs may be abbreviated as FA, PW, WYFA, and NDFA, respectively. Multiple batches of Wyoming FGD waste ash were used out of necessity, designated as WYFA-1, WYFA-2, and WYFA-3 when necessary. The WYFA-2 and WYFA-3 ash samples contained large, hydrated nodules with ettringite, so they were both processed with a sieve before use such that all SCM particles had a diameter of 2mm or less. Specimens made with WYFA-3 were treated in an oven at 150°C for at least eight hours to decompose residual ettringite; this treatment decreased the loss on ignition (LOI) of WYFA-3 to a value closer to that of WYFA-1, which was not heat-treated. The purpose of this treatment was to make WYFA-3 specimens perform similarly to WYFA-1 specimens, because of inconsistency in the material. The SCM abbreviations and descriptions including the treatments applied to the WYFA samples are shown in Table 2. Specimens made with WYFA-2 did not have their ash treated in an oven and were used only for length change testing according to the ASTM C157 standard.

Table 2: Summary of all SCMs

SCM	Long Title	Notes
FA	Class C fly ash	Rush Island, MO plant
PW	Paper recycling waste	From Epic Minerals, LLC
WYFA-1	Wyoming FGD waste ash	No hydrated nodules
WYFA-2	Wyoming FGD waste ash	Hydrated nodules untreated
WYFA-3	Wyoming FGD waste ash	Hydrated nodules heat-treated
NDFA	North Dakota fly ash	Coyote lignite plant

The four SCMs are shown in Figure 2.

Figure 2: The four SCMs. From left to right: Class C fly ash (FA), paper recycling waste (PW), Wyoming FGD waste ash (WYFA-1), North Dakota fly ash (NDFA)

The hydrated nodules found in WYFA-2 and WYFA-3 are shown in Figure 3.

Figure 3: Hydrated nodules in WYFA-2 and WYFA-3, which were sieved before use. WYFA-3 was also heat-treated at 150°C to dehydrate and make it more similar to WYFA-1, which did not have these nodules and had LOI half as large. Scale bar shows inches.

3.2 Mix Proportions and Mixing Procedures

This section describes the relative quantities of components used in mixes of pastes, mortars, and concrete, as well as the treatments used in their production.

3.2.1 Cement Pastes for Hydration Study

All pastes used in this study were made with a constant ratio of water to cementitious material ("water/cement ratio") of 0.5. Cementitious mass or cementitious material is the sum of SCM mass and BCSA mass. Paste components were measured according to the proportions shown in Table 3, and were mixed using a Labnet Vortex Mixer for 45 seconds. The mixing procedure was used for pastes used in isothermal calorimetry and later for the creation of specimens used in hydration stoppage. These were then used for further analysis.

Table 3: Relative proportions of paste component masses (dimensionless)

Component	BCSA	BCSA + 10% SCM	BCSA + 20% SCM	BCSA + 30% SCM
BCSA	10	9	8	7
SCM	-	1	2	3
Water	5	5	5	5

3.2.2 Stopping the Hydration of Pastes

Hydration stoppage was performed for cement paste samples according to the "RILEM TC-238 SCM recommendation on hydration stoppage by solvent exchange for the study of hydrate assemblages" [37], a standard developed specifically for use in XRD and thermogravimetry.

After mixing a paste, hydration stoppage was performed at 4hr, 24hr, and 28d. To stop the hydration of a paste specimen, a small piece was broken off with a clean chisel. It was then wrapped in paper and hit with a hammer to make small pieces. The pieces were ground into a powder using a mortar and pestle, then processed using a No. 18 sieve such that all remaining particles were smaller than 1mm in diameter. The crushed particles were then immersed in approximately forty milliliters of isopropanol for 15 minutes before being poured into a Büchner funnel with a filter paper. In the Büchner funnel, specimens were rinsed and vacuum-filtered once with ten milliliters of isopropanol, then twice with ten milliliters of diethyl ether. Quantities of isopropanol and diethyl ether were reduced from RILEM procedure recommendations to minimize chemical waste with no effect on coverage. For the final drying step, specimens were dried in a 43°C oven for 10 minutes. Hydration-stopped paste specimens were used in X-ray diffraction (XRD) and Rietveld analysis, thermogravimetric analysis (TGA), and scanning electron microscopy (SEM). The process of stopping paste hydration is depicted in Figure 4.

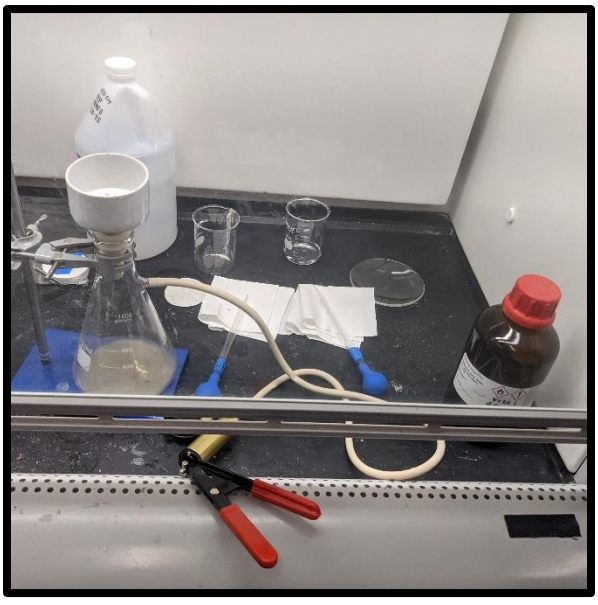

Figure 4: Stopping the hydration of a cement paste with isopropanol and diethyl ether.

3.2.3 Cement mortars

Mortars are specimens that contain cement and sand, and, unlike concrete, no coarse aggregate. Two types of mortars were tested: those made with a constant water/cement ratio of 0.5, called "constant-water" specimens, and those made to achieve constant workability according to the ASTM C1437 standard, called "constant-flow" specimens. Example constant-water mortar mixes are shown in Table 4.

Table 4: Relative proportions of component masses of constant-water mortars (dimensionless)

Component	BCSA	BCSA + 10% SCM	BCSA + 20% SCM	BCSA + 30% SCM
C778 Sand	1375	1375	1375	1375
BCSA	500	450	400	350
SCM	-	50	100	150
Water	250	250	250	250

Depending on the SCM used in each mortar and its weight fraction, the workability of a mortar would not necessarily remain constant at a water/cement ratio of 50%. Thus, water/cement ratios were found using the flow test described in ASTM C1437: immediately after mixing, mortar specimens were put into a conical mold on a flow table, then the mold was removed such that the wet mortar stood on its own. The flow table was then dropped 25 times in 15 seconds, and four diameters were measured using calipers compliant with the ASTM C230 standard, with an angular separation of 45° between any pair of adjacent diameters. Two example flow tests are

shown in Figure 5. If a mortar was so dry that it could not maintain a cohesive border of which four diameters could be measured, then the flow was recorded as unmeasurable.

Figure 5: Testing flow by varying water proportion; Left: A specimen ready to have its diameters measured after dropping the flow table; Right: A specimen too dry to have its flow measured.

The calipers used had increments spaced evenly every four millimeters. A specimen achieved constant workability if the sum of four diameters was equal to 110 ± 5 increments; this water/cement ratio was recorded. For constant-flow mortars using any of the three batches of WYFA, the same water/cement ratios were used, regardless of possible batch variation. The flow values of constant-water mortars were recorded as well.

Mortars were mixed using a stand mixer according to the ASTM C305 standard. The appropriate quantity of water was measured into a mixing bowl, and all cementitious material was added at once while mixing at 140rpm, henceforth referred to as “slow” speed. Mixing continued at slow

speed for 30 seconds, then all sand was added continuously and evenly over the subsequent 30 seconds. After all sand was added, the mixing speed was increased to 285rpm, henceforth referred to as “medium” speed, for 30 seconds. The walls of the mixing bowl were scraped clean with a rubber spatula within 15 seconds after medium-speed mixing finished, and the specimen was allowed to rest in the mixing bowl for 75 more seconds, for a total of 90 seconds without mixing. Finally, the specimen was mixed at medium speed for 60 seconds. The mortar was then ready for molding. The total mixing time of a mortar was four minutes, from the moment cement touched water to the moment the final mixing step finished. The timing of mixing a mortar is illustrated in Figure 6.

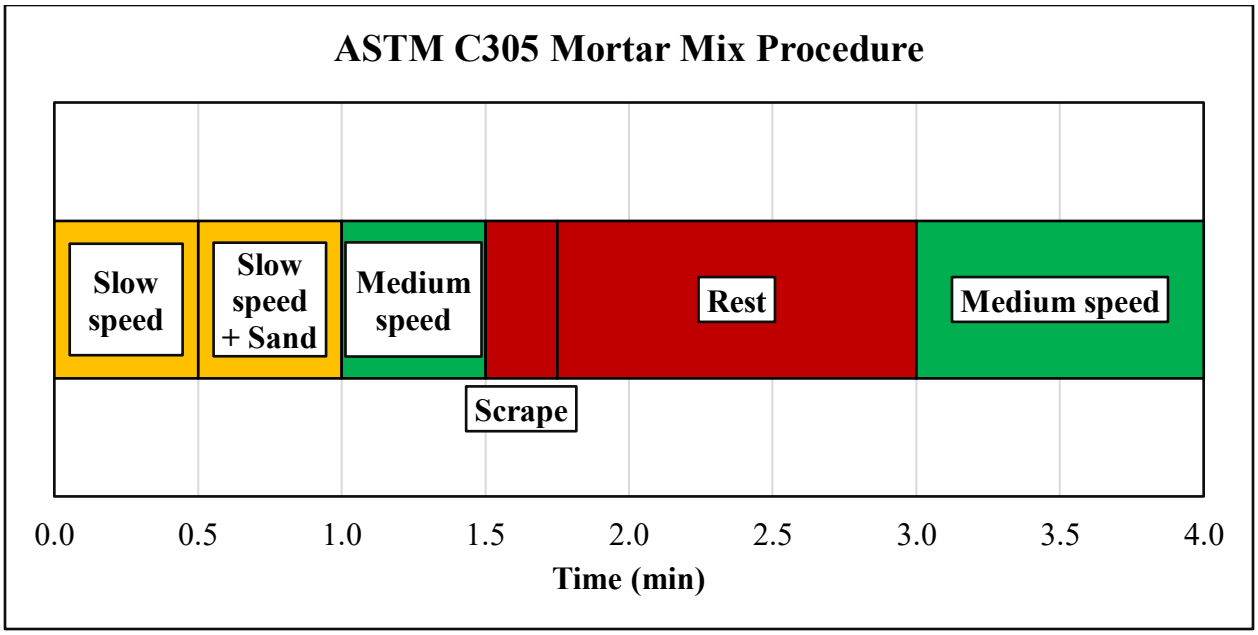

Figure 6: Steps of mixing a mortar, as described in the ASTM C305 standard. Yellow corresponds to slow mixing speed (0-60 seconds), green corresponds to medium mixing speed (60-90 seconds, 180-240 seconds), and red corresponds to mixer turned off (90-180 seconds).

Some mortar cube specimens used for compressive strength testing are depicted in Figure 7.

Figure 7: Several mortar cubes in molds after mixing, later used to test compressive strength

Mortars were used for testing set times, length change, compressive strength, and carbon intensity. For measuring compressive strength, mortars were put into 2” cube-shaped brass molds in two layers according to the ASTM C109 standard, with each layer tamped with a rubber tamper in four sets of eight tamps. Cubes that were strength-tested at or below 24hr of age cured in air, while cubes that were strength-tested at later ages cured in a lime solution after a day had passed since mixing. For measuring length change, mortars were put into molds shaped like a rectangular prism 10” in length with a 1” square cross section according to the ASTM C157 standard. These bars were cured in air at 23°C and 50% relative humidity. Mortars were also used to test set times according to the ASTM C191 standard with a Vicat needle apparatus.

3.2.4 Concrete for Compressive Strength Testing

WYFA was selected for testing in BCSA concrete because of its minimal detriment to the strength of BCSA mortars. Concrete was not made according to any ASTM standard because the ASTM C192 standard for concrete mixing is better suited for use with slower-setting Portland cement, not BCSA. MasterGlenium 3400 admixture was used as a superplasticizer to reduce the required amount of water for sufficient workability, thus increasing the strength of the concrete. MasterSet DELVO admixture was used as a retarder, allowing greater working time for molding the concrete. The four concrete mix designs are described in Table 5.

Table 5: Weights of components of concrete mixes (lb)

Component	BCSA	10% WYFA-3	20% WYFA-3	30% WYFA-3
BCSA	39.92	35.93	31.94	27.94
WYFA-3 SCM	-	3.99	7.98	11.98
Fine Aggregate	88.35	88.35	88.35	88.35
Coarse Aggregate	116.41	116.41	116.41	116.41
Water	0.548	0.747	0.848	0.898
Superplasticizer	0.229	0.229	0.229	0.229
Retarder	0.223	0.223	0.223	0.223

Before mixing the concrete, in three separate buckets the coarse and fine aggregates were intermixed, the cementitious materials (BCSA and WYFA-3 SCM) were intermixed, and the two admixtures were added to the water. Before adding any cement, roughly 80% of the aggregate mixture and water were put into a portable electric cement mixer. The mixer ran for an arbitrary

period on the order of minutes until the aggregates were evenly wetted, at which point all cementitious material was added at once, followed by all remaining water. The amount of water differs between mixes because water was added as needed to achieve a near-constant consistency. The concrete was allowed to homogenize in the mixer before the remaining aggregate was added. The concrete was allowed to homogenize in the mixer again before being poured into a wheelbarrow for transportation; WYFA-3 concrete is poured into a wheelbarrow in Figure 8. Each concrete mix took roughly four minutes to complete before molding. Concrete was put into cylindrical plastic molds 4” in diameter and 8” tall (abbreviated as 4”×8”) in two layers; each layer was tamped 25 times with a metal rod. Example cylinders can be seen in Figure 8. Like mortar cubes, concrete cylinders with their strengths tested at 4hr and 24hr were cured in air, while all later-age specimens were cured in a solution of water and lime, with temperature uncontrolled.

Figure 8: Left: pouring WYFA-3 concrete before it is put into cylindrical molds; Right: 4”×8” concrete cylinders used for mechanical testing

3.3 Analytical Methods for SCMs, Cement Pastes, Mortars, and Concrete

In this section the procedures used for testing specimens are described, including that of SCMs, pastes, mortars, and BCSA/WYFA-3 concrete.

3.3.1 Chemical Compositions of Materials via X-Ray Fluorescence

Chemical compositions of SCMs were determined via X-ray fluorescence (XRF) using a Bruker S8 TIGER wavelength-dispersive spectrometer. Powder specimens were pressed into pellets before analysis. The sums of component fractions were not normalized, so they do not necessarily equal 100%.

3.3.2 Loss on Ignition of SCMs, and Thermogravimetry of Pastes

Thermogravimetric analysis (TGA) was performed using a Mettler Toledo TGA/DSC 3+ thermogravimetric analyzer.

Loss on ignition (LOI) was measured for each SCM by way of thermogravimetry. Roughly 150μg of each SCM, including all three WYFA samples, were loaded into 300μL alumina crucibles. The TGA used a nitrogen atmosphere with a gas flow rate of 50mL/min as the temperature raised from 25°C to 1000°C at a rate of 10°C/min. The LOI values were obtained from this data by calculating the percentage change in mass of each SCM after the test finished.

Pastes subject to hydration stoppage at 28 days of age were put into 35μL alumina crucibles. Specimens were subject to a nitrogen atmosphere at 20psi with a gas flow rate of 50mL/min. Temperature was raised from 35°C to 900°C at a rate of 10°C/min while the mass was measured

continuously. The derivative of the mass function was taken, showing negative, endothermic peaks corresponding to the release of water and carbon dioxide from hydrated and carbonated phases within the pastes at characteristic temperatures. This included those phases undetectable via XRD due to their amorphous character. Graphs of the mass derivative were smoothed with a Savitsky-Golay filter across a region with a width of 20 points using the proprietary scientific graphing software Origin 2026.

3.3.3 Scanning Electron Microscopy

Powder specimens were attached to metal stands using conductive carbon tape. In an electron microscope, non-conductive specimens accumulate charge on their surface, showing bright spots in the final image. To minimize this effect, SCMs and pastes were given a five-nanometer-thick conductive coating of gold using an argon plasma sputter coater and imaged within two days of sputtering. Gold sputtering is depicted in Figure 9. Microscopic imaging was performed on all SCMs, as well as those pastes containing 30% SCM with hydration stopped at 24hr and 28d of age. Microscopic imaging was performed using an FEI Nova 230 NanoSEM scanning electron microscope, shown in Figure 9, under high vacuum with an accelerating voltage of 10kV, a spot size setting of 3.0, and a working distance of approximately 8mm. Electrons were detected using an Everhart-Thornley detector.

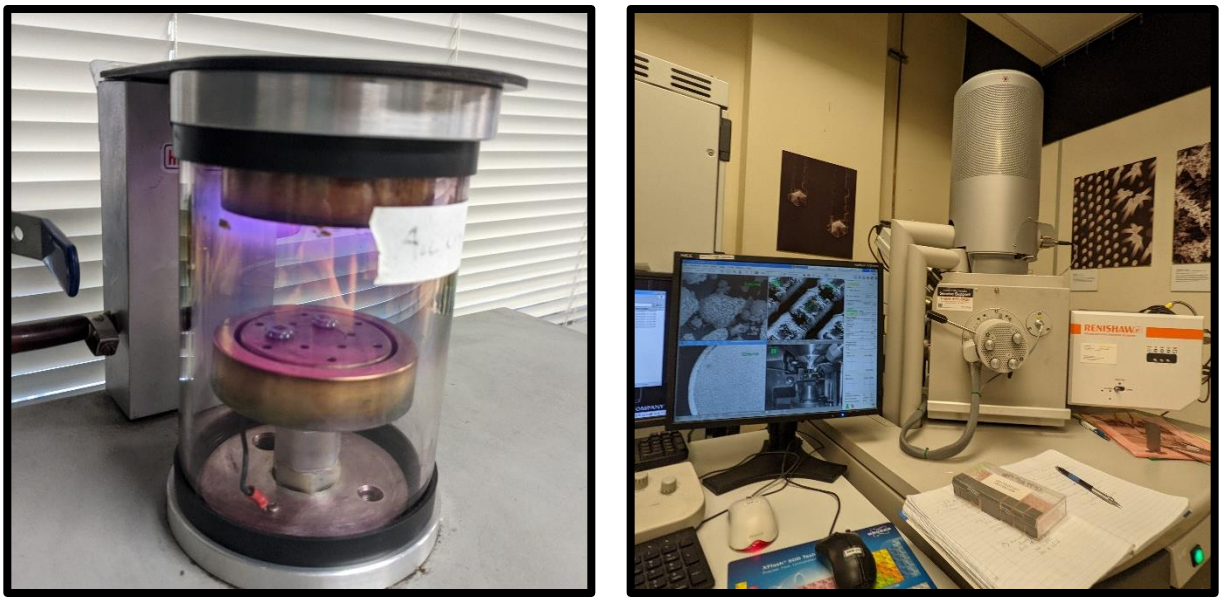

Figure 9: Left: Sputter-coating specimens with gold; Right: Imaging via SEM

3.3.4 XRD: Phase Quantification of Pastes via Rietveld Refinement

Powder X-ray diffraction (XRD) scans of raw SCMs and of all hydration-stopped pastes were performed using a Bruker D8 ENDEAVOR X-ray diffractometer. A No. 200 sieve was used to remove particles larger than 75μm in diameter before scanning. The powder specimens were put into cylindrical plastic molds that were loaded into the diffractometer; this is shown in Figure 10. The X-ray generator used a voltage of 40kV and a current of 25mA to emit Cu-Kα X-ray radiation. All diffraction scans used 2θ values ranging from 5° to 65° with a step size of 0.02° and a dwell time of 0.1s. During scans, specimens were rotated about φ at a constant rate of 15rpm. Each scan lasted slightly over five minutes. Paste phase quantification via Rietveld refinement was performed using Profex 5.6.1 [38], a free and open-source program that uses the BGMN Rietveld refinement kernel. All CIF files representing crystal structures were

downloaded from the Crystallography Open Database (COD) [39, 40, 41, 42, 43, 44, 45, 46, 47] and are identified in this text by their COD identification number.

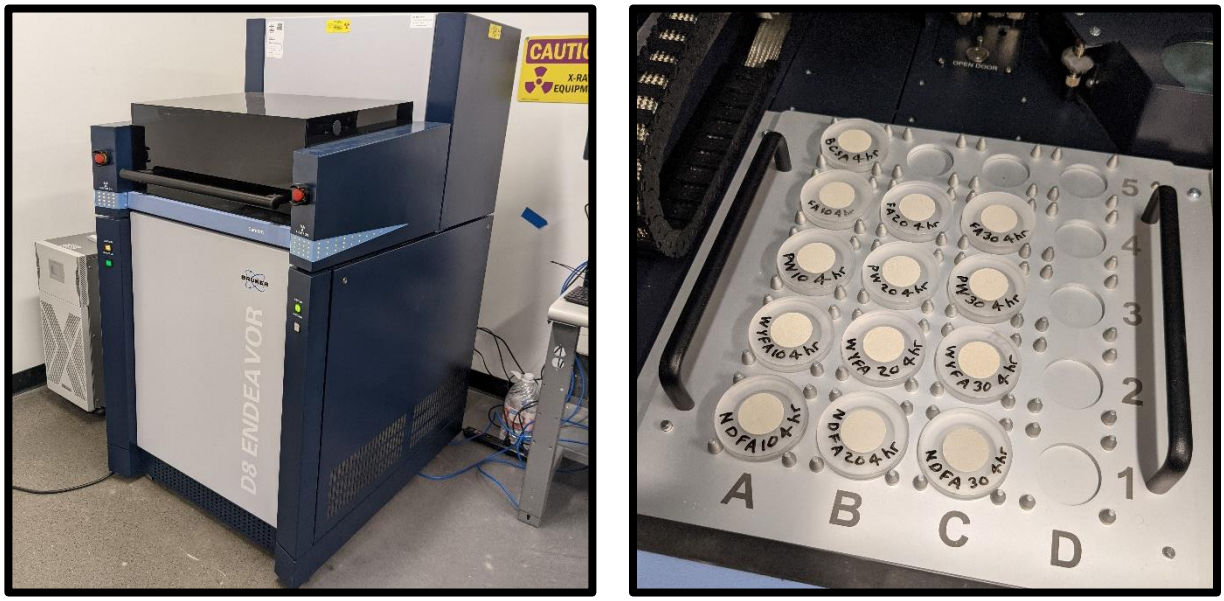

Figure 10: Left: X-ray diffractometer; Right: Several pastes sit inside the diffractometer.

3.3.5 Isothermal Calorimetry of Pastes

Isothermal calorimetry was performed according to the ASTM C1702 standard. Cement pastes containing 0%, 10%, 20%, and 30% SCM by mass were tested using all four SCMs. The cementitious mass, being the sum of BCSA mass and SCM mass, was ten grams in all tests. Five grams of water were used, giving a water/cement ratio of 0.5, equivalent to that used in constant-water mortars. Before heat flow and cumulative heat release of a paste were measured as a function of time, the cementitious mass and water were conditioned within the chamber of the calorimeter for at least two hours at 23°C to equilibrate their temperatures before testing. Pastes were mixed using a Labnet Vortex Mixer for 45 seconds. A Calmetrix I-Cal 2000 HPC isothermal calorimeter was used to measure heat flow and cumulative heat release within pastes

up to 24hr after mixing. For the first six hours after logging began, data was polled every five seconds. For the remainder of the 24-hour testing period, data was polled every 30 seconds. Heat flow (mW/g) and cumulative heat release (J/g) were normalized by dividing by the cementitious mass.

3.3.6 Isothermal R^3 Calorimetry

R^3 calorimetry, short for "rapid, relevant, reliable," is a novel type of calorimetry developed by Avet, et al, [48] and iterated upon by the RILEM Technical Committee [49] for rapid estimation of SCM performance in Portland cement. The procedure may not be suitable for comparing SCMs in BCSA: BCSA cement and Portland cement hydrate via distinct chemical pathways. The data may find utility as a broad overview of SCM efficacy in OPC by simulating its chemical environment. In this study, the procedure was performed according to the ASTM C1897 standard. The same Calmetrix I-Cal 2000 HPC isothermal calorimeter was used for isothermal calorimetry of pastes and isothermal R^3 calorimetry. One test was performed per SCM, and each test lasted seven days within the calorimeter. A bulk solution was prepared for the test using one liter of deionized water, four grams of potassium hydroxide, and 20 grams of potassium sulfate. For each test, 1.52g SCM, 4.55g calcium hydroxide, and 0.76g calcium carbonate were weighed and combined. A cup containing 8.18g of the potassium solution was also weighed. The SCM cup and potassium solution cup conditioned within the calorimeter for 24hr at 40°C, the temperature of the test.

Measurements of heat flow and cumulative heat release were polled every 30 seconds throughout the entire duration of the test. The SCM cup was mixed with the cup of potassium solution for

two minutes, and the cup was inserted into the calorimeter chamber. After this, the test continued for seven days.

The average heat flow over the last six hours of the test was used as a baseline value: the expected behavior of the heat flow was to approach a constant value with zero gradient or curvature as the test terminated, corresponding to the completion of the reaction. This heat flow was subtracted from the heat flow of the SCM cup such that the reaction heat flow values approached zero as the test finished, removing any error from miscalibration of the calorimeter for long-term measurements. Heat flow was shown as a function of time, with the first 75 minutes of the test after SCM mixing being removed per ASTM C1897 recommendation. The cumulative heat outputs up to three days and seven days were calculated as the integrals of the heat flow curves. Heat flow and cumulative heat values were normalized to SCM mass.

3.3.7 Mortar Set Times

The initial set time of a mortar describes the duration of the period in which the mortar maintains plasticity. After the final set time has passed, a mortar completely solidifies and begins to develop its strength. Set times were tested using a Vicat needle apparatus according to the ASTM C191 standard. Testing proceeded as follows: a small amount of mortar was inserted into a rubber cone on a plastic plate. The needle of the Vicat testing apparatus was held in place just above the surface of the finished mortar. Periodically, the needle would be dropped into the mortar: the initial set time was recorded as the time elapsed before the needle penetrated fewer than 25mm into the mortar, and the final set time was recorded as the time elapsed until the needle did not leave any mark on the surface of the mortar. The Vicat apparatus is depicted in

Figure 11. Set times were measured for control mortars made using 100% BCSA cement; as well as those mortars containing 10%, 20%, and 30% SCM by mass, for both constant-water and constant-flow specimens.

Figure 11: Testing set time of a mortar puck using a Vicat needle apparatus

3.3.8 Length Change of Mortars

Mortars' change in length was measured as a function of time according to the ASTM C157 standard. Before measuring the length of a mortar bar, the length of a metal reference bar was measured in a length comparator. Then, the length of the mortar bar was measured, and the difference in these two comparator measurements was recorded. The relative length change could be calculated according to Equation (6).

$$\Delta L_x = \frac{D - D_i}{G} \times 100\% \tag{6}$$

In Equation (6), D refers to the difference between the comparator readings of the specimen and the reference bar at any age; D_i refers to the difference between the comparator readings of the specimen and the reference bar at the initial age (24 hours in this study); G refers to the gage length, here 10"; and ΔL_x is the percent change in length relative to the initial length. The average and standard deviation of two values was taken for each mortar design.

3.3.9 Compressive Strength of Mortars

The compressive strength of mortar cubes was measured at 4hr, 24hr, 7d, 28d, and 90d of age, for both constant-water and constant-flow mortars. Two-inch mortar cubes were loaded directly into a hydraulic press to measure their compressive strength. Mortar cubes were subject to a loading rate between 200 and 400lb/s, according to the ASTM C109 standard. The compressive strength was recorded as the maximum load per unit area applied to the specimen before failure. Most specimens were taken as the average and standard deviation of three strengths, but some values had to be taken as an average and standard deviation of two strengths, due to specimen malformation or the presence of outliers.

3.3.10 Compressive Strength of Concrete

Concrete cylinders were strength-tested in a hydraulic press using a target loading rate of 440lb/s, or 35psi/s, according to the ASTM C39 standard. The loading rate was maintained within 88lb/s, or 7psi/s, of the target value. A specimen after breaking is shown in Figure 12.

Figure 12: Concrete cylinder (4”×8”) after mechanical failure in hydraulic press

3.3.11 Global Warming Potentials and Carbon Intensities of Mortars and Concrete

BCSA cement has a global warming potential (GWP) of 0.673 [5]. That is, the manufacture of one kilogram of BCSA cement emits 0.673 kilograms of CO_2-equivalent greenhouse gases. Carbon emissions of specimens containing SCMs were calculated by considering all SCMs to have zero GWP. Thus, a BCSA mortar specimen with 30% of its mass replaced with an SCM will have a GWP of 0.471, which is 70% as large as that of BCSA. Concrete GWP is calculated differently, measured instead as CO_2-equivalent emissions per unit volume of concrete. This is calculated by multiplying the cement GWP, measured in kg CO_2-eq per unit mass of cement, by the amount of cement used per unit volume of concrete, then multiplying by a dimensionless factor to account for emissions from sources aside from cement in the concrete, e.g. aggregates.

The carbon intensity of a specimen is defined as its GWP divided by its strength for a mortar, or its volumetric emissions divided by its strength for concrete. Carbon intensity serves as a figure

of merit for low-GWP cements: an optimal specimen will have the lowest possible carbon intensity.

The GWP and carbon intensity values of BCSA/WYFA-3 concrete were compared to literature values of concrete made with Portland cement.

4. Results

All results observed during testing are tabulated in this section. Tests performed on SCMs, cement pastes, mortars, and BCSA/WYFA-3 concrete are summarized individually in Table 6, Table 7, Table 8, and Table 9, respectively. The use of different WYFA samples (WYFA-1, WYFA-2, WYFA-3) is complex and thus clarified in later sections.

Table 6: Summary of tests performed on SCMs

SCM	XRF & LOI	SEM	XRD (No Rietveld)	R^3 Calorimetry
FA	✓	✓	✓	✓
PW	✓	✓	✓	✓
WYFA-1	✓	✓	✓	✓
WYFA-2	✓	-	✓	-
WYFA-3	✓	-	✓	-
NDFA	✓	✓	✓	✓

Table 7: Summary of tests performed on cement pastes

Paste Type	TGA	SEM	XRD & Rietveld	C1702 Calorimetry
BCSA (Control)	28d	24hr, 28d	4hr, 24hr, 28d	✓
BCSA + 10% SCM	28d	-	4hr, 24hr, 28d	✓
BCSA + 20% SCM	28d	-	4hr, 24hr, 28d	✓

BCSA + 30% SCM	28d	24hr, 28d	4hr, 24hr, 28d	✓

All tests in the mortar table, Table 8, were performed on both constant-water and constant-flow specimens with all four SCMs. The column labelled “Flow” in Table 8 refers to the measurement of flow at constant water for constant-water specimens, and the water/cement ratio necessary to achieve constant flow for constant-flow specimens.

Table 8: Summary of tests performed on constant-water and constant-flow mortars

Mortar Type	Flow	Set Time	Length Change	Compressive Strength	GWP	Carbon Intensity
BCSA (Control)	✓	✓	7d, 28d, 90d	4hr, 24hr, 7d, 28d, 90d	✓	4hr, 24hr, 7d, 28d, 90d
BCSA + 10% SCM	✓	✓	7d, 28d, 90d	4hr, 24hr, 7d, 28d, 90d	✓	4hr, 24hr, 7d, 28d, 90d
BCSA + 20% SCM	✓	✓	7d, 28d, 90d	4hr, 24hr, 7d, 28d, 90d	✓	4hr, 24hr, 7d, 28d, 90d
BCSA + 30% SCM	✓	✓	7d, 28d, 90d	4hr, 24hr, 7d, 28d, 90d	✓	4hr, 24hr, 7d, 28d, 90d

Data from concrete was compared to reference values from literature, and this is reflected in Table 9. No OPC was used or tested in this study.

Table 9: Summary of tests performed on BCSA/WYFA-3 concrete, and OPC reference values

Concrete Type	Compressive Strength	GWP	Carbon Intensity
Portland (Literature)	4d, 7d, 14d, 28d	✓	4d, 7d, 14d, 28d
BCSA (Control)	4hr, 24hr, 3d, 7d, 14d, 28d, 56d	✓	4hr, 24hr, 3d, 7d, 14d, 28d, 56d
BCSA + 10% WYFA-3	4hr, 24hr, 3d, 7d, 14d, 28d, 56d	✓	4hr, 24hr, 3d, 7d, 14d, 28d, 56d
BCSA + 20% WYFA-3	4hr, 24hr, 3d, 7d, 14d, 28d, 56d	✓	4hr, 24hr, 3d, 7d, 14d, 28d, 56d
BCSA + 30% WYFA-3	4hr, 24hr, 3d, 7d, 14d, 28d, 56d	✓	4hr, 24hr, 3d, 7d, 14d, 28d, 56d

4.1 Analysis of SCMs

4.1.1 X-Ray Fluorescence & Loss on Ignition

The chemical composition of all SCMs obtained via XRF is shown in Table 10. All values less than 0.5% were removed. Composition sums were not normalized to 100%. Loss-on-ignition (LOI) values were obtained via thermogravimetry.

Table 10: XRF chemical compositions & TGA loss on ignition of all SCMs

Compound	FA	PW	WYFA-1	WYFA-2	WYFA-3	NDFA
SiO_2	48.3%	27.1%	16.2%	14.0%	15.3%	14.5%

Al_2O_3	17.8%	14.6%	9.2%	8.2%	9.0%	6.1%
Fe_2O_3	10.7%	2.2%	4.6%	4.3%	4.4%	5.9%
CaO	7.1%	49.9%	33.4%	35.5%	35.8%	25.0%
K_2O	2.6%	-	-	-	-	0.9%
MgO	1.6%	1.9%	3.9%	3.2%	3.5%	2.7%
SO_3	1.6%	2.9%	15.8%	15.3%	15.8%	27.3%
Na_2O	1.3%	-	2.2%	2.0%	2.2%	8.3%
TiO_2	0.9%	-	-	0.7%	0.7%	-
P_2O_5	0.5%	-	0.8%	0.6%	0.7%	-
BaO	-	-	0.6%	0.5%	0.5%	0.9%
CO_2	-	0.8%	-	-	-	-
Sum	92.4%	99.5%	86.7%	84.3%	88.0%	91.5%
LOI	1.6%	2.8%	9.3%	20.8%	10.6%	20.9%

The compositional profiles of each SCM are also shown in Figure 13. This is the same data as in the preceding table, Table 10.

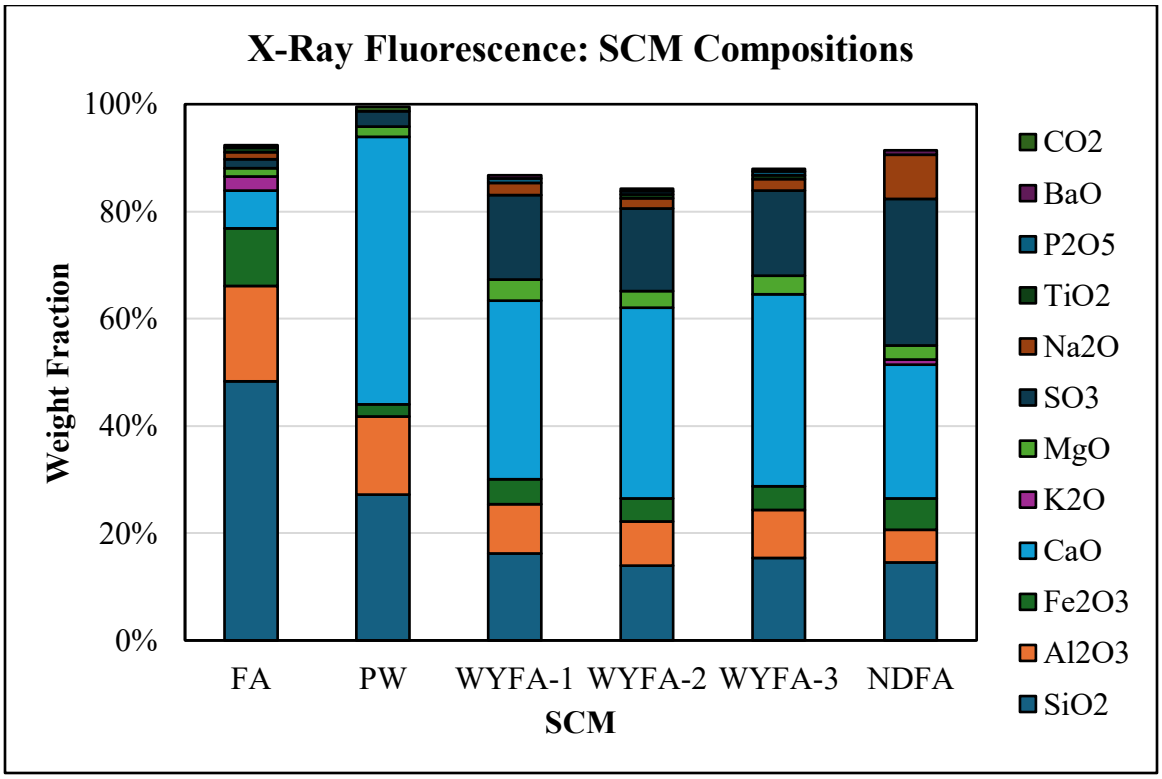

Figure 13: Compositions of all SCMs as measured via XRF, also written in Table 10

Class C fly ash (FA) had a very high amount of silica. Paper recycling waste (PW) contained the most lime. All three Wyoming specimens had very similar compositions, with lime, sulfate, and silica being the most prominent components. WYFA-2 had a high LOI corresponding to its elevated moisture content in its hydrated nodules, which was not present in WYFA-3 due to its heat treatment. The North Dakota fly ash (NDFA) had the largest sulfate content of all SCMs but otherwise had a similar composition profile to that of the three WYFA samples.

4.1.2 X-Ray Diffraction

No SCM compositions were analyzed via Rietveld refinement due to the complexity of their phase content as well as the presence of amorphous phases. However, they were scanned via XRD with select peaks identified, allowing some of the mineral content to be ascertained without knowledge of their relative quantities.

The X-ray diffraction profile of class C fly ash (FA) is shown in Figure 14.

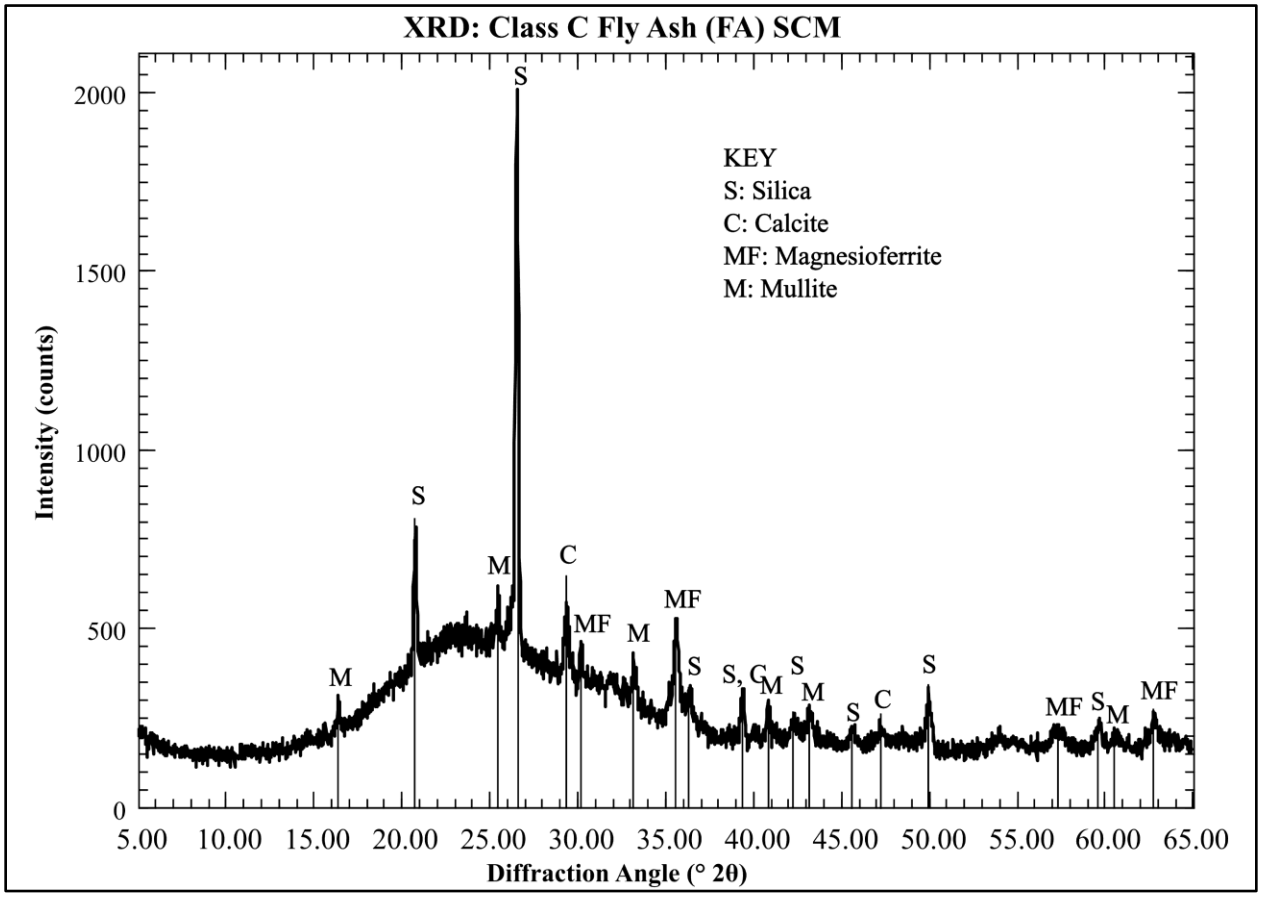

Figure 14: XRD of class C fly ash SCM (FA). Key phases include silica (COD: 9013321), calcite (COD: 9014216), magnesioferrite (COD: 9007273), and mullite (COD: 9001322), as well as amorphous content (not annotated).

The XRD data from the class C fly ash SCM showed peaks from silica, calcite, magnesioferrite, and mullite. Additionally, a large broad peak between roughly 15 and 40 degrees corresponds to amorphous content within the ash.

The paper recycling waste SCM (PW) X-ray diffraction data is shown in Figure 15.

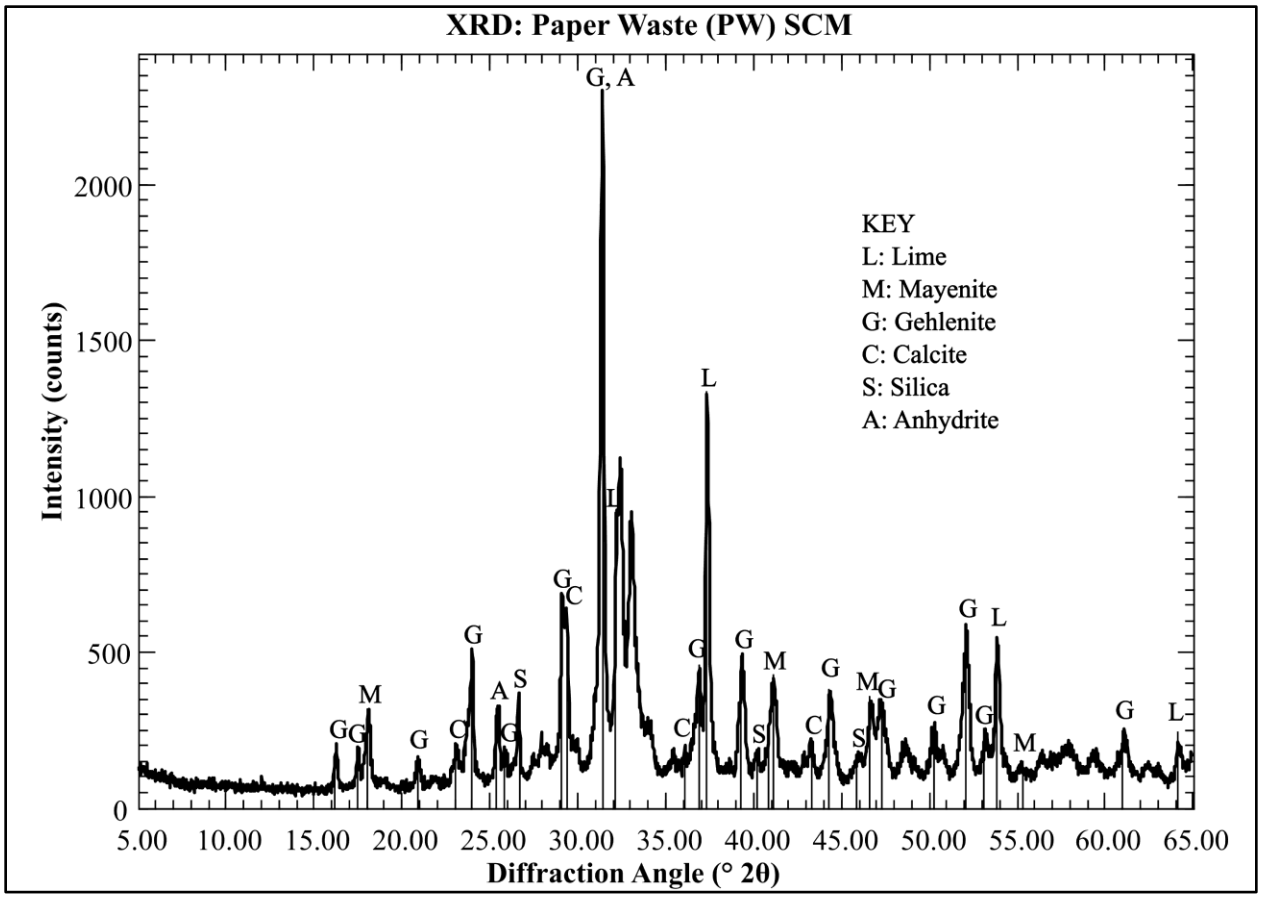

Figure 15: XRD of paper recycling waste SCM (PW). Key annotated phases include lime (COD: 9006694), mayenite (COD: 2102955), gehlenite (COD: 1000048), calcite (COD: 9014216), silica (COD: 9013321), and anhydrite (COD: 9017809).

X-ray diffraction data of the paper recycling waste SCM showed evidence of large quantities of free lime, as well as mayenite, gehlenite, calcite, silica, and anhydrite.

XRD of the WYFA-1, WYFA-2, and WYFA-3 SCMs can be seen in Figure 16.

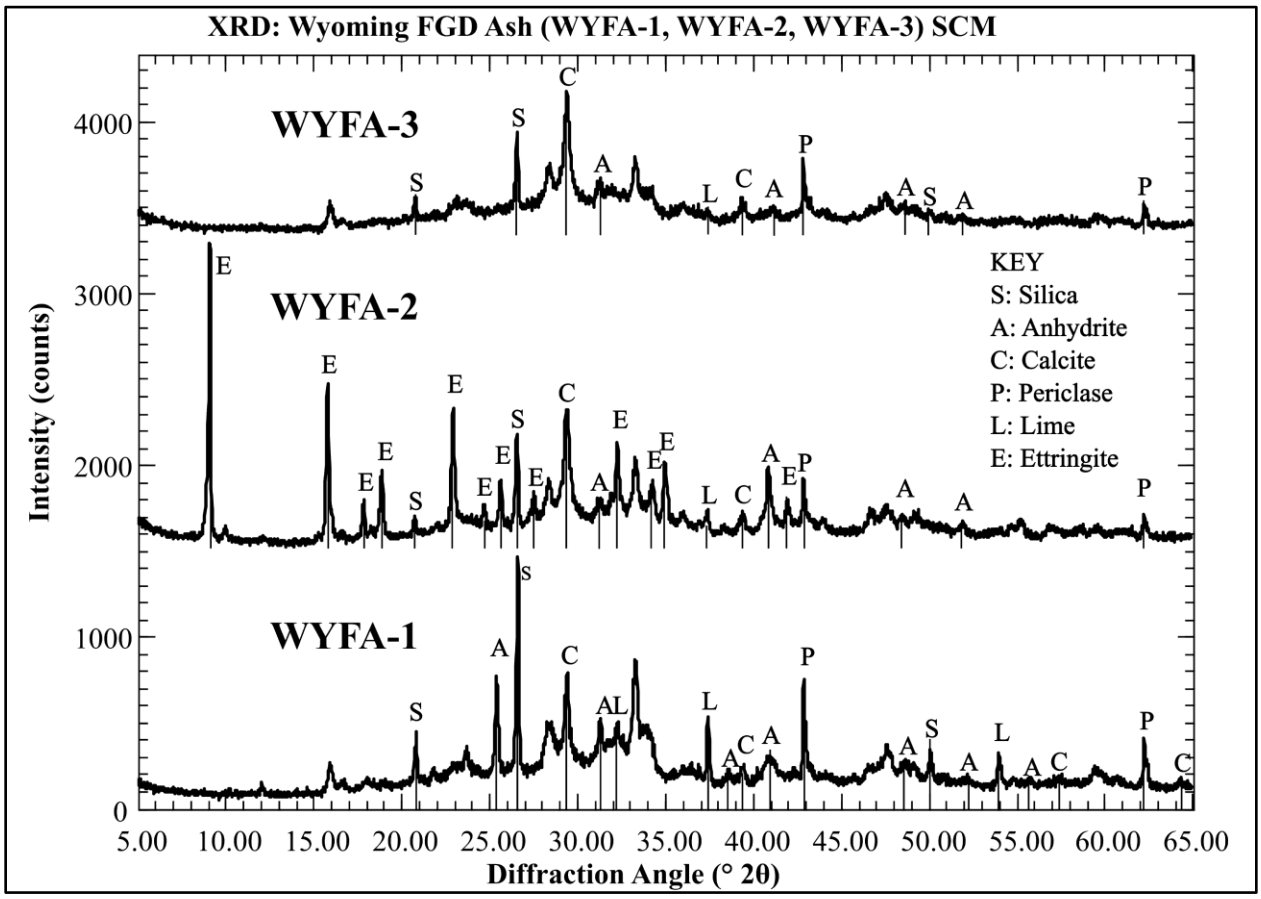

Figure 16: XRD of Wyoming FGD waste ash (WYFA-1, WYFA-2, and WYFA-3) SCMs. Annotated phases include silica (COD: 9013321), anhydrite (COD: 9017809), calcite (COD: 9014216), periclase (COD: 9006784), lime (COD: 9006694), and ettringite (COD: 9015084). WYFA-2 is the only WYFA sample to show signs of ettringite.

XRD of the WYFA-1 and WYFA-3 SCMs showed peaks from silica, anhydrite, calcite, periclase, and lime. XRD of the WYFA-2 SCM, which was hydrated, showed peaks from all these phases, as well as strong peaks from ettringite. WYFA-3, despite showing the same hydrated nodules as WYFA-2, did not show ettringite peaks, due to its heat treatment. The presence of ettringite in the hydrated SCM, even in the absence of BCSA cement, indicates that it may engage in favorable reactions with BCSA.

XRD results of the North Dakota fly ash (NDFA) SCM can be seen in Figure 17.

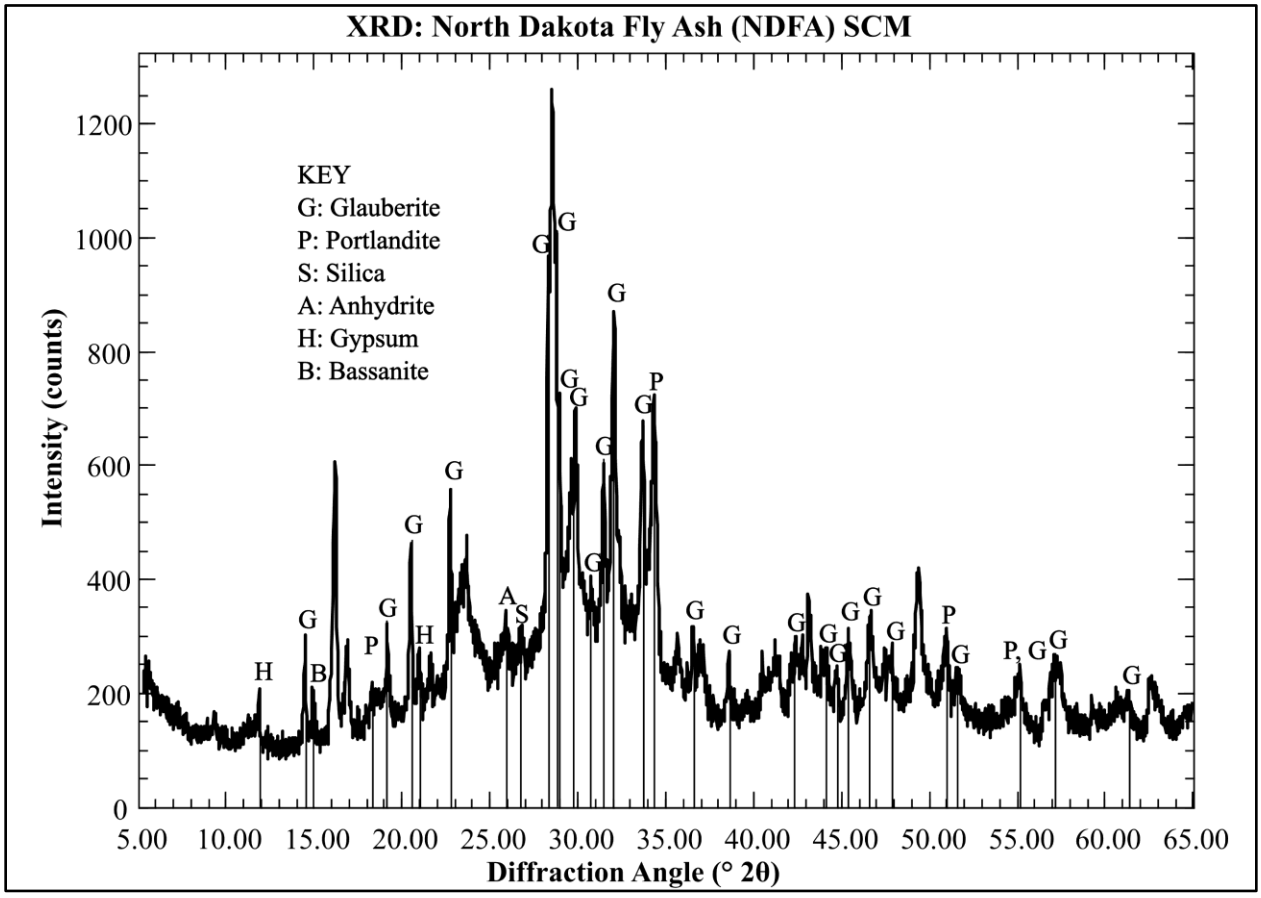

Figure 17: XRD of NDFA SCM with annotated phases. Annotated phases include glauberite (COD: 9000154), portlandite (COD: 9006832), silica (COD: 9013321), anhydrite (COD: 9017809), gypsum (COD: 9017313), and bassanite (COD: 2105042).

Per XRD data, the NDFA SCM contained glauberite, portlandite, silica, anhydrite, gypsum, and bassanite. XRD of similar North Dakota lignite fly ash from literature has also shown evidence of glauberite [50].

4.2 Thermogravimetry of Cement Pastes

Thermogravimetric data of hydration-stopped cement pastes is shown in Figure 18 (28d FA pastes), Figure 19 (28d PW pastes), Figure 20 (28d WYFA-1 pastes), and Figure 21 (28d NDFA pastes). These specimens had their hydration stopped at 28d, and contained 0%, 10%, 20%, and 30% SCM. All graphs show the temperature at which each phase had its most intense mass derivative, but the decomposition of all phases occurred over a range of temperatures. The temperature at which a phase decomposes depends heavily on the equipment used as well as measurement conditions, making peak identification a highly situational endeavor [51, p. 188]. Scrivener, et al, write approximate reference values for many phases in cement [51, pp. 190-195], and these values are listed in Table 11 alongside the peak positions observed in this study.

Table 11: Decomposition temperatures of various phases under DTG

Phase	Reference Temperature (Scrivener et al [51, pp. 190-195])	Observed Temperature
Ettringite (AFt)	100°C	120°C
Stratlingite	200°C	170°C
AFm	200-300°C	210°C

AH_3	270°C	245°C
CČ	600-800°C	690°C
Wollastonite (CS)	800°C	750-900°C

DTG data from 28-day-old pastes made with class C fly ash (FA) is shown in Figure 18.

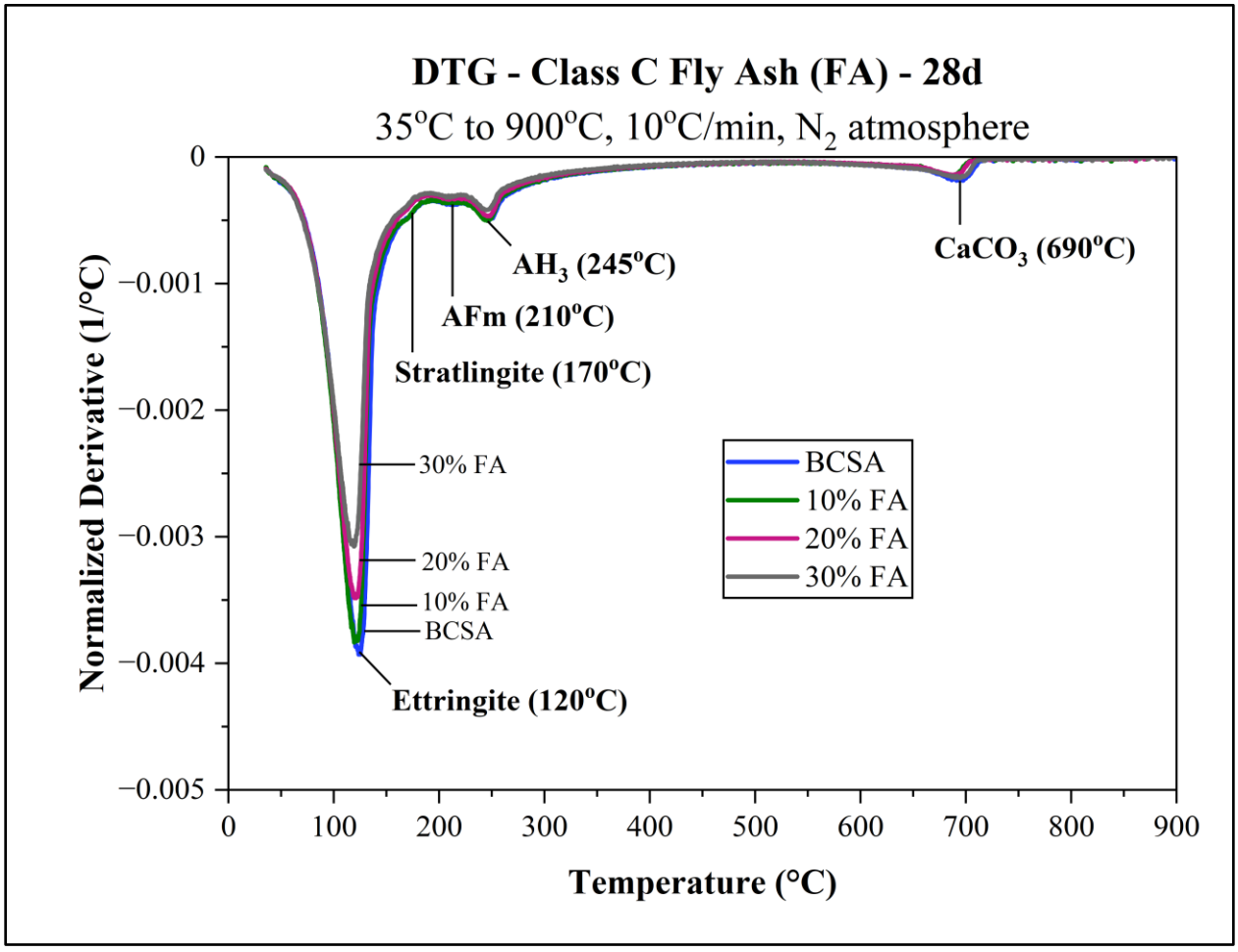

Figure 18: DTG data from pastes made with class C fly ash (FA)

Specimens made with class C fly ash showed decreasing ettringite content with higher SCM fractions. All specimens showed a small, weak stratlingite peak, which slightly weakened with higher SCM content. Content of AFm phases also slightly decreased with higher SCM content. AH_3 content decreased with higher SCM content. Calcium carbonate content remained mostly constant.

DTG data from 28-day-old pastes made with paper recycling waste (PW) is shown in Figure 19.

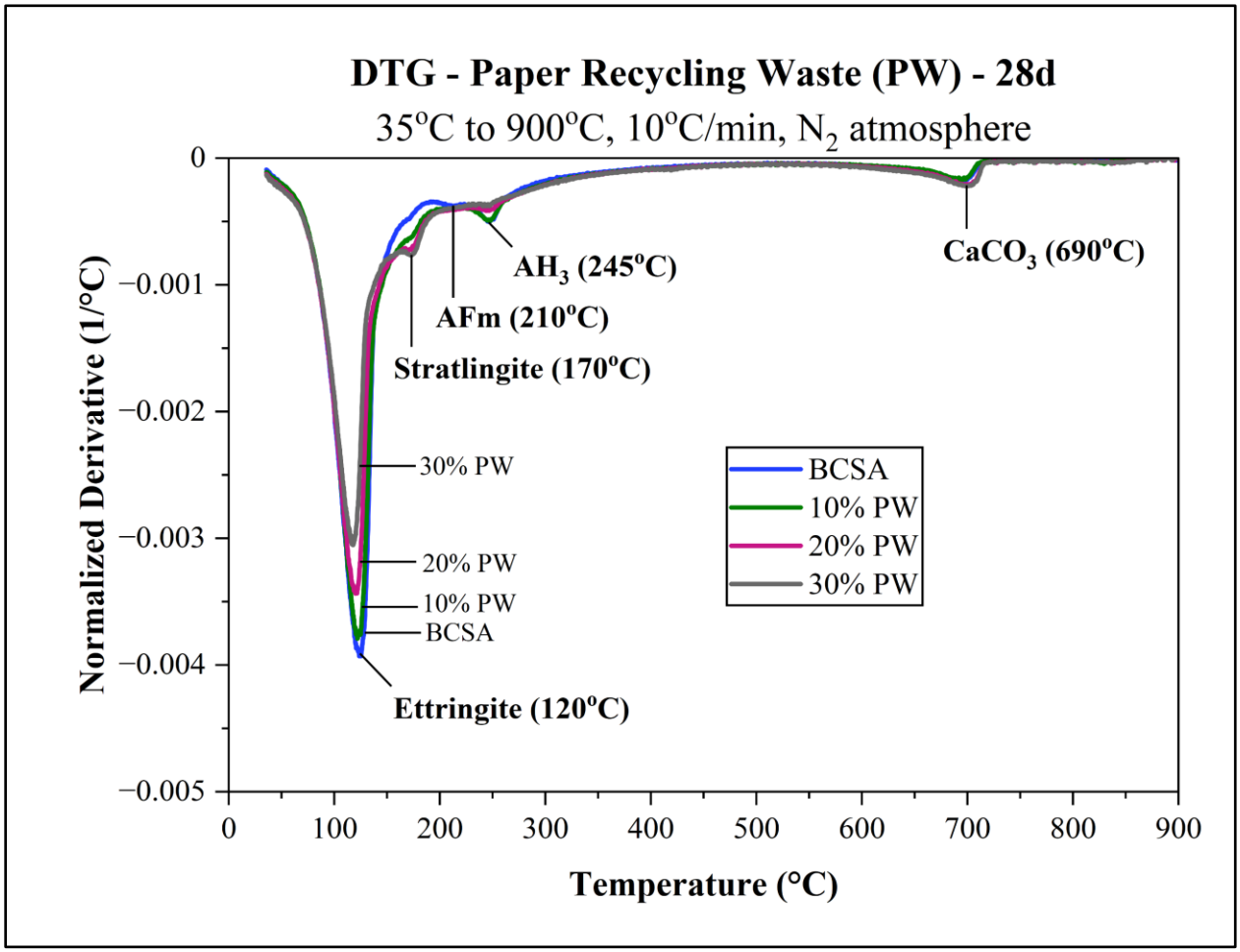

Figure 19: DTG data from pastes made with paper recycling waste (PW)

Specimens made with paper recycling waste exhibited reductions in ettringite content to a similar degree as those pastes made with FA. Stratlingite content increased with SCM content. AFm phases remained relatively unaffected. AH_3 content significantly decreased with higher SCM content. Calcium carbonate content remained mostly unaffected.

DTG data from 28-day-old pastes made with Wyoming FGD waste ash (WYFA-1) is shown in Figure 20.

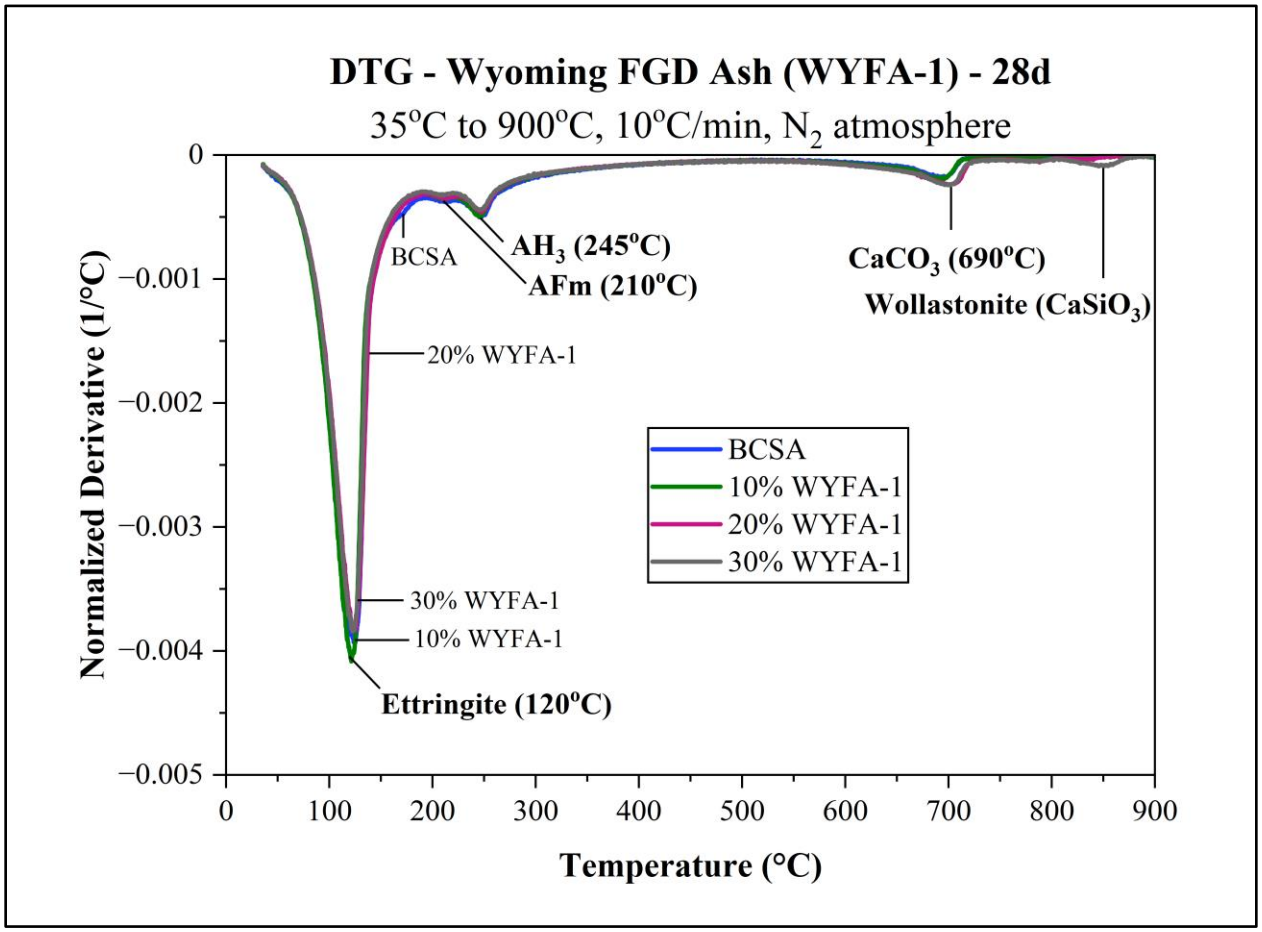

Figure 20: DTG data from pastes made with Wyoming FGD waste ash (WYFA-1)

In pastes made with Wyoming FGD waste ash (WYFA-1), ettringite content remained constant. The paste with the highest ettringite content by a slight amount contained 10% WYFA-1. No stratlingite was present, even when the control showed a possible weak peak. AFm phases remained mostly unaffected, as did AH_3 content. Calcium carbonate content increased with higher SCM content. The 30% SCM paste also showed evidence of wollastonite formation.

DTG data from 28-day-old pastes made with North Dakota fly ash (NDFA) is shown in Figure 21.

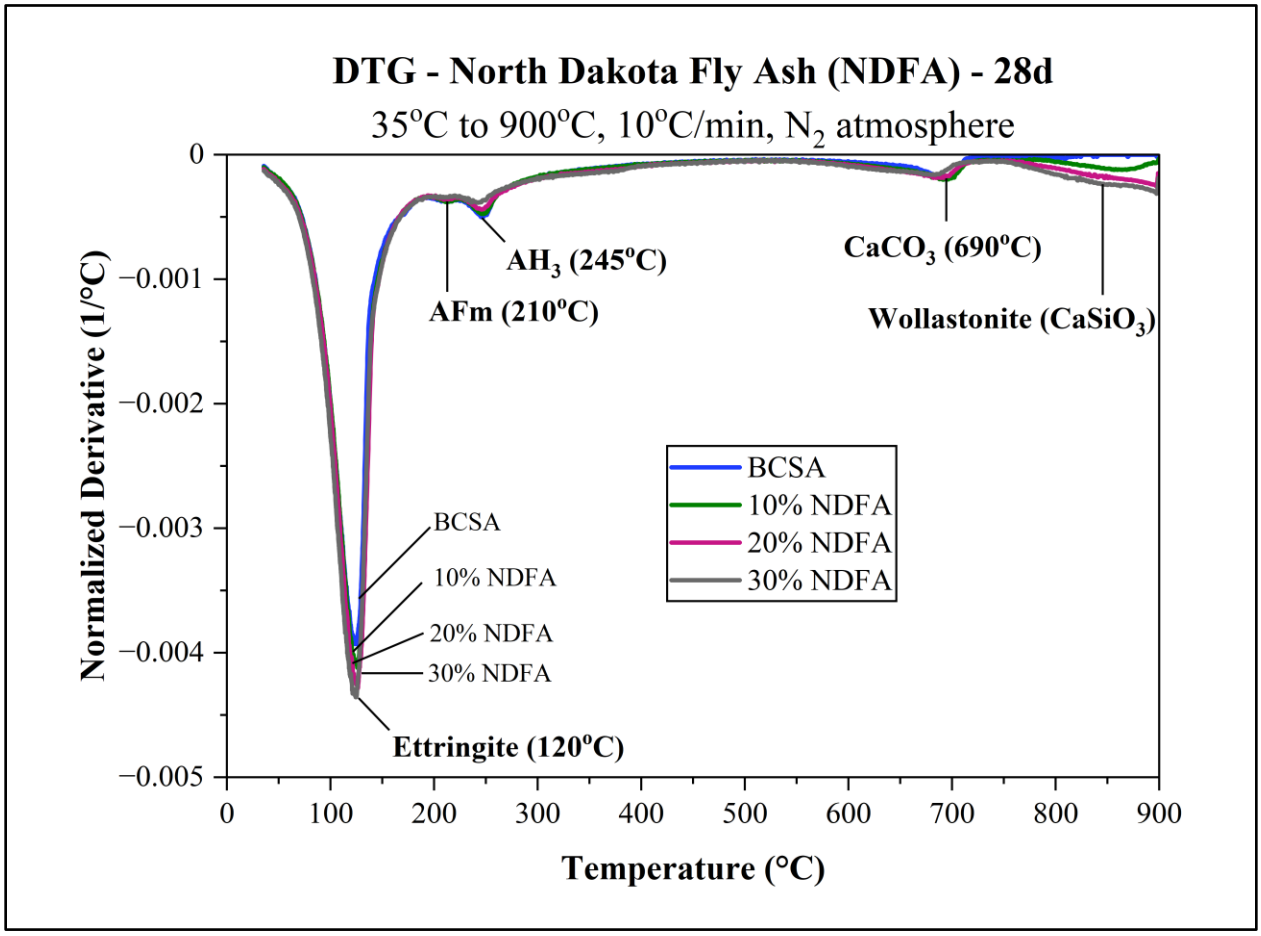

Figure 21: DTG data from pastes made with North Dakota fly ash (NDFA)

Pastes made with North Dakota fly ash (NDFA) showed increasing ettringite content for greater SCM content. No stratlingite was present. AFm phases remained unaffected. AH_3 content decreased for higher SCM fractions. Calcium carbonate content decreased slightly with SCM addition. All three NDFA pastes showed evidence of wollastonite formation, which increased with SCM content.

4.3 Scanning Electron Microscopy

An electron microscope was used to image the SCMs, as well as control BCSA pastes containing 0% SCM and pastes containing 30% SCM, with hydration stopped at 24hr and 28d. This allowed qualitative characterization of the morphology of the pure SCMs, and the ettringite of the pastes. These images are shown in Figure 22 (SCMs), Figure 23 (pastes without SCM), Figure 24 (30% FA pastes), Figure 25 (30% PW pastes), Figure 26 (30% WYFA-1 pastes), and Figure 27 (30% NDFA pastes). Because the SEM micrographs are of pastes, which do not contain sand, the images purely reflect the phase development within the cement itself, and the interactions between BCSA and the SCMs.

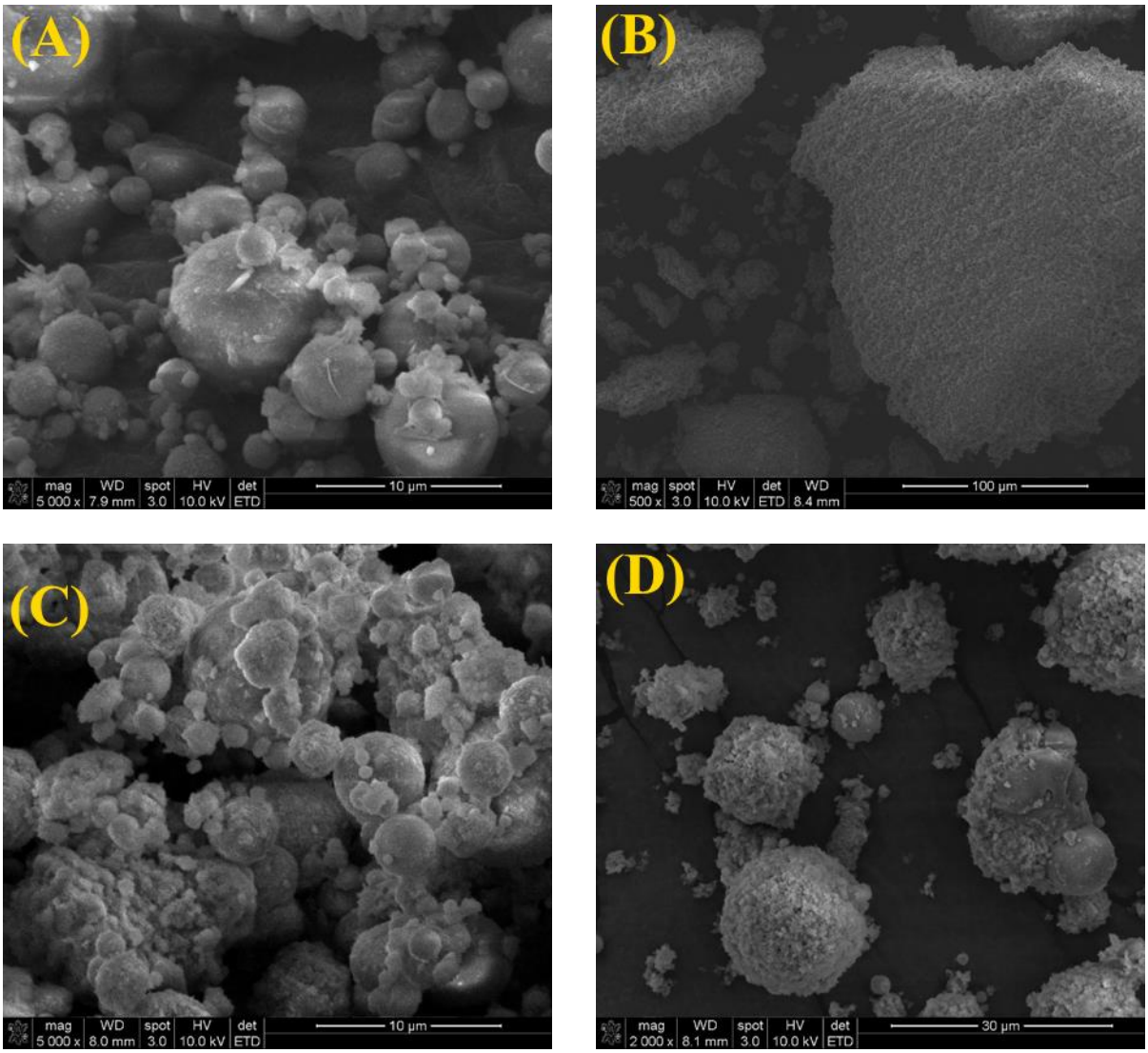

Figure 22: SCMs imaged via electron microscope. A: Class C Fly Ash (FA); B: Paper Recycling Waste (PW); C: Wyoming FGD Waste Ash (WYFA-1); D: North Dakota Fly Ash (NDFA)

The three ash SCMs had similar morphologies between them. The constituent particles of the paper recycling waste SCM were very large in comparison to the other three SCMs.

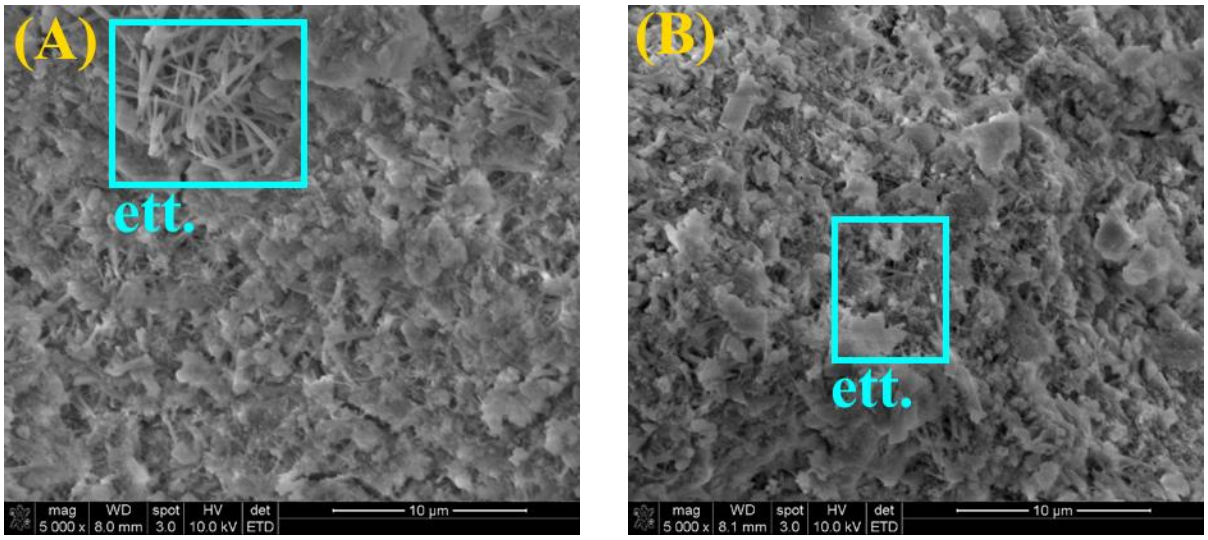

Figure 23: SEM images of pastes with no SCM. A: BCSA paste at 24hr; B: BCSA paste at 28d

Imaging BCSA serves as a control for observation of ettringite. At 28d the ettringite is less visible, due to the densification of the cement matrix with the precipitation of more C-S-H.

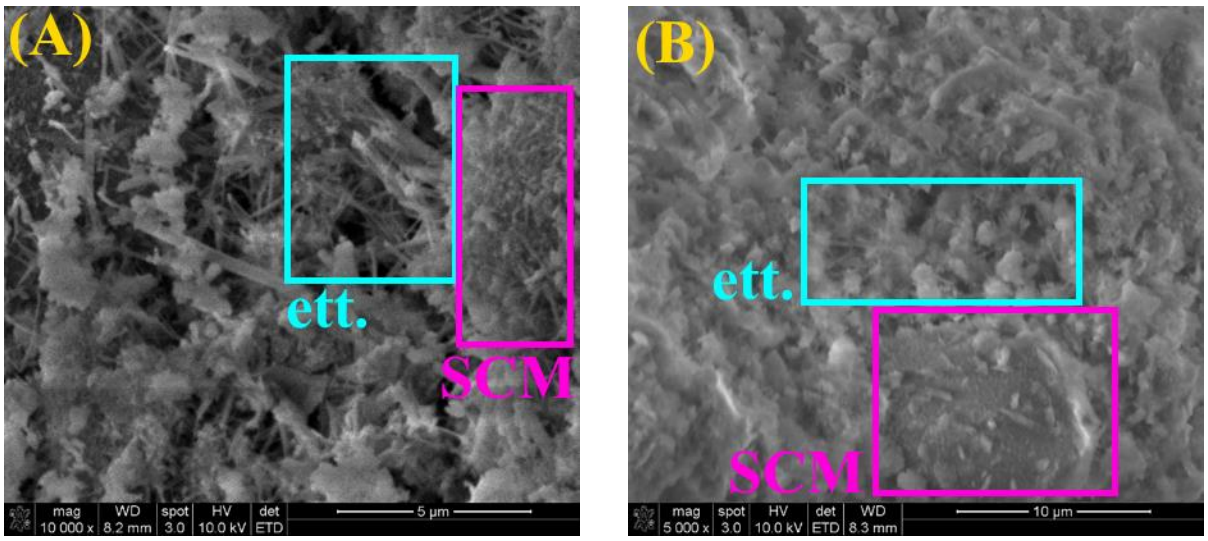

Figure 24: SEM images of pastes containing 30% FA. A: FA paste at 24hr; B: FA paste at 28d

Pastes made with class C fly ash still showed high quantities of ettringite.

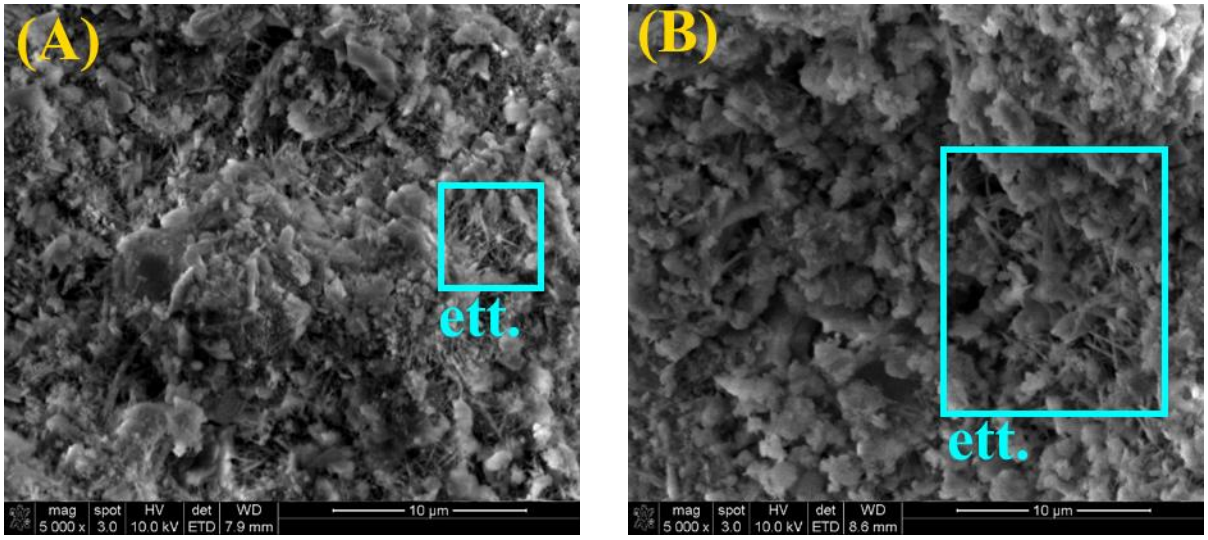

Figure 25: SEM images of pastes containing 30% PW. A: PW paste at 24hr; B: PW paste at 28d

Because the particles of the paper recycling waste SCM were very large, they cannot be shown in the selected micrographs. Paper recycling waste specimens still showed significant ettringite crystallization, but the needles themselves may be thinner than those in other specimens.

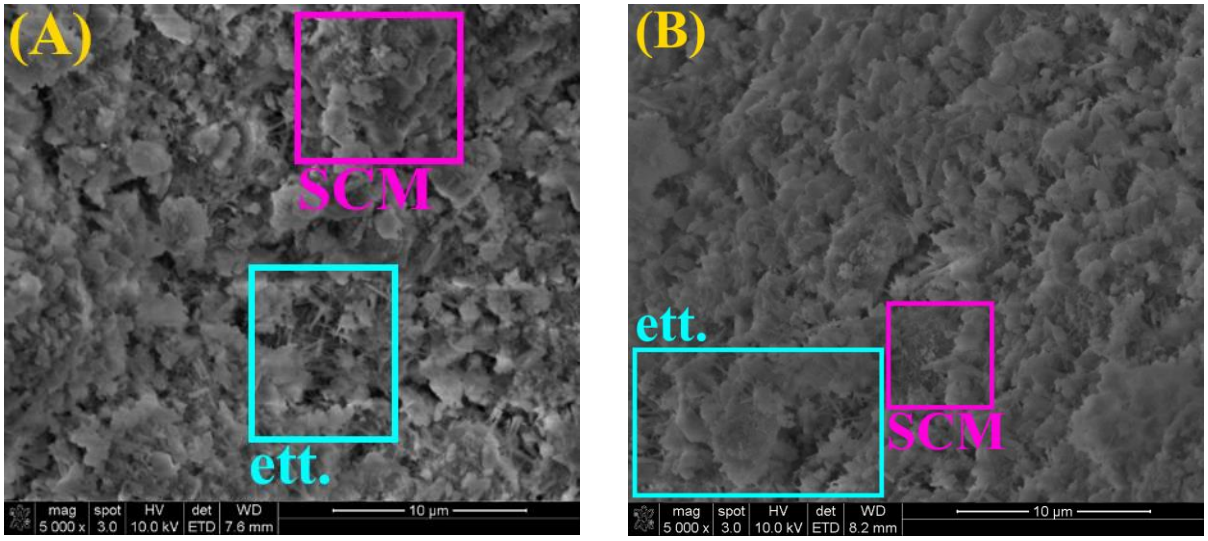

Figure 26: SEM images of pastes containing 30% WYFA-1. A: WYFA-1 paste at 24hr; B: WYFA-1 paste at 28d

The WYFA-1 specimens showed similar ettringite development to that found in the other specimens. Again, the ettringite needles seem to be less exposed due to the precipitation of C-S-H.

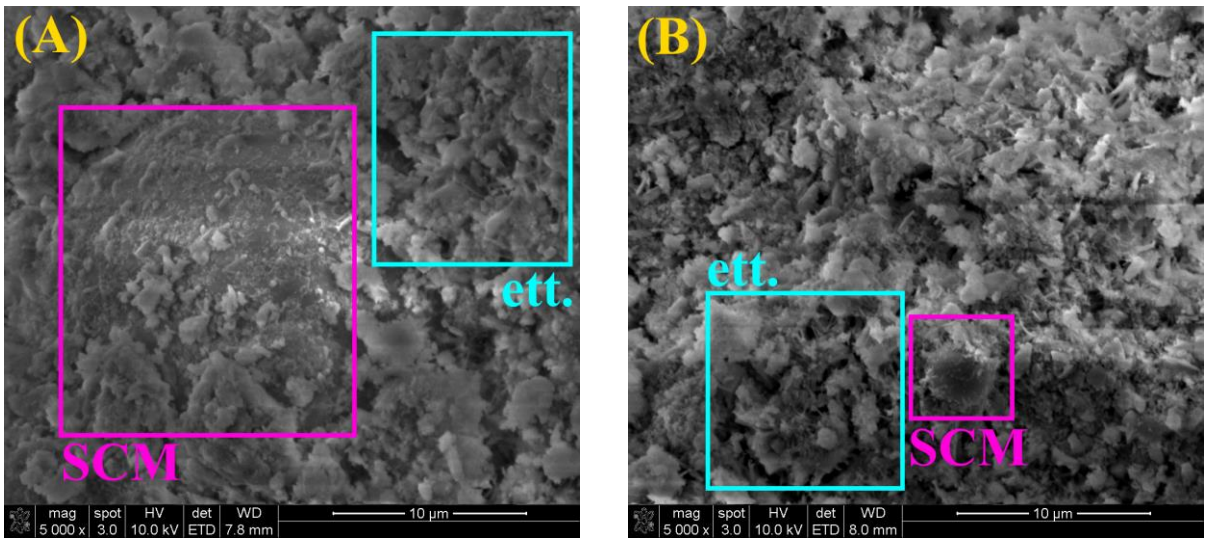

Figure 27: SEM images of pastes containing 30% NDFA. A: NDFA paste at 24hr; B: NDFA paste at 28d.

The development of ettringite within the NDFA specimens is similar to that within the other paste specimens. Ettringite needles still form within close range of the SCM at 24hr and at 28d. The ettringite seems to be better-developed at 28d in comparison to that found at 24hr. Artifacts of the NDFA SCM appeared as 10µm spheres, which are larger than artifacts of WYFA-1. The inert artifacts of WYFA-1 are much smaller than those of NDFA, leading to more efficient

particle packing in WYFA-1 and a lower strength reduction after addition of WYFA-1 in comparison to NDFA.

4.4 Phase Quantification in Pastes via Rietveld Refinement

In the pastes used for hydration study, the quantities of belite, ye'elimite, ettringite, and stratlingite were calculated via XRD and Rietveld refinement. These values are shown in Figure 28, Figure 29, Figure 30, and Figure 31. Pastes were prepared for hydration study at 4hr, 24hr, and 28d, so Rietveld quantities correspond to these ages. Stratlingite was not present in any WYFA-1, NDFA, or control (BCSA) pastes.

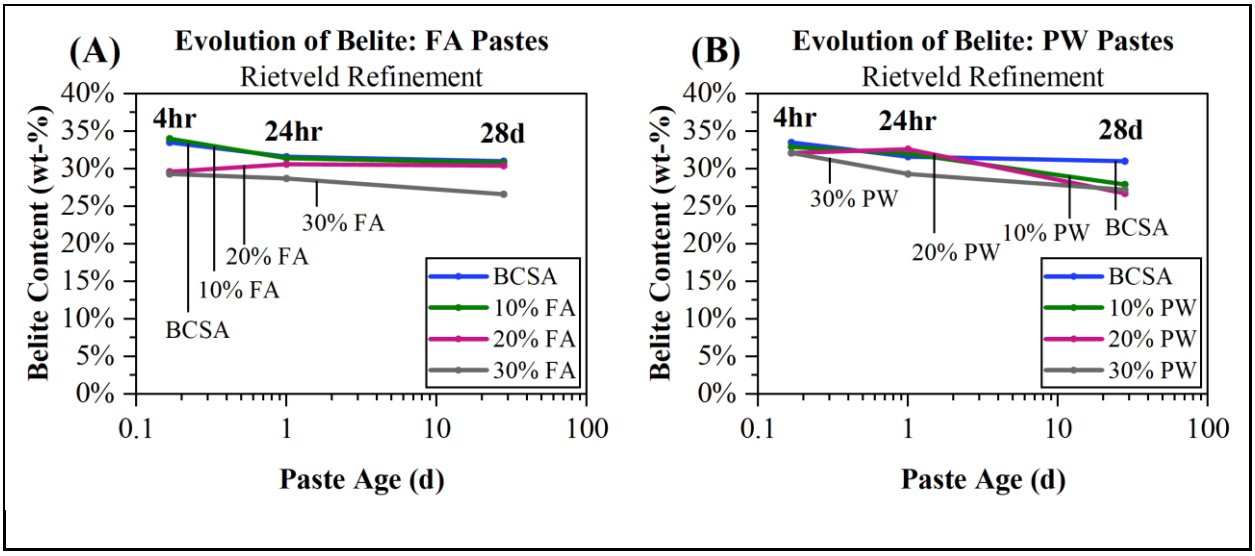

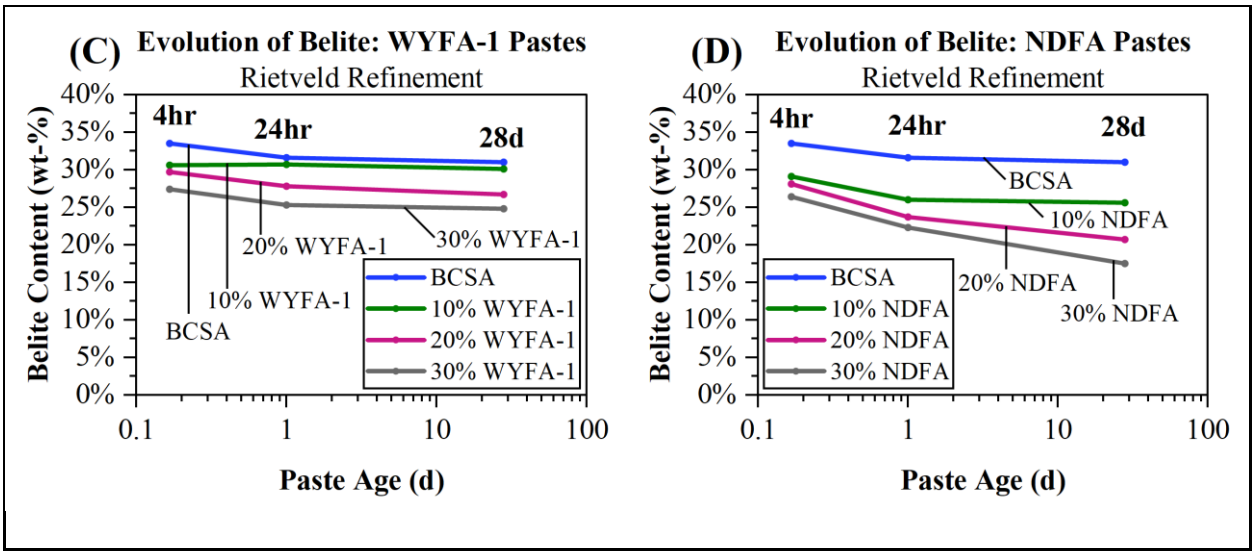

Figure 28: Belite weight fraction over time, calculated via Rietveld refinement; A: in FA pastes; B: in PW pastes; C: in WYFA-1 pastes; D: in NDFA pastes

Pastes containing NDFA consumed the most belite in their hydration, followed by those pastes containing WYFA-1. This may be due to pozzolanic activity between NDFA and belite: the NDFA SCM contains portlandite, as seen in its XRD scan (Figure 17), which can react with belite to form C-S-H. Pastes containing FA and PW showed similar levels of belite consumption, but PW pastes had a higher reduction in belite content for lower SCM fractions in comparison to FA pastes.

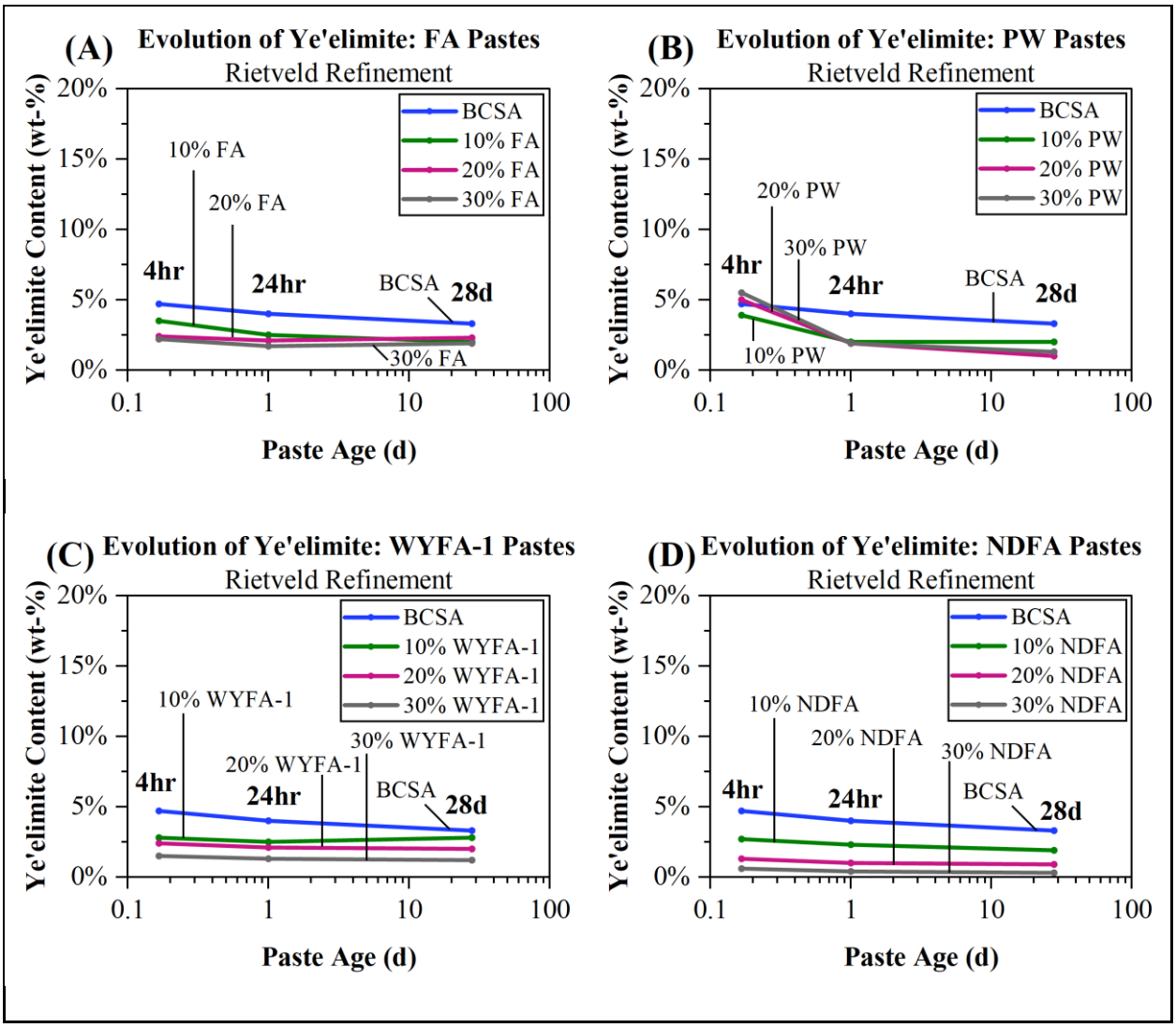

Figure 29: Ye'elimite weight fraction over time, calculated via Rietveld refinement; A: in FA pastes; B: in PW pastes; C: in WYFA-1 pastes; D: in NDFA pastes

Pastes made with NDFA had the highest consumption of ye'elimite with hydration. Because ye'elimite hydrates very quickly, any variation in ye'elimite content after 24hr can be explained by the production of other crystalline phases later within the paste's development.

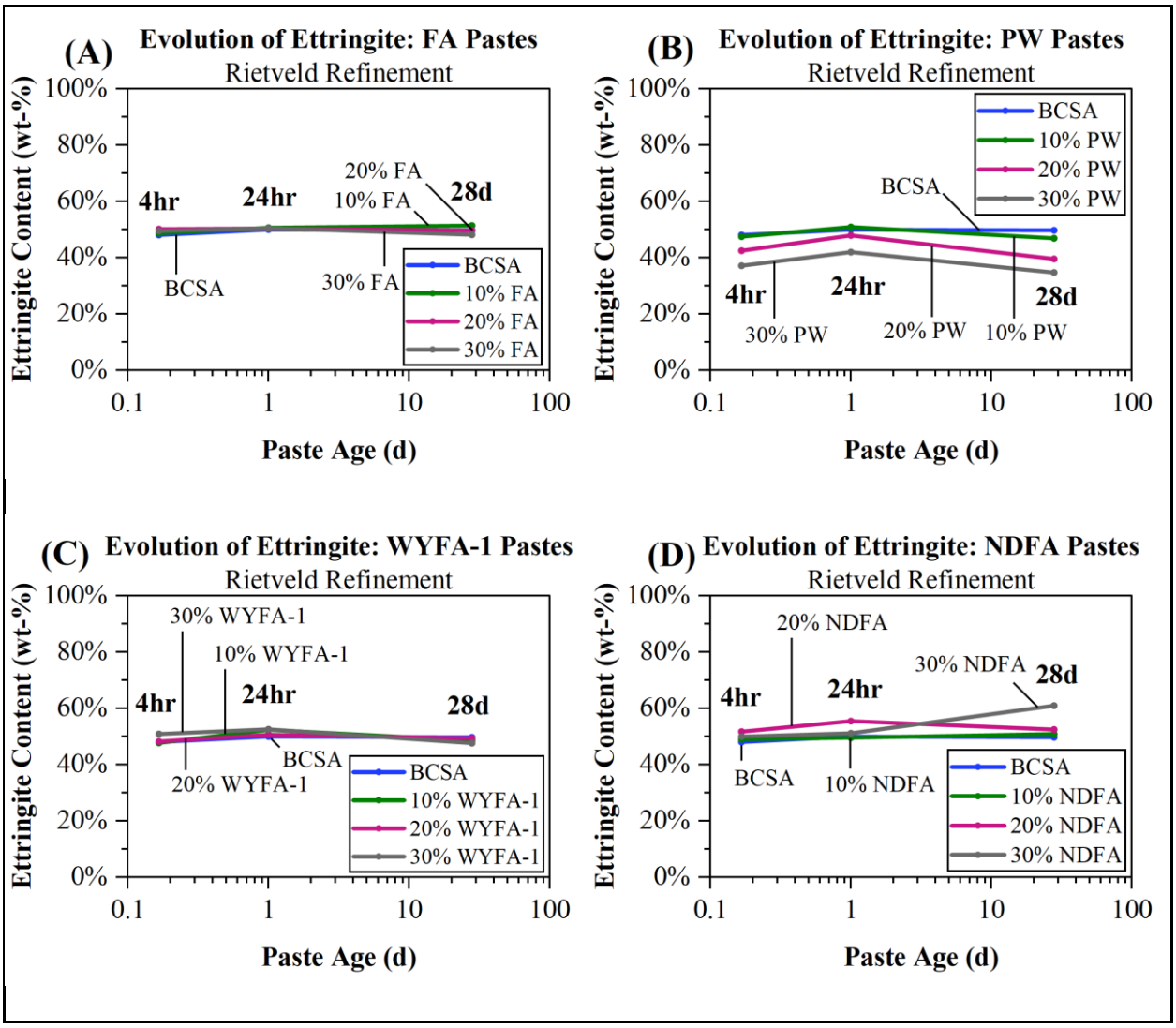

Figure 30: Ettringite weight fraction over time, calculated via Rietveld refinement; A: in FA pastes; B: in PW pastes; C: in WYFA-1 pastes; D: in NDFA pastes

Similar to the TGA data, pastes containing NDFA showed some increase in ettringite content. WYFA-1 pastes and FA pastes did not show much change in ettringite content. PW-containing specimens showed a significant decrease in ettringite content. The amount of ettringite may seem to decrease in many specimens between 24hr and 28d, but this is illusory and explained by the production of other crystalline phases in that time, e.g. stratlingite in FA and PW paste

specimens. Because Rietveld analysis necessarily shows all phases summing to 100%, the production of other crystalline phases can cause individual phase fractions to seemingly decrease when that is not necessarily the case.

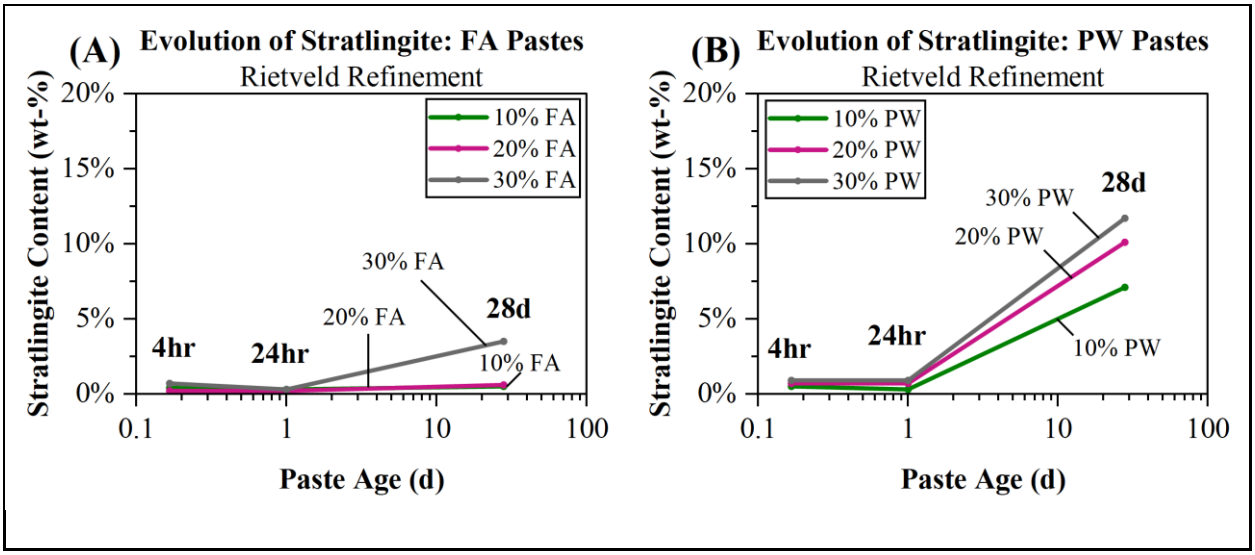

Figure 31: Stratlingite weight fraction over time, calculated via Rietveld refinement; A: in FA pastes; B: in PW pastes

FA and PW pastes showed stratlingite development between 24hr and 28d. No other pastes showed stratlingite development in their diffraction data during phase identification, so stratlingite was not included. Specimens containing class C fly ash (FA) did not show significant amounts of stratlingite below an SCM fraction of 20%. Specimens containing paper recycling waste (PW) showed consistent signs of stratlingite crystallization at all SCM fractions. Stratlingite did not form before the period between 24hr and 28d after mixing. This is because stratlingite is a product of belite hydration, a far slower reaction than that of the hydration of ye'elimite [21]. The absence of AH_3 in the PW DTG data indicates that it may have reacted with dissolved belite to produce stratlingite.

4.5 Isothermal Calorimetry of Cement Pastes

Heat flow of constant-water pastes, as measured as a function of time according to the ASTM C1702 standard for isothermal calorimetry, can be seen up to six hours after mixing in Figure 32, and up to 24 hours after mixing in Figure 33. In BCSA cement, there are two main peaks, both occurring within six hours after mixing a paste. The first peak, visible within 15 minutes of mixing, corresponds to the dissolution of clinker phases and the initial production of hydration products, including ettringite, AH_3, and secondary gypsum from hemihydrate [52, 53]. After the first peak, an induction period follows, where clinker phases and calcium sulfate dissolve while ettringite slowly crystallizes [52]. The second peak corresponds to the dissolution and hydration reaction of calcium sulfoaluminate and calcium sulfate producing ettringite and aluminum hydroxide [52]. The change in peak position corresponds to an SCM being an accelerator or a retarder: a paste containing an SCM that acts as an accelerator will react more quickly, while a paste containing an SCM that acts as a retarder will react more slowly. Cumulative heat output corresponds to reactivity of an SCM with BCSA: an SCM that is more reactive with BCSA will produce more heat, while an inert one that reduces ettringite crystallization will produce less heat. There is not a general correlation between set times, strength, and calorimetry, due to dependence on relative proportions of binder, water, and aggregate [51, pp. 56-57]. However, given a specific mortar or concrete mix design, it is possible to derive such correlations [51, pp. 56-57]. Calorimetry may be more convenient or reproducible within a study and thus preferred over set- and strength-testing.

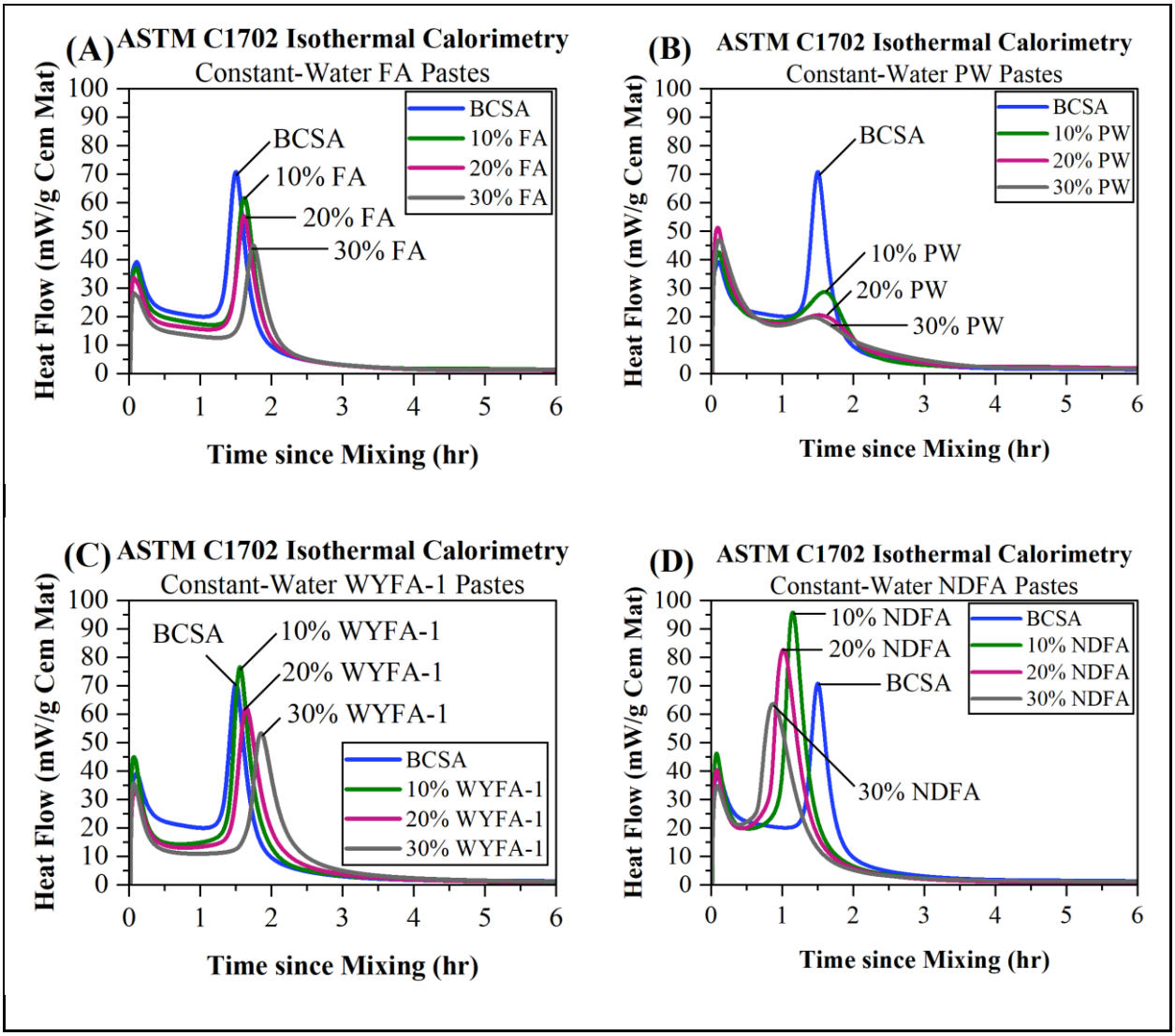

Figure 32: Heat flow of pastes containing SCMs as a function of time, as measured via isothermal calorimetry up to six hours after mixing. A: FA pastes; B: PW pastes; C: WYFA-1 pastes; D: NDFA pastes. The same BCSA control is shown in all four graphs.

The purpose of Figure 32 is to better show the chemical activity within the cement at very early ages. The heat flow drops nearly to zero between four and six hours after mixing across all specimens, making knowledge of the heat flow at later ages less useful.

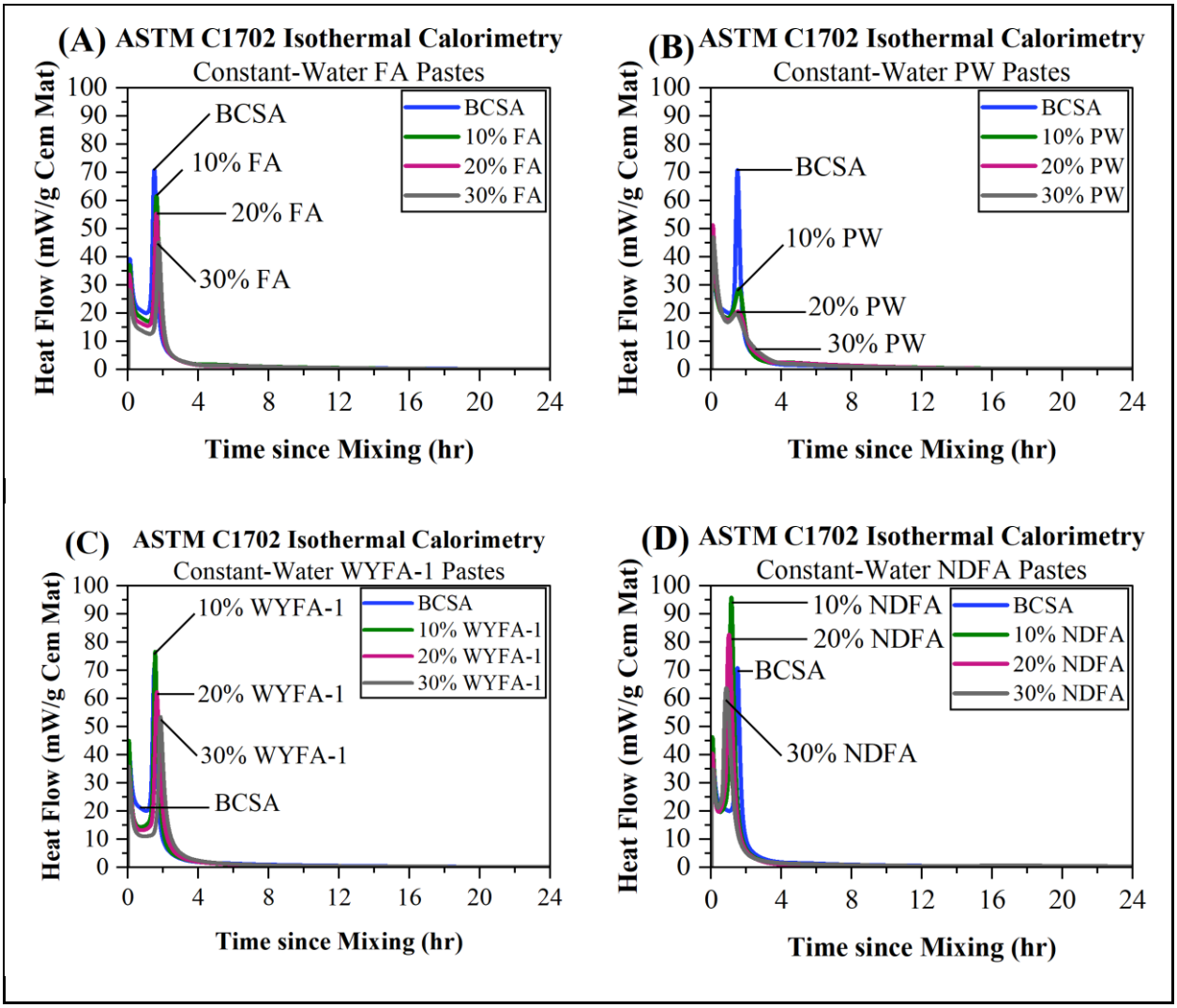

Figure 33: Heat flow of pastes containing SCMs as a function of time, as measured via isothermal calorimetry up to 24 hours after mixing. A: FA pastes; B: PW pastes; C: WYFA-1 pastes; D: NDFA pastes. The same BCSA control is shown in all four graphs.

Class C fly ash (FA) delayed the second peak in heat flow, due to its inert content, and reduced the intensity of both peaks as SCM content increased. The paper recycling waste product (PW) had a mixed effect on the initial peak in heat flow, increasing its intensity overall but having the

strongest effect at 20% SCM. It also strongly reduced the intensity of the second peak with increasing SCM content. Wyoming FGD waste ash (WYFA-1) increased the intensity of the first peak with 10% SCM, but reduced the peak intensity at 20% and 30% SCM. Additionally, WYFA-1 acted as a retarder on the second peak, increasing its intensity with 10% SCM, but reducing its intensity at 20% and 30% SCM. North Dakota fly ash (NDFA) uniformly acted as an accelerator, with higher-NDFA-content pastes showing progressively earlier positions of their second peaks. Importantly, NDFA pastes showed greater maximum heat flow at 20% and 30% SCM.

General reactivity of an SCM with BCSA cement can be quantified according to the cumulative heat output of a paste containing that SCM. The cumulative heat output, being the integral of the data from the heat flow graphs in Figure 32 and Figure 33, is shown in Figure 34.

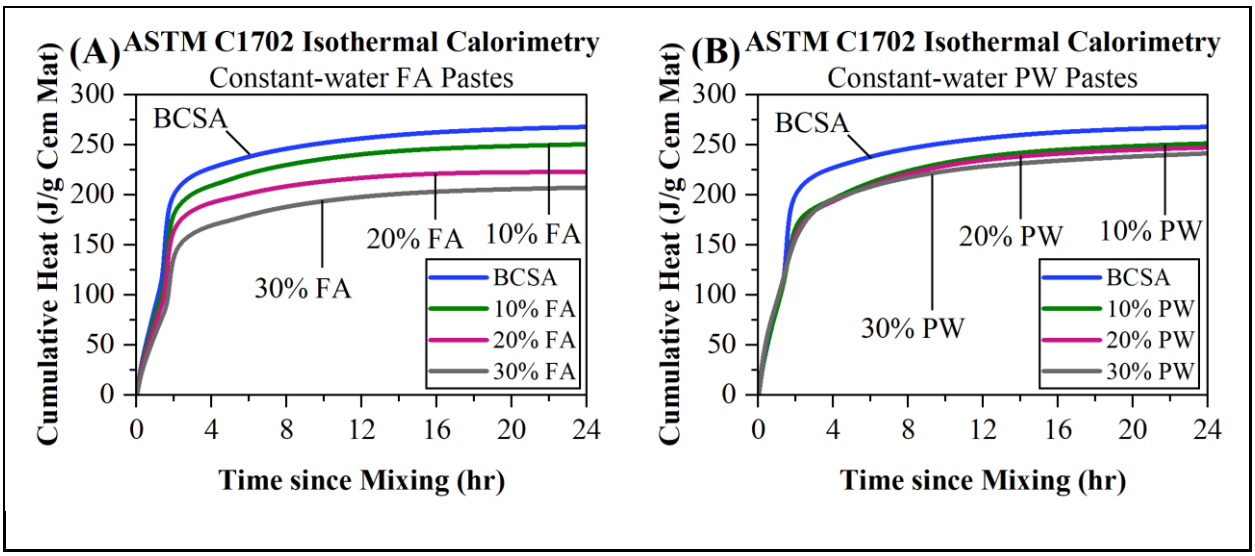

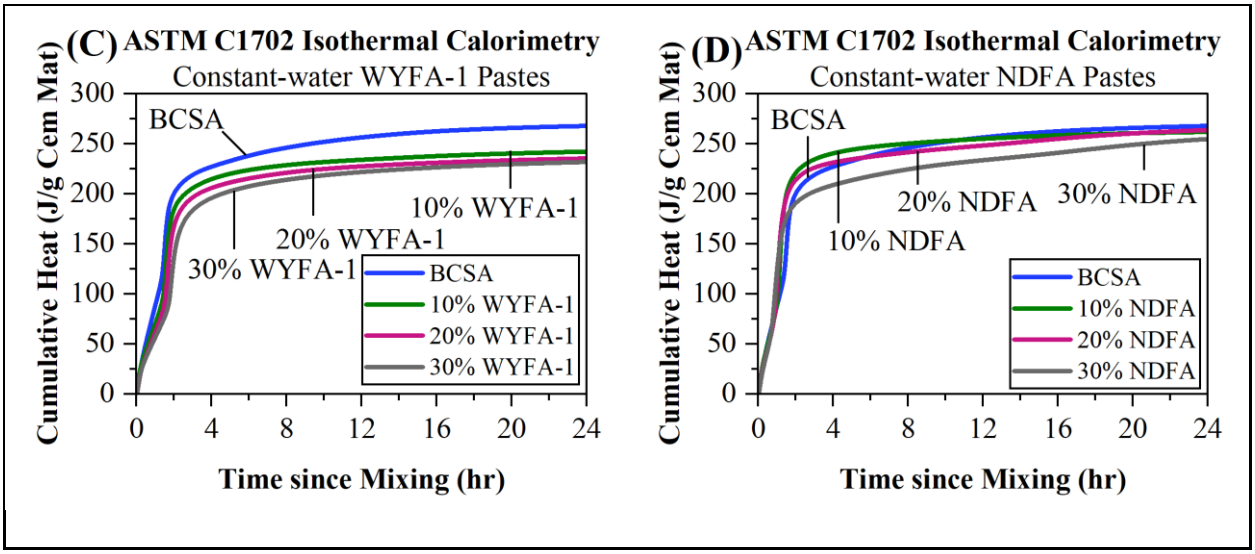

Figure 34: Cumulative heat release of pastes containing SCMs as a function of time, as measured via isothermal calorimetry up to 24 hours after mixing. A: FA pastes; B: PW pastes; C: WYFA-1 pastes; D: NDFA pastes. The same BCSA control data is shown in all four graphs.

All specimens showed a reduction in cumulative heat output with higher SCM content except those containing North Dakota fly ash. The 20% NDFA paste released more heat than the 10% NDFA paste by a narrow margin of 2 J/g. The reduction of cumulative heat from the 30% NDFA paste in comparison to the 20% NDFA paste may be due to the consumption of all BCSA reactants, or the depletion of water, limiting the extent of hydration within the paste. After 24hr of measurement, NDFA showed the highest degree of reactivity with BCSA under calorimetry out of all SCMs, having the highest cumulative heat output. The 24-hour heat output of all pastes is tabulated in Figure 35.

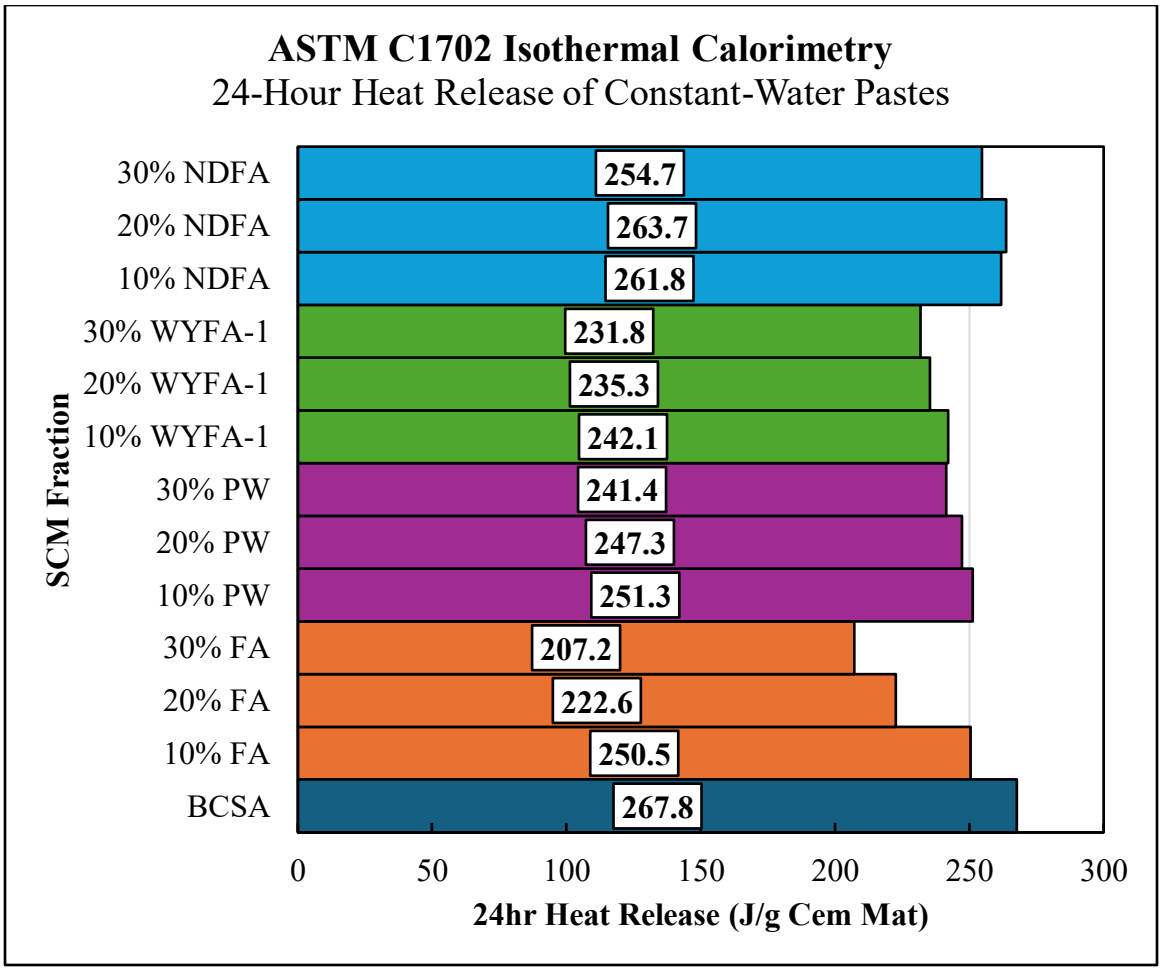

Figure 35: 24-hour cumulative heat release of all pastes under ASTM C1702 calorimetry

Importantly, class C fly ash seems to be the least reactive. Pastes made with class C fly ash showed the greatest reduction in cumulative heat release after 24hr, in contrast to those made with PW, WYFA-1, and NDFA.

4.6 Isothermal R^3 Calorimetry

The heat flow is shown as a function of time in Figure 36.

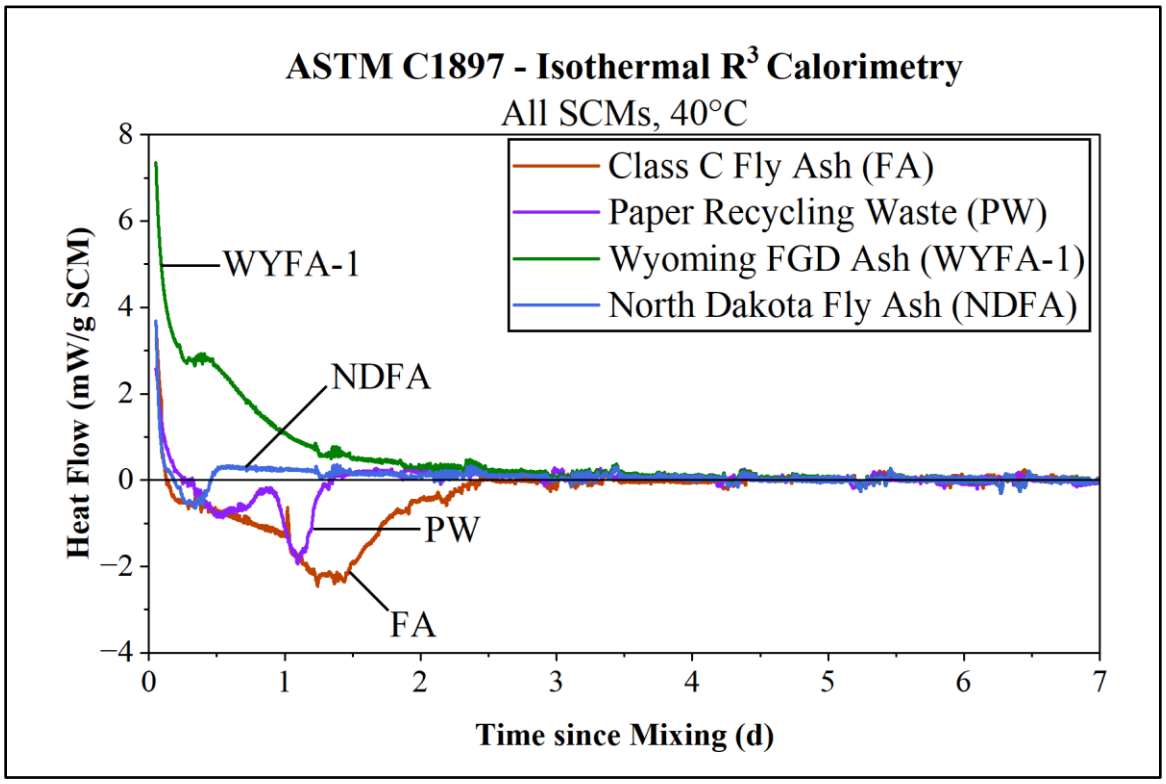

Figure 36: Isothermal R^3 calorimetry over one week. Heat flow as a function of time after 75min. Values were normalized with respect to specimen size by dividing by SCM weight.

As described in the Methods section, the heat flow was increased adjusted by a constant value for all four specimens such that it approached zero at the end of the test. The first 75 minutes of the measurements were removed, per ASTM C1897 guidelines. Wyoming FGD waste ash was the only SCM to consistently remain exothermic as its heat flow gradually decreased to zero. North Dakota fly ash alternated between endothermic and exothermic behavior. Paper recycling

waste and class C fly ash showed consistent endothermic behavior, except at the beginning of their tests.

The cumulative heat release for each SCM is shown as a function of time in Figure 37.

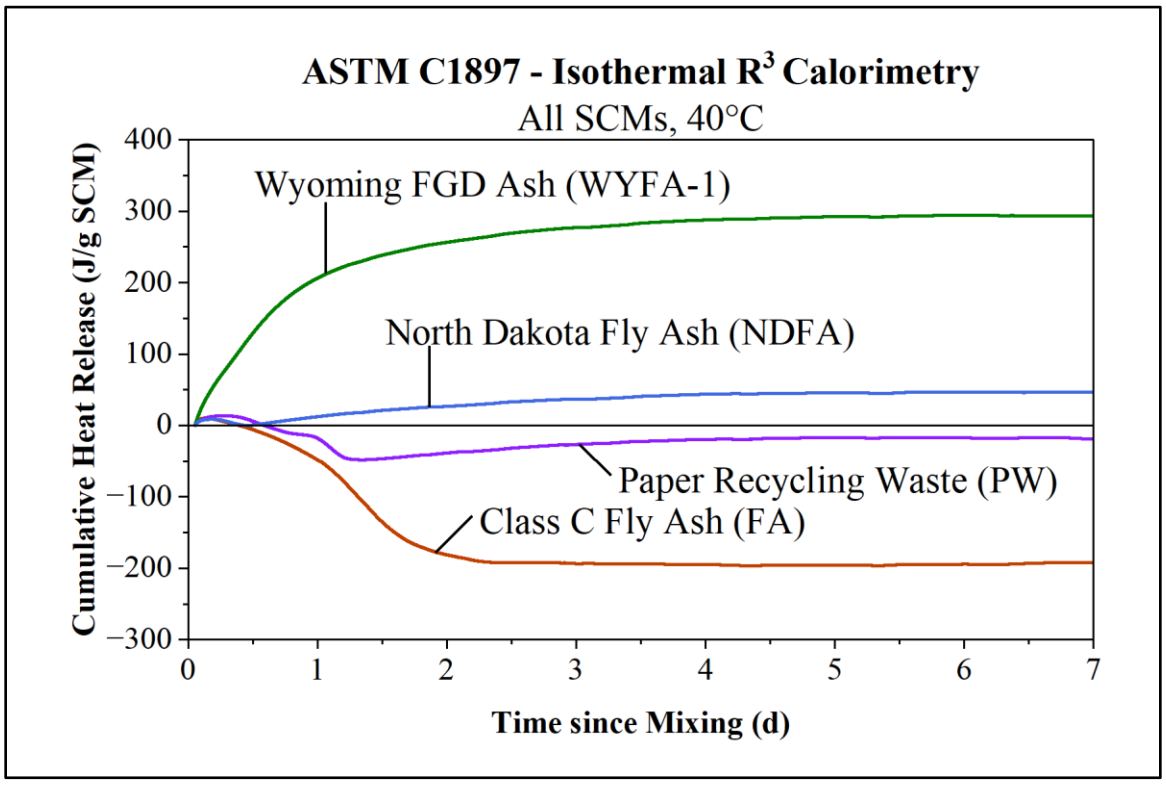

Figure 37: Isothermal R^3 calorimetry over one week. Cumulative heat as a function of time after 75min. Values were normalized with respect to specimen size by dividing by SCM weight.

The cumulative heat release of each SCM approached a constant value, because the heat flow curves were adjusted by a constant value such that they approached zero over time. The Wyoming and North Dakota SCMs were the only ones to remain exothermic with net positive heat release. Paper recycling waste and class C fly ash showed endothermic behavior, but class C fly ash was more endothermic.

Cumulative heat release values after three and seven days are tabulated in Figure 38.

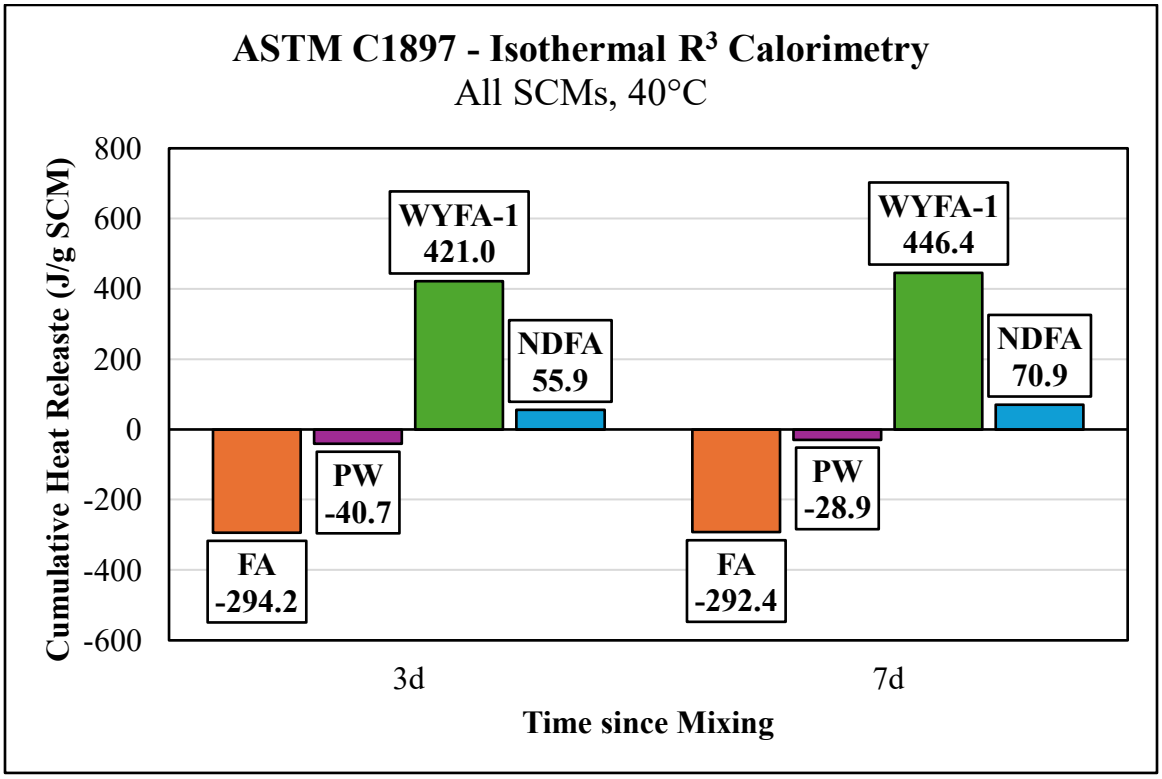

Figure 38: Isothermal R^3 calorimetry. Cumulative heat after three and seven days. Values were normalized with respect to specimen size by dividing by SCM weight.

The cumulative heat release values at three and seven days are quite similar for all four specimens. This is reflected in the fact that the heat flow curves are all near zero after three days, making any possible change very small. Between three and seven days after mixing, the FA specimen released +1.8 J/g SCM, the PW specimen released +11.8 J/g SCM, the WYFA-1 specimen released +25.4 J/g SCM, and the NDFA specimen released +15.0 J/g SCM. The average behavior across all specimens in this span of time was exothermic.

These results imply that WYFA-1 would perform the best as an SCM in OPC, followed by NDFA, PW, and FA, in that order.

4.7 Mortar Flow Testing

The water/cement ratios of constant-flow mortars are listed in Table 12; the water quantity for a constant-flow mortar is found by multiplying the water/cement ratio by the sum of the masses of BCSA and SCM, which is constant regardless of the SCM fraction.

Table 12: Water/cement ratios of constant-flow mortars (dimensionless)

SCM	SCM Weight Fraction	Constant-Flow Water/Cement Ratio	Flow at 50% Water/Cement
Control BCSA	-	0.524	89.5
Class C Fly Ash (FA)	10%	0.520	95.5
	20%	0.500	112.5
	30%	0.480	123
Paper Recycling Waste (PW)	10%	0.570	50
	20%	0.641	Dry, unmeasurable
	30%	0.701	Dry, unmeasurable
Wyoming FGD Waste Ash (WYFA-1)	10%	0.500	106
	20%	0.494	120.5
	30%	0.490	Unavailable, ran out of SCM
	10%	0.532	74.5

North Dakota Fly Ash (NDFA)	20%	0.556	43.5
	30%	0.584	Dry, unmeasurable

For all SCMs, an increase in water/cement ratio coincided with a decrease in flow at constant water, and vice versa. The PW specimens required the most water of all specimens to achieve constant flow and could not have their flow measured at constant water above 10% SCM content. This is likely due to a high presence of free lime within the SCM quickly reacting with most of the water added to the mortar, making the mix very dry. NDFA also degraded workability but not as strongly as PW. FA and WYFA-1 specimens both improved the workability of the mortars with higher SCM content. This is because the unreactive components of FA and WYFA-1 that do not consume water are round in shape as seen in SEM imaging.

4.8 Mortar Set Times

Set times of mortars were measured using a Vicat needle according to the ASTM C191 standard. The results are tabulated in Figure 39 and Figure 40. The lack of sample variance is a limitation of this data. The ASTM C191 standard provides values for the single-operator standard deviations of initial and final set times: the standard deviation for initial set is 12 minutes for an initial set between 49 and 202 minutes (between 5.9% and 24% of the measurement), and the standard deviation for final set is 20 minutes for a final set between 185 and 312 minutes (between 6.4% and 11% of the measurement). Unfortunately, these official values were not designed for cements like BCSA that set very quickly, and the time intervals do not overlap with those observed in this study. A rough estimate for standard deviation can be extrapolated using

the relative deviation: an initial set of 30 minutes corresponds to error between 1.8 and 7.3 minutes, and a final set time of 40 minutes corresponds to a standard deviation between 2.6 and 4.3 minutes.

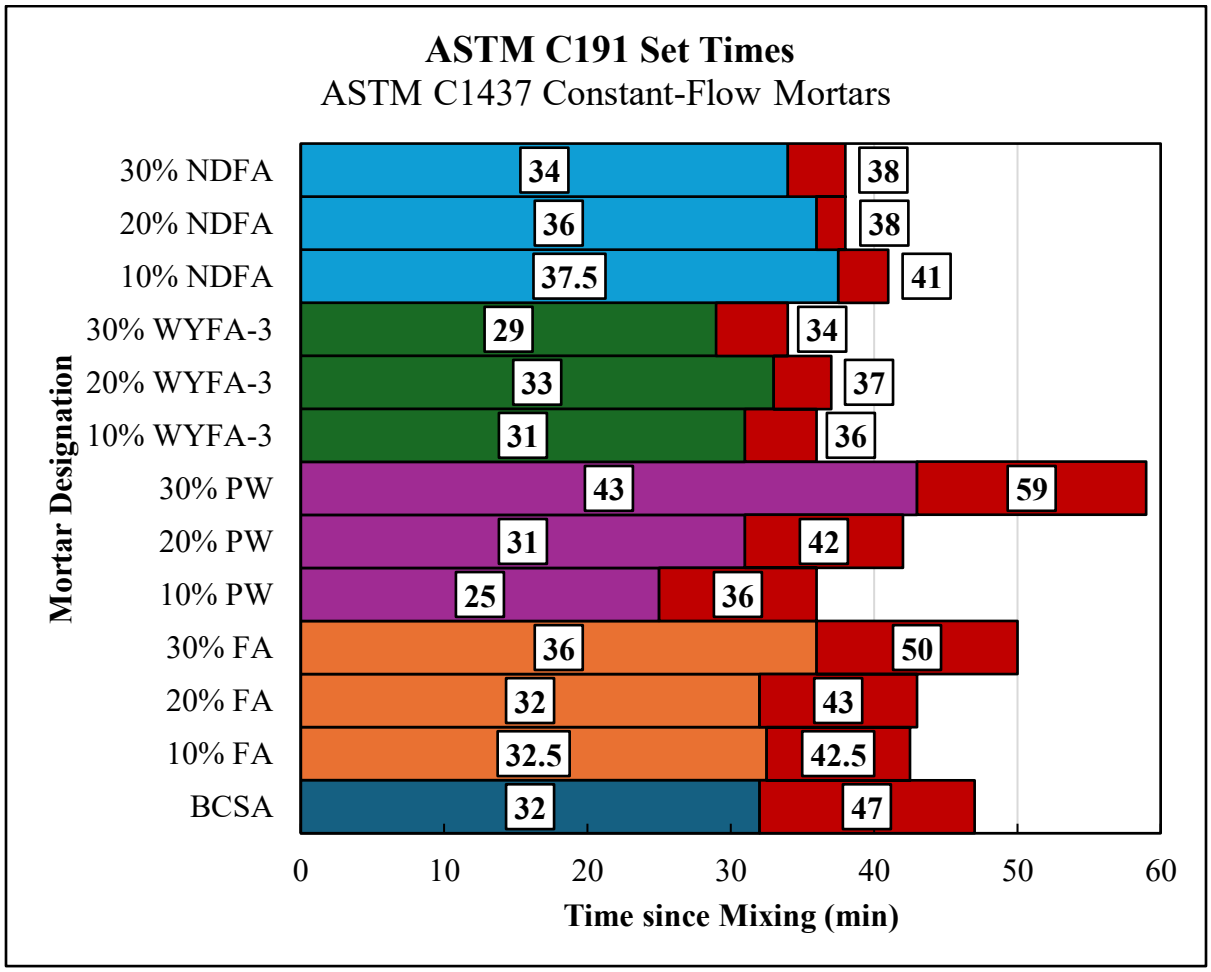

Figure 39: Set times of constant-flow mortars, measured with a Vicat needle per ASTM C191. The first segment indicates initial set time, while the second indicates final set time.

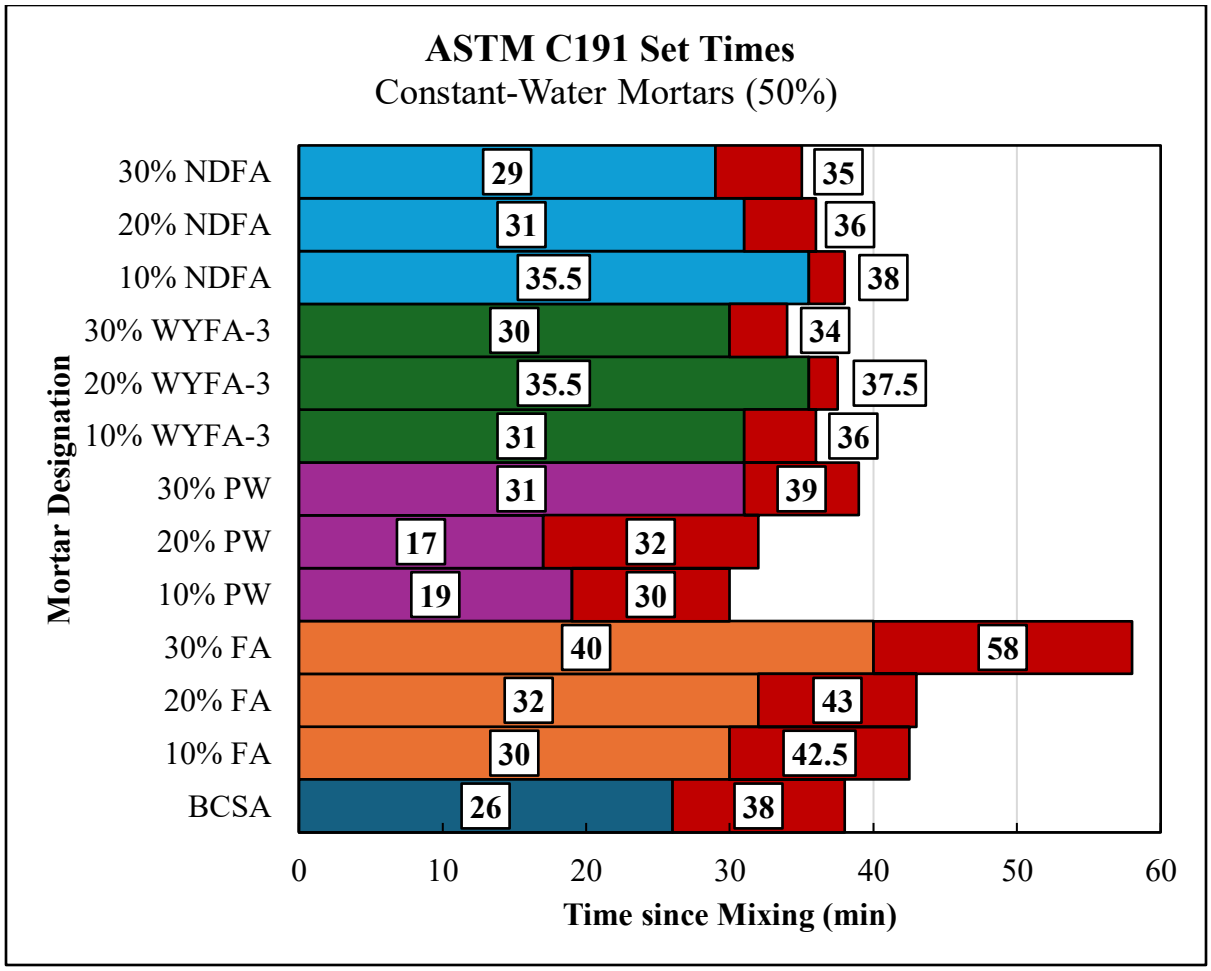

Figure 40: Set times of constant-water mortars, measured with a Vicat needle per ASTM C191. The first segment indicates initial set time, while the second indicates final set time.

Mortars made with less water generally had faster set times. BCSA had a set time of 32-47 minutes at constant flow, and 26-38 minutes at constant water. At constant-flow, FA had little effect on the set time below 30% SCM, in comparison to the control. At 30% SCM under constant flow, FA acted as a retarder, slowing the initial set time by 4 minutes and the final set time by 3 minutes. In the constant-water setting, FA also acted as a retarder, uniformly increasing the initial set time by 14 minutes and the final set time by 20 minutes.

PW showed mixed behavior as a retarder and an accelerator in both constant-water and constant-flow mortars. This may be due to flash-setting caused by free lime content in the SCM. At constant flow, it reduced the initial and final set times by 7 and 11 minutes at 10% mass replacement, had little effect on the set time at 20% mass replacement, and delayed the initial and final set times by 11 and 12 minutes at 30% mass replacement. Under constant flow, PW reduced set times at 10% and 20% SCM, and increased set times at 30% SCM.

WYFA-3 acted as a mild accelerator in both the constant-flow and constant-water mortars. However, in both settings the SCM showed a maximum in setting time at 20% SCM content. Its accelerating properties were stronger in constant-water mortars.

The NDFA SCM delayed initial set in both constant-water and constant-flow mortars. But its final set times were all still faster than that of control BCSA specimens. The set time of NDFA mortars had a maximum at 10% SCM content, which decreased with further SCM addition.

4.9 Mortar Length Change

The length change of all constant-flow mortars, according to ASTM C157 standard, are depicted as a function of time in Figure 41.

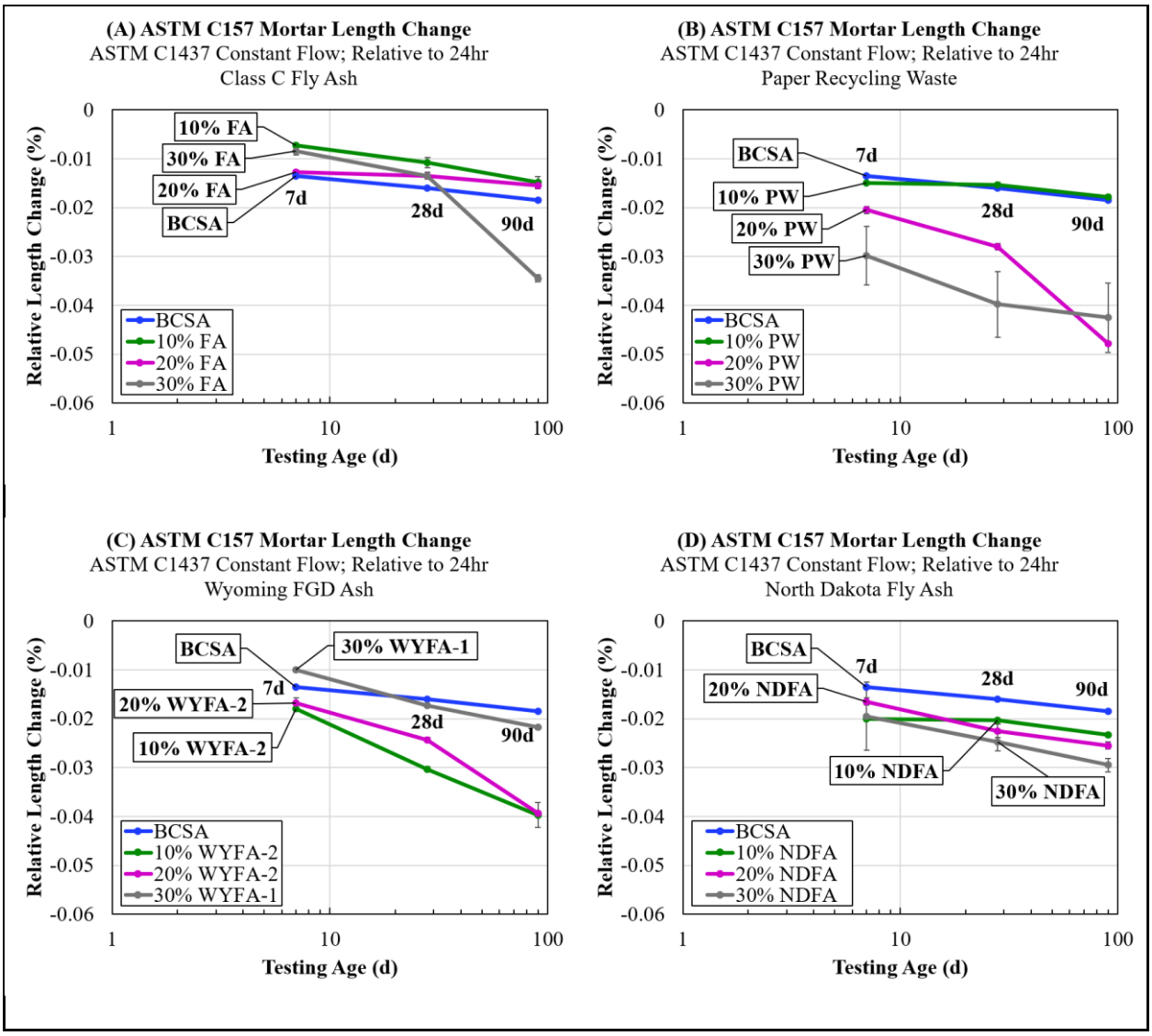

Figure 41: ASTM C157 length change of all constant-flow mortars. A: Class C fly ash; B: Paper recycling waste; C: Wyoming FGD waste ash (WYFA-1 & 2); D: North Dakota fly ash

Among WYFA specimens, the 30% WYFA-1 specimens showed the least change in length, in comparison to the WYFA-2 specimens. This may indicate a difference in microstructure due to the fact that the WYFA-2 SCM already contained ettringite in its raw form. The 20% and 30% PW specimens had the greatest length contraction across all mortars, possibly due to decreased

ettringite content in PW-containing specimens according to Rietveld analysis, in addition to the high water content of constant-flow PW mortars. Ordinarily the ettringite would absorb any free water, reducing drying shrinkage, but this effect is weakened due to the reduced crystallization of ettringite. The NDFA and FA specimens showed length change of similar degree, except in the 30% FA specimen, which suddenly showed significant contraction at ninety days of age.

The ASTM C157 length change data for constant-water mortars is depicted in Figure 42.

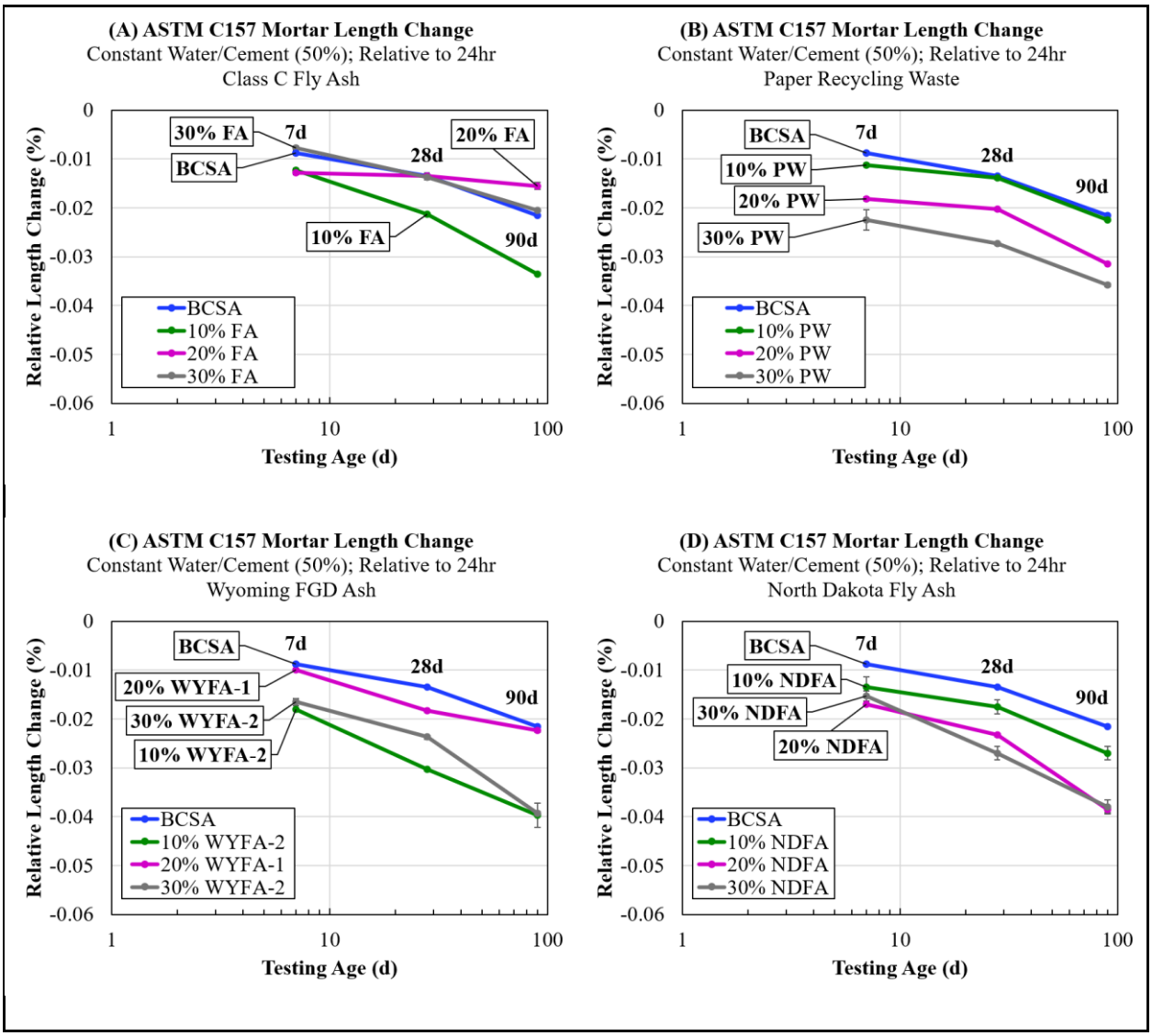

Figure 42: ASTM C157 length change of all constant-water mortars. A: Class C fly ash; B: Paper recycling waste; C: Wyoming FGD waste ash (WYFA-1 & 2); D: North Dakota fly ash

Like in the constant-flow specimens, WYFA-2 showed similar degrees of length contraction at both 10% and 30% SCM content, in contrast to that of WYFA-1, which showed less length contraction. The fact that this happened across both constant-water and constant-flow WYFA specimens shows that specimen variability is an important factor to take into account when designing cement mixes. All constant-water mortars showed similar degrees of length contraction except those mortars made with FA. FA constant-water mortars showed the least change in drying shrinkage in comparison to the control BCSA specimens.

4.10 Compressive Strength

Compressive strengths of mortars and BCSA/WYFA-3 concrete are included in this section.

4.10.1 Compressive Strength of Mortars

The strengths of constant-flow mortars, per ASTM C305, are recorded in Figure 43. Some of these constant-flow mortar strength values are averages of two strengths, instead of three, including: 10% FA at 90 days, 20% PW at 4 hours, 10% WYFA-1 at 28 days, 30% WYFA-1 at 28 and 90 days, and 30% NDFA at 7 and 28 days.

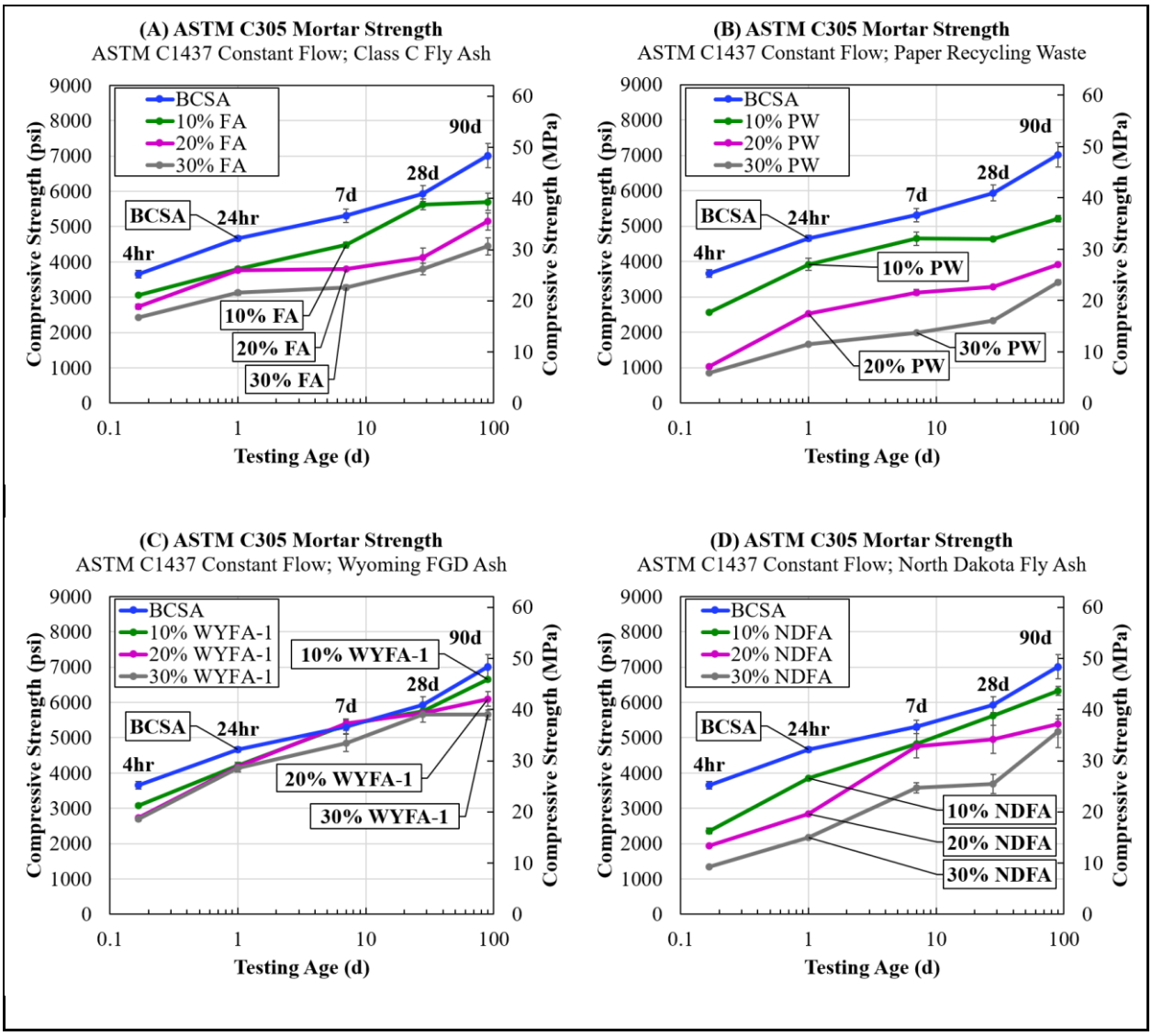

Figure 43: Compressive strength of constant-flow mortars. A: Mortars containing class C fly ash; B: Mortars containing paper recycling waste; C: Mortars containing Wyoming FGD waste ash (WYFA-1); D: Mortars containing North Dakota fly ash.

Among constant-flow mortars, those made with WYFA-1 performed the best, and those made with PW performed the worst. This is true at both early and later ages. Specimens made with 10% PW showed similar performance to those made with 10% FA, but FA mortars better

maintained their strength with higher SCM content in comparison to those made with PW. NDFA mortars performed well at later ages, but, in comparison to other SCMs, did not perform well at early ages. NDFA and FA mortars performed similarly at 10% and 30% SCM content, but NDFA outperformed FA at 20% SCM content, with a particularly pronounced effect at later ages.

Strengths of constant-water mortars are shown in Figure 44. The graph of strengths of WYFA mortars says that WYFA-1 and WYFA-3 were used because of limited availability of the WYFA-1 SCM. The strengths of 20% and 30% WYFA constant-water mortars measured at four hours and seven days were taken using the WYFA-3 SCM instead of the WYFA-1 SCM. Some of these constant-water mortar strength values are averages of two cubes, instead of three. This includes the following strengths: BCSA (control) at 4 hours, 30% PW at 24 hours, 30% WYFA-1 at 90 days, and 10% and 30% NDFA at 7 days.

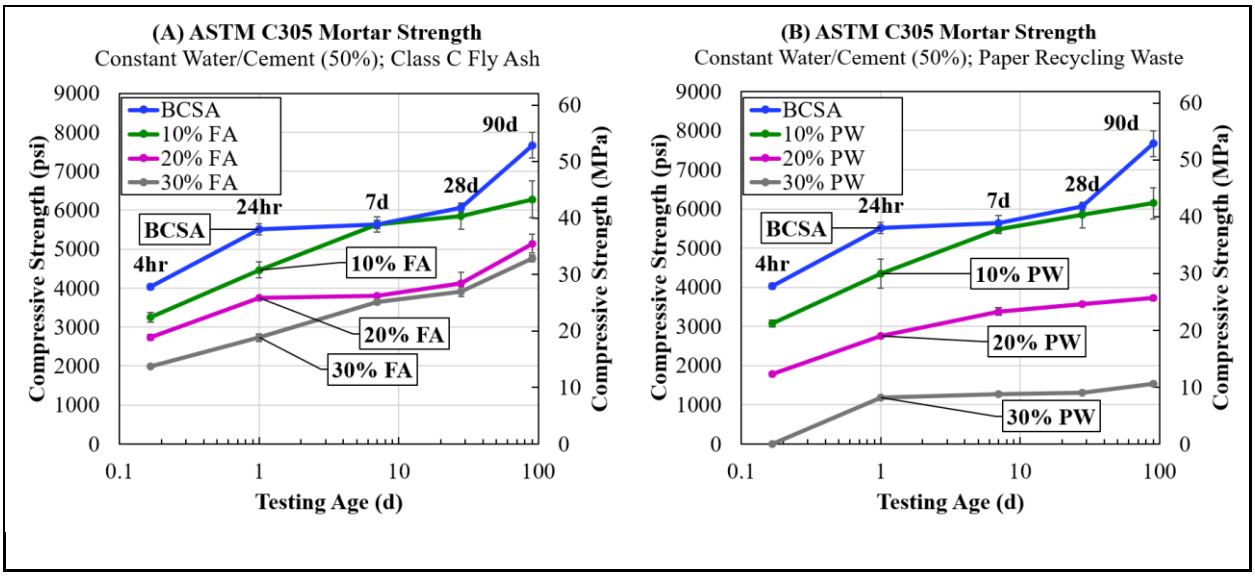

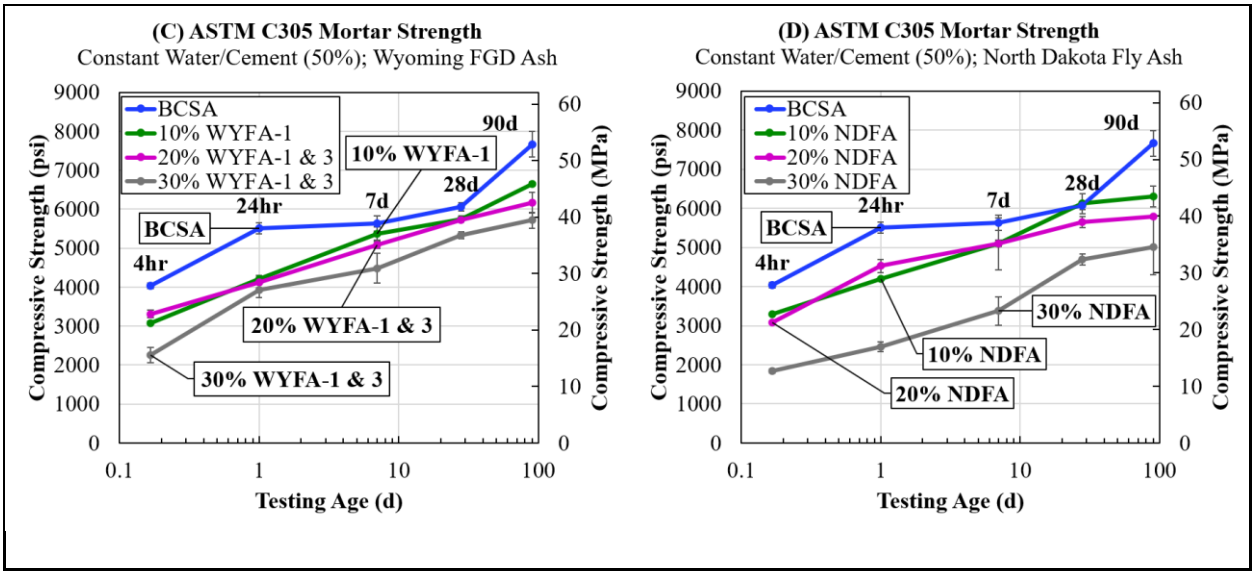

Figure 44: Compressive strength of constant-water mortars. A: Mortars containing class C fly ash; B: Mortars containing paper recycling waste; C: Mortars containing Wyoming FGD waste ash (WYFA-1 & WYFA-3); D: Mortars containing North Dakota fly ash

Among the constant-water mortars, those containing WYFA generally exhibited the highest strength. Like in the constant-flow mortars, the FA and NDFA SCMs performed similarly at 10% and 30% SCM content, but NDFA generally outperformed FA with higher strength values at 20% SCM content, especially at later ages. The 30% PW constant-water mortar with strength measured at four hours after mixing showed zero strength: the specimen failed so quickly that it could not have a strength value register in the display of the hydraulic press. PW generally had the greatest detrimental effect on the strength of constant-water mortars.

4.10.2 Compressive Strength of WYFA-3 Concrete

The compressive strength of 4”×8” concrete cylinders, as measured according to ASTM C39, are depicted in Figure 45. This includes observed values of BCSA/WYFA-3 concrete, as well as literature values for concrete made with Portland cement.

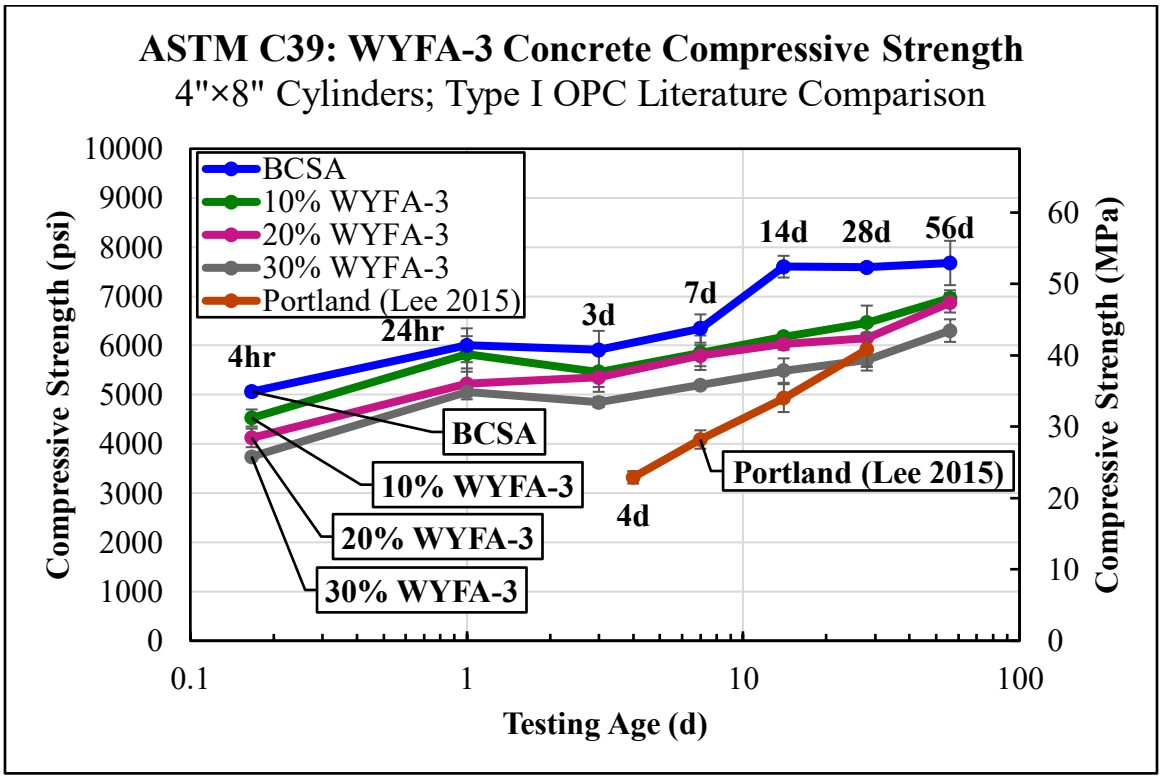

Figure 45: Compressive strengths of 4"×8" BCSA concrete cylinders containing WYFA-3 SCM. Reference values for Type I Portland cement from Lee, et al, are also included [54].

The strength of BCSA/WYFA-3 concrete seemingly decreased for higher SCM fractions. The strength seemed to be lower at three days than it was at 24hr for 10% and 30% SCM specimens not because of a decrease in real strength, but because there is no expected microstructural change in this time: the strength from ettringite would have already fully developed at 24hr,

while the hydration of belite would not measurably increase the strength until seven days after mixing. Therefore, the specimens tested at 24hr and three days were practically the same, and the apparent decrease in strength appeared due to natural variation.

Literature data from Portland cement is included for comparison [54]. The strength of concrete made with Portland cement did not match the strength of BCSA/WYFA-3 concrete until 28 days had passed since mixing. This shows the significant early strength that can be achieved with BCSA.

4.11 Global Warming Potential and Carbon Intensity

The Global Warming Potentials (GWPs) of all mortars and the volumetric emissions of the WYFA-3 concrete specimens are calculated in this section. These values show how intensely a mortar or concrete specimen emits CO_2 during its production. The carbon intensities of mortars and WYFA-3 concrete specimens are also calculated in this section by dividing the volumetric emissions of the concrete by its strength. The carbon intensity serves as a figure of merit: an ideal specimen will have low CO_2 emissions and high strength, and thus a low carbon intensity.

4.11.1 Global Warming Potentials of Mortars and Concrete

The GWP of a mortar is calculated by linearly interpolating the GWP of BCSA cement (673 kg CO_2-eq per metric ton of BCSA cement [5]) with the GWP of the SCM. All SCMs in this study are taken to have GWP values of zero. Thus, as an example, a mortar with 30% SCM by mass will have a GWP value that is 70% as large as that of unmodified BCSA cement. The GWP values of mortars are tabulated in Table 13 and are the same for both constant-flow and constant-

water mortars. GWP is a dimensionless quantity due to unit cancellation. The specimens with the highest SCM content had the lowest GWP values, owing to their reduced cement content.

Table 13: Global Warming Potentials of BCSA mortars with SCMs

Mortar Designation	Mortar GWP (kg CO_2-eq/kg cement)
100% BCSA	0.673
90% BCSA + 10% SCM	0.606
80% BCSA + 20% SCM	0.538
70% BCSA + 30% SCM	0.471

The GWP of concrete was calculated as a volumetric quantity: the equivalent CO_2 emissions per unit volume of concrete. The calculation is shown in Equation (7).

$$\text{GWP} = (1 - f)\left(0.673\frac{\text{kg } CO_2\text{-eq}}{\text{kg cement}}\right)\left(362.5\frac{\text{kg cement}}{\text{m}^3 \text{ concrete}}\right) \div 85\% \quad (7)$$

In the equation, f is the SCM weight fraction, being 0%, 10%, 20%, or 30%, depending on the mix design, and $(1 - f)$ is thus the BCSA weight fraction; 0.673, a dimensionless value, is the GWP of BCSA cement; and 362.5 is the assumed mass of cement used per cubic meter of concrete, measured in kg/m^3. The product of these values is divided by 85% to account for the carbon emissions of the remaining components of the concrete mix: it is assumed that 85% of concrete emissions are from the cement itself, and the remaining 15% of emissions come from all other components of the concrete. Quantifying the emissions of concrete made from Portland cement is useful for comparison. Portland cement has a GWP of 0.919 kg CO_2-equivalent per kg of cement produced [6]. Thus, using Equation (7) again, but replacing 0.673 with this value, the volumetric CO_2 release of concrete made with Portland cement is 392 kg CO_2-eq/m^3 concrete, or

661 lb CO_2-eq/yd^3 concrete. The emissions of Portland concrete and BCSA/WYFA-3 concrete are compared in Figure 46.

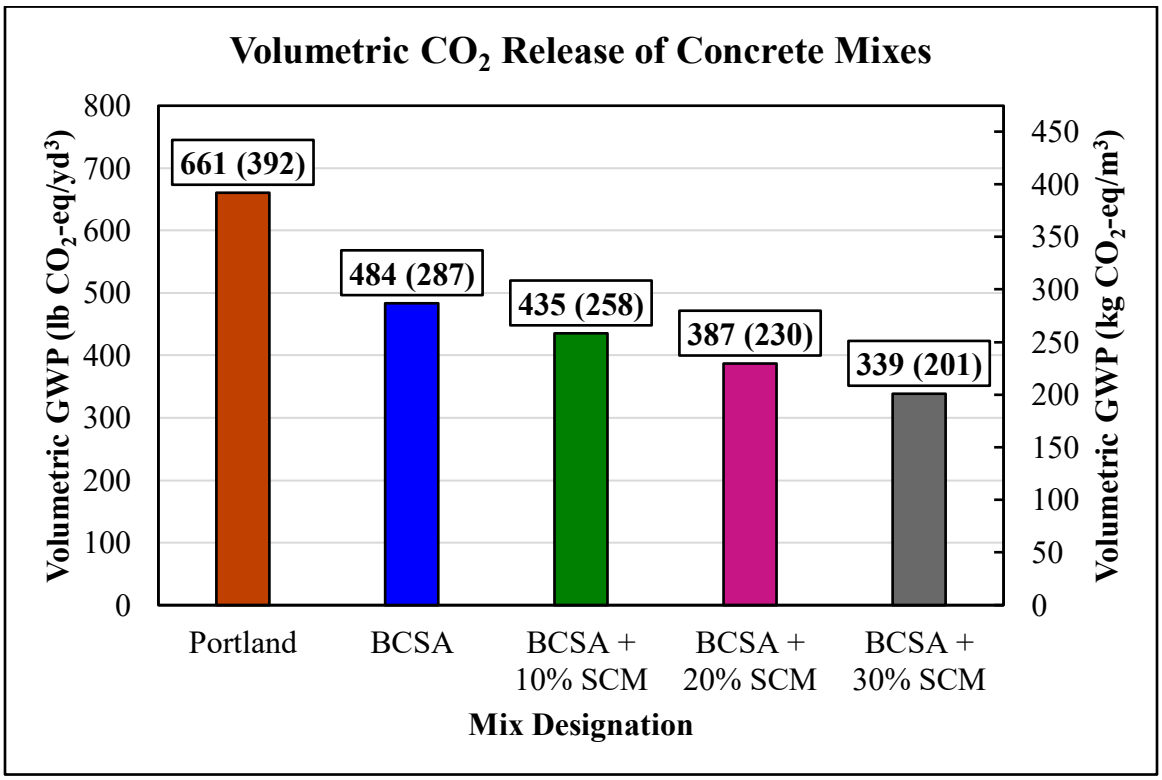

Figure 46: Comparison of CO_2 emissions across Portland and BCSA/WYFA-3 concrete mixes. Emissions of Portland cement calculated with GWP from Portland Cement Association [6].

Under this paradigm, BCSA concrete can emit as little as 51.3% of the carbon released by concrete made using Portland cement, by replacing 30% of the cementitious mass with zero-GWP SCM. This percentage could be even lower for greater SCM fractions. These values are independent of the SCM used or the concrete's strength and depend solely on the type of cement used and its SCM fraction.

4.11.2 Carbon Intensity of Mortars

A mortar's carbon intensity was calculated by dividing its GWP by its ASTM C109 compressive strength.

The carbon intensities of constant-flow mortars are depicted in Figure 47. These values are calculated using the strengths from Figure 43 and the GWPs from Table 13.

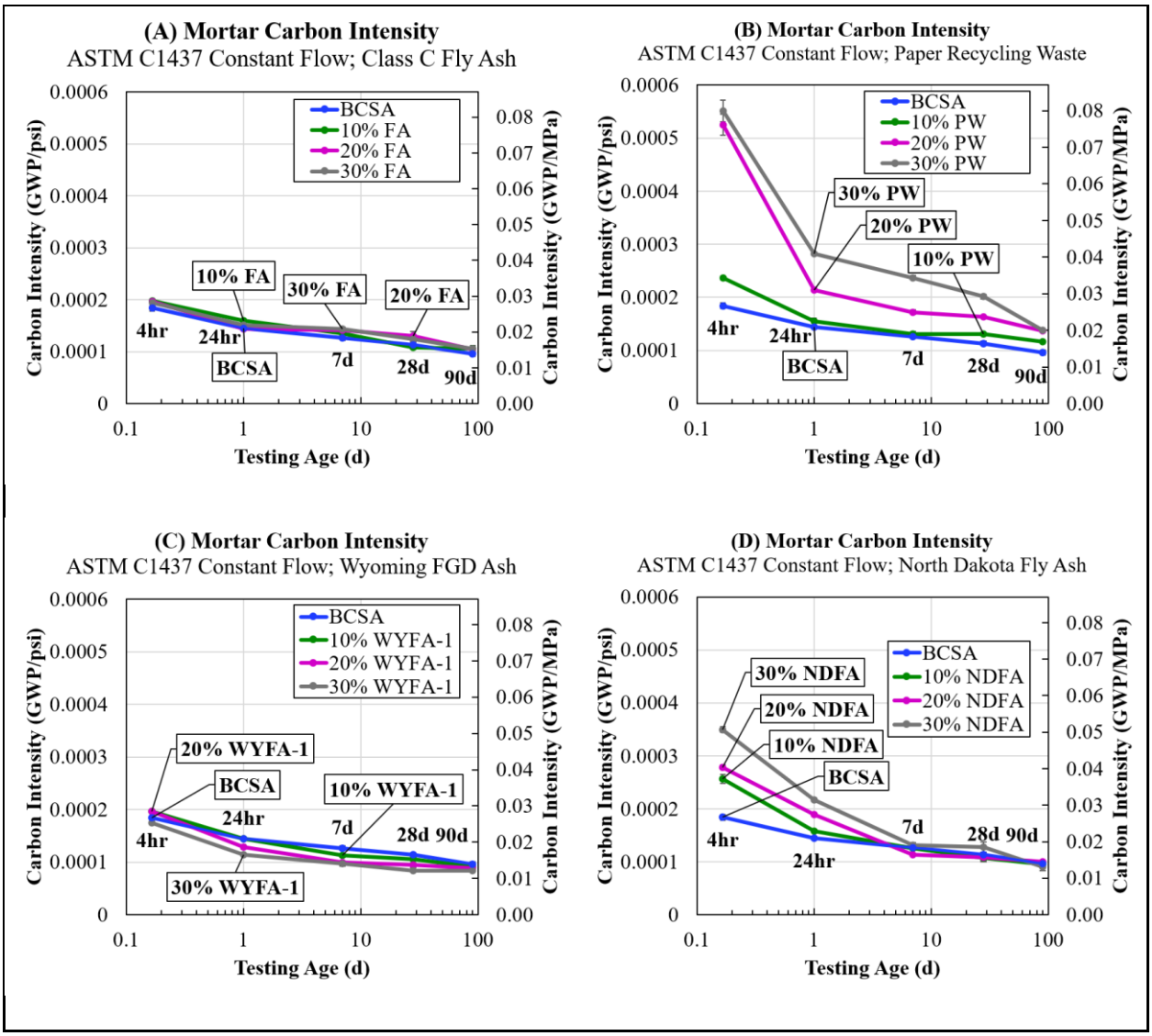

Figure 47: Carbon intensities of constant-flow mortars. A: Mortars containing class C fly ash; B: Mortars containing paper recycling waste; C: Mortars containing Wyoming FGD waste ash (WYFA-1); D: Mortars containing North Dakota fly ash

Among the constant-flow mortars, those made with WYFA-1 were the only ones to have the carbon intensity be consistently lower than that of the control. FA mortars performed similarly to WYFA-1, but its carbon intensities were generally outperformed by the control. NDFA mortars were much worse than the control at early ages, but maintained a carbon intensity similar to that of BCSA at ninety days of age. PW mortars were consistently outperformed by the control values, with higher SCM content making the carbon intensity even higher. This is because of the intense deleterious effect PW had on the strength of the mortars.

Carbon intensities of constant-water mortars are depicted in Figure 48. These values were calculated using the strengths shown in Figure 44 and the GWP values from Table 13. WYFA-3 was used in the 20% and 30% mortars tested at four hours and seven days.

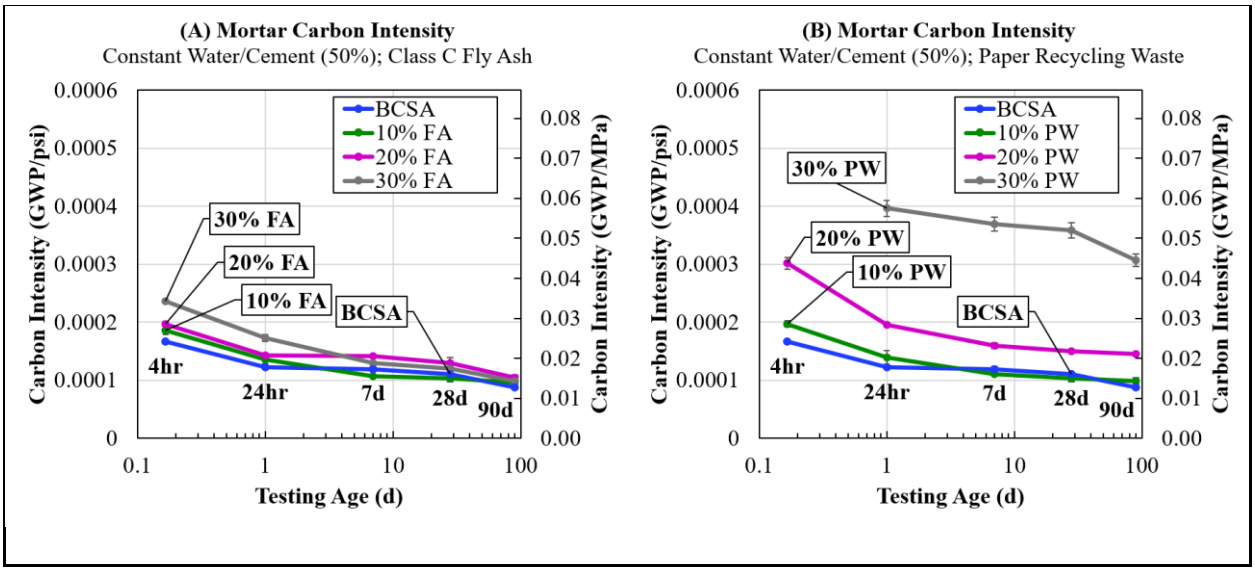

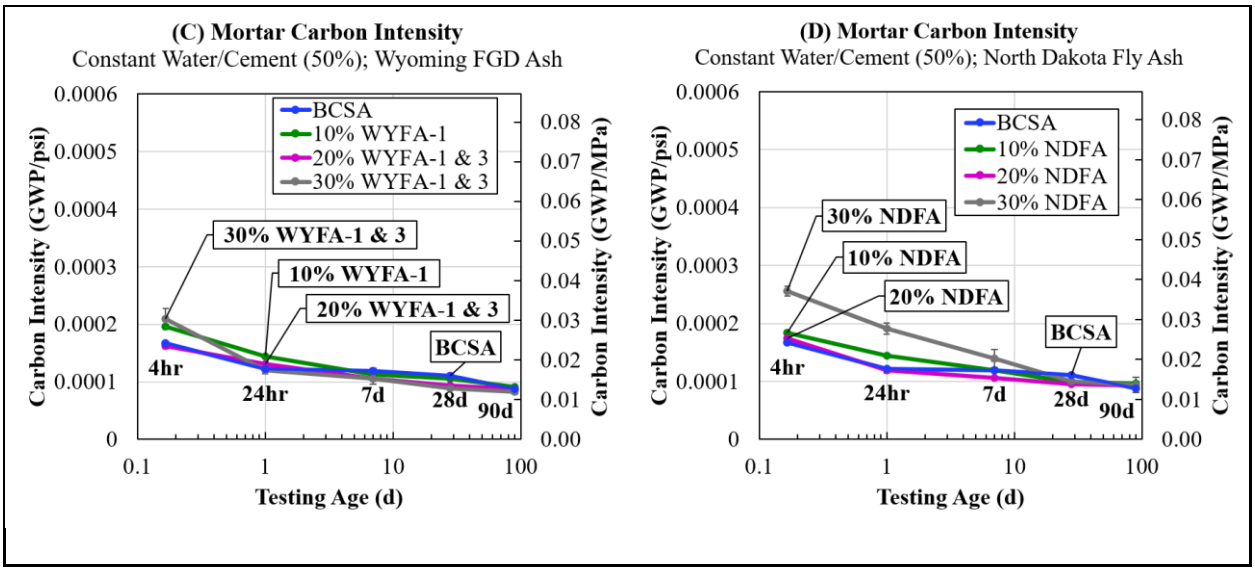

Figure 48: Carbon intensities of constant-water mortars. A: Mortars containing class C fly ash; B: mortars containing paper recycling waste; C: Mortars containing Wyoming FGD waste ash (WYFA-1 & WYFA-3); D: Mortars containing North Dakota fly ash

Like in the constant-flow mortars, WYFA had the best performance in constant-water mortars, and generally outperformed the control, especially after seven days of age. The FA and NDFA mortars had a similar degree of performance within the constant-water mortars, but NDFA mortars slightly outperformed FA at later ages. Constant-water mortars made with PW had the generally highest carbon intensity across all specimens, in a similar fashion to the constant-flow mortars. The 30% PW mortars do not have a carbon intensity at 4hr because the strength at that time was zero, resulting in an undefined carbon intensity.

4.11.3 Carbon Intensity of WYFA-3 Concrete

The carbon intensity of concrete was calculated by dividing the volumetric emissions of the concrete, shown in Figure 46, by the ASTM C39 strength of the concrete at each age, shown in Figure 45. These carbon intensity values are plotted in Figure 49.

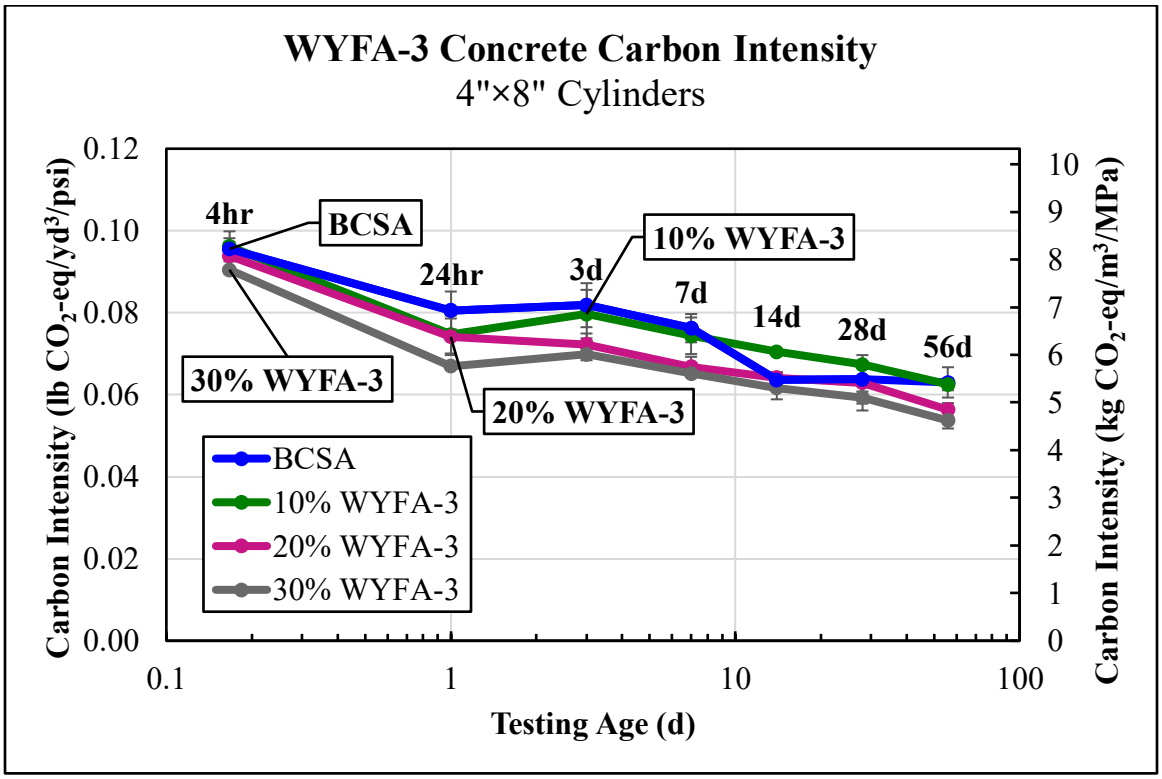

Figure 49: Carbon intensity of BCSA/WYFA-3 concrete specimens as a function of time.

Specimens containing 30% WYFA-3 outperformed the BCSA control specimen across the entire duration of testing: the carbon intensity of 30% WYFA-3 concrete was lower than that of BCSA at all ages. 20% WYFA-3 concrete outperformed at nearly all ages, except at 14 days by a small margin. 10% WYFA-3 concrete outperformed BCSA concrete at all ages except 14 days and 28 days. This is because, as seen in Figure 45, the 10% WYFA-3 specimen had a delay in its

strength development in comparison to BCSA at 14 days after mixing, and this gap later decreased as BCSA concrete's strength stayed relatively constant while the strength of WYFA-3 concrete continued to develop up to 56 days. Specimens containing more SCM outperformed those specimens with less SCM, showing that, to a point, WYFA-3 can effectively reduce the carbon intensity of BCSA concrete.

Using literature values for the strength of Portland concrete [54] and the volumetric emissions of Portland concrete calculated with data from the Portland Cement Association [6] shown in Figure 46, reference values for the carbon intensity of Portland concrete were calculated for comparison with the carbon intensity of BCSA/WYFA-3 concrete. These OPC carbon intensity values are shown alongside the BCSA/WYFA-3 carbon intensity values in Figure 50.

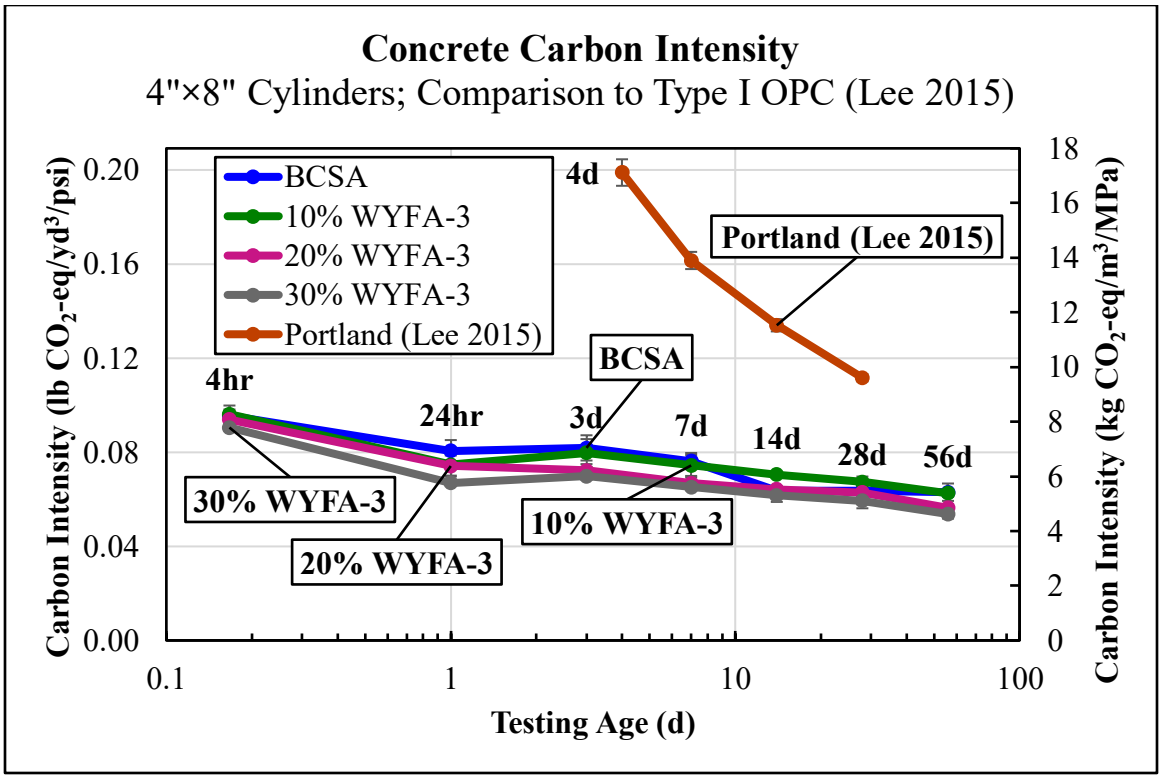

Figure 50: Carbon intensity of BCSA/WYFA-3 concrete, with carbon intensity of Portland concrete. Carbon intensity calculated using strength by Lee, et al, and GWP by Portland Cement Association [54, 6].

The carbon intensity of all BCSA/WYFA-3 concrete specimens is far below the carbon intensity of Portland concrete at all ages. Even though Portland concrete matches the strength of BCSA/WYFA-3 concrete at 28 days of age, the amount of CO_2 Portland concrete emits (661 lb/yd^3) is significantly higher than what BCSA concrete emits (484 lb/yd^3). Because carbon intensity is proportional to CO_2 emitted, and strength remained comparable across specimens, the carbon intensity was significantly higher in OPC.

4.12 Tabulation of Selected Observed Quantities in Mortars

Some properties of constant-water mortars are summarized in Table 14 for ease of comparison. In the last column of the table, "CI" is an abbreviation for carbon intensity.

Table 14: Select observed quantities of constant-water mortars

Mortar Type	Flow	Initial & Final Set Times (min)	90d Length Change	GWP	90d CI (psi^{-1}, MPa^{-1})
BCSA	89.5	32-47	-0.022%	0.673	8.78×10^{-5}, 1.27×10^{-2}
30% FA	123	36-50	-0.021%	0.471	9.90×10^{-5}, 1.44×10^{-2}
30% PW	-	43-59	-0.036%	0.471	3.07×10^{-4}, 4.45×10^{-2}
30% WYFA	N/A	29-34	-0.039%	0.471	8.24×10^{-5}, 1.20×10^{-2}
30% NDFA	-	34-38	-0.038%	0.471	9.39×10^{-5}, 1.36×10^{-2}

Table 15 contains the same set of values as observed in constant-flow mortars. The necessary water/cement ratio to achieve constant flow is written in the table instead of the flow at constant water.

Table 15: Select observed quantities of constant-flow mortars

Mortar Type	Water/Cement	Initial & Final Set Times (min)	90d Length Change	GWP	90d CI (psi^{-1}, MPa^{-1})
BCSA	0.524	32-47	-0.019%	0.673	9.60×10^{-5}, 1.39×10^{-2}
30% FA	0.480	36-50	-0.035%	0.471	1.06×10^{-4}, 1.54×10^{-2}
30% PW	0.701	43-59	-0.043%	0.471	1.38×10^{-4}, 2.00×10^{-2}
30% WYFA	0.490	29-34	-0.022%	0.471	8.33×10^{-5}, 1.21×10^{-2}
30% NDFA	0.584	34-38	-0.030%	0.471	9.10×10^{-5}, 1.32×10^{-2}

Early and late strengths of high-SCM mortars are tabulated in Table 16.

Table 16: 4hr & 90d strengths of control mortars & 30% SCM mortars

Mortar Type	Constant-Water 4hr Strength (psi, MPa)	Constant-Flow 4hr Strength (psi, MPa)	Constant-Water 90d Strength (psi, MPa)	Constant-Flow 90d Strength (psi, MPa)
BCSA	4034, 27.81	3658, 25.22	7664, 52.84	7008, 48.32
30% FA	1994, 13.75	2426, 16.73	4760, 32.82	4441, 30.62
30% PW	-	854, 5.89	1533, 10.57	3414, 23.54
30% WYFA	2256, 15.55	2690, 18.55	5719, 39.43	5656, 39.00
30% NDFA	1841, 12.69	1347, 9.285	5017, 34.59	5179, 35.71

5. Conclusions

5.1 Class C Fly Ash

Fly ash may receive a class C designation per the ASTM C618 standard due to elevated sulfate content; lower-sulfate fly ash is designated as class F. The classification of this SCM under the ASTM C618 standard may permit better reproducibility between studies. Due to its high sulfate content, class C fly ash (FA) is generally unacceptable for use as an SCM in OPC. However, due to the difference in chemistry and sulfate balance between BCSA and OPC, class C fly ash can be used in substantial quantities in BCSA without incurring significant detriment to early or late strength in mortars, as observed in this study. Class C fly ash is not pozzolanic in the BCSA system due to BCSA's lack of necessary portlandite for pozzolanic reactions to take place. FA was tested using R^3 isothermal calorimetry as a proxy for the SCM's performance in OPC: the SCM showed strong endothermic activity, confirming the SCM likely does not perform well in OPC. Within mortars, the addition of FA improved workability: less water was needed to maintain constant flow, and the flow measured using constant water increased. SEM micrographs showed the FA particles were spherical, improving their microscopic packing ability. This shape explains the improvement in mortar workability and may mitigate the loss of compressive strength. As observed under SEM, ettringite development in FA pastes proceeded unremarkably in comparison to the control BCSA specimens. According to DTG data of cement pastes, the addition of FA to BCSA limited the crystallization of ettringite, which has negative implications for the impact of FA on the early strength of BCSA mortars. Rietveld analysis of BCSA pastes containing FA, in contrast, did not show any significant change in ettringite crystallization with the addition of FA to pastes. Rietveld analysis showed some crystallization of stratlingite in FA pastes between 7 and 28 days after mixing, when 30% FA was used by mass. This most likely

formed as a product of a reaction between the AH_3 of the cement and the silica of the SCM. XRD and XRF data showed that the SCM contained high quantities of silica that cannot react with BCSA. This contributed to the slight reduction in drying shrinkage observed in mortars: the inert components of the SCM, as well as the reduced need for water in FA mortars, limited the degree of length change within FA mortar specimens. The substantial inert content of FA significantly affected heat release in FA pastes under calorimetry: in addition to reducing the intensity of the main exothermic peak, which corresponds to interference with ye'elimite reacting to form ettringite, class C fly ash also slightly delayed the onset of the exothermic peak due to its inert silica content. This correlates with the observed set delay in FA mortars. Mortars made with FA showed acceptable compressive strength, with the greatest decrease in strength occurring between 10% SCM and 20% SCM mortars, and with greatest effect at 28 days after mixing. Class C fly ash did not reduce the carbon intensity of mortars; it instead maintained carbon intensity values relatively close to those of the control specimens at all ages. Despite the carbon intensity not decreasing with the addition of FA, the use of FA remains beneficial due to its reduction in mortar GWP. The substantial inert silica content of class C fly ash explains its behavior as an SCM in BCSA. Because silica does not react in the presence of water, all hydration mechanisms were chemically inhibited by FA. This delayed and minimized heat evolution, ettringite crystallization, and C-S-H precipitation. At a macroscopic scale, reaction interference contributed to set delays and strength reduction, but the inert content may have simultaneously limited the degree of drying shrinkage in comparison to other SCMs.

5.2 Paper Recycling Waste

Paper recycling waste (PW) is an unregulated industrial by-product, not defined by any standard such as the ASTM C618 standard used for fly ash. The lack of regulation presents difficulties for reproduction of the effects of PW as an SCM. XRF data showed that the SCM contained high quantities of calcium oxide, likely corresponding to free lime, which matched XRD data of the SCM. The high free lime content of PW necessitated a high amount of water to achieve constant workability in mortars per the ASTM C1437 standard. Lime content reduced workability in constant-water PW mortars so strongly that extreme dryness entirely prevented flow measurement at 20% and 30% SCM. For the same reason, the 30% PW constant-water mortar did not have any compressive strength at four hours. DTG data as well as Rietveld refinement showed that PW reduced the crystallization of ettringite in BCSA pastes to a similar degree as class C fly ash. Reduced ettringite crystallization and the high water content of PW mortars effected the relatively high degree of observed drying shrinkage. Pastes containing PW showed evidence of stratlingite forming between 7 and 28 days after mixing, according to Rietveld refinement and DTG data, and DTG data also showed a reduction in AH_3 content. As sulfates depleted in the cement system, belite may have begun to react with AH_3 and water to form stratlingite, as written in Equation (3). Therefore, in BCSA/PW specimens, belite may preferentially form stratlingite in place of C-S-H as it hydrates, reducing the maximum possible durability at later ages. The PW SCM showed mixed behavior as a set retarder and accelerator depending on the fraction used—flash-setting took place in 10% PW mortars with both constant flow and constant water, but in 30% PW mortars the SCM acted as a retarder. The SCM may delay setting due to interference with ye'elimite hydration and its subsequent production of ettringite. Under isothermal calorimetry of BCSA cement pastes, addition of PW caused the

primary exothermic peak to strongly decrease in intensity, but the initial dissolution peak simultaneously intensified, mitigating the difference in cumulative heat release in PW pastes but resulting in a net decrease in reactivity. This corresponds to reduced ettringite crystallization due to insufficient sulfur or alumina in PW. SEM images of pastes made with PW showed that ettringite needles may have grown thinner and shorter than in control pastes. Under SEM imaging, the PW particles themselves were much larger than the particles of any other SCM. The PW mortars showed a very sharp decrease in strength at four hours due to the inhibited hydration of ye'elimite at early ages. They generally exhibited lower compressive strength in comparison to mortars made with all other SCMs. Due to their low strength, the carbon intensity of PW mortars was also generally higher than that of all other mortars, including control specimens. However, paper recycling waste, like all other SCMs studied, reduced the GWP of cement by up to 30%. Under R^3 isothermal calorimetry, paper recycling waste showed mild endothermic behavior, indicating that its use in OPC is likely ill-advised. The behavior of PW as an SCM can broadly be attributed to high free lime content: the fast hydration of lime limited the amount of water available to react with belite and ye'elimite, effecting microstructural change in the form of reduced ettringite and C-S-H content. The SCM caused sulfate depletion in the cement as evidenced by stratlingite formation and AH_3 reduction, further inhibiting the C-S-H hydration pathway. These are the mechanisms by which strength in PW mortars decreased. Length change can also be attributed to free lime: high water content in constant-flow PW mortars caused extensive drying shrinkage, while constant-water PW mortars were exceptionally dry and shrank much less. Free lime hydration contributed to flash setting in lower-PW-content mortars, but constant-flow PW mortars with 30% PW exhibited set delay due to excessive water content

interfering with reaction kinetics, and 30% PW constant-water mortars did so due to water depletion inhibiting solidification.

5.3 Wyoming FGD Waste Ash

The composition of flue gas desulphurization products is not regulated according to any ASTM standard, which may negatively impact reproducibility in future studies. Three samples of FGD waste ash from the Wyoming test reactor, abbreviated as WYFA-1, WYFA-2, and WYFA-3, were observed as an SCM in BCSA. The WYFA SCM was rich in calcium oxide, silica, and sulfate per XRF measurement; all three samples were of similar chemical constitution. WYFA-2 and WYFA-3 contained solidified hydrated nodules while WYFA-1 did not, likely due to differences in storage and handling between the samples before shipment and possible exposure to humidity. This difference emphasizes the importance of proper SCM storage for the purpose of reproducibility. Hydration of the SCM caused the LOI of WYFA-2 and WYFA-3 to be much higher than that of WYFA-1. This was resolved by heating WYFA-3 in an oven at 150°C for several hours, decomposing any ettringite within the SCM and making WYFA-3 practically identical to WYFA-1. As a result of this treatment, XRD scans showed no peaks belonging to ettringite in WYFA-3, which were otherwise present in WYFA-2. Due to the heat treatment, the LOI of WYFA-3 also decreased to a value more closely matching that of WYFA-1. The crystallization of ettringite within WYFA-2 and WYFA-3, even in the absence of ye'elimite from cement, indicates that the SCM should not strongly interfere with early hydration in BCSA. Results from DTG and Rietveld refinement matched this conclusion: the addition of WYFA-1 to BCSA pastes had a negligible effect on the crystallization of ettringite, even in those pastes

containing as much as 30% WYFA-1. Pastes made with WYFA-1 showed some evidence of wollastonite formation under DTG. SEM images of WYFA-1 pastes showed unremarkable ettringite development, matching DTG and Rietveld evidence that WYFA-1 does not affect ettringite production. WYFA-2 mortars consistently showed a higher degree of drying shrinkage in comparison to WYFA-1 mortars; the higher LOI of WYFA-2 in comparison to WYFA-1 may have limited the extent of hydration, increasing the amount of residual free water and elevating the degree of length change. The WYFA-1 mortars showed a similar degree of length contraction to control specimens even in constant-flow mortars containing 30% WYFA-1. Heat release in cement pastes was slightly delayed under calorimetry; the primary exothermic peak showed an increase in intensity in the paste containing 10% WYFA-1, but the intensity decreased uniformly thereafter with higher SCM fractions. The greatest decrease in cumulative heat release of WYFA-1 pastes took place between the 0% and 10% SCM specimens; higher-SCM-content pastes showed similar cumulative heat development. Isothermal calorimetry of WYFA-1 under the R^3 specification showed the highest cumulative heat release out of all SCMs tested, implying the SCM may react favorably in OPC blends, but this demands further study due to the high sulfur content of the SCM. The effect of WYFA-1 on workability in mortars was quantified: adding the SCM reduced the amount of water in mortars necessary for constant flow, and with constant water the flow of WYFA-1 mortars increased with SCM content. The flow at constant water for 20% and 30% WYFA-1 mortars could not be measured due to insufficient available quantities of the SCM. WYFA-3 reduced the final set time in all specimens but showed mixed behavior as a retarder and accelerator of the initial set. WYFA-1 and WYFA-3 mortars showed the highest compressive strength among all mortars made with SCMs. The WYFA SCM reduced carbon intensity in mortars in comparison to the control specimens, which generally was not the

case among most mortars made with the other three SCMs of this study. Because of this improvement in carbon intensity, WYFA-3 was selected for further examination in BCSA concrete. The 30% BCSA/WYFA-3 concrete specimens showed a reduction in compressive strength by roughly 1500psi (10MPa) at 4 hours and at 56 days after mixing; the control BCSA concrete approached its final observed strength at 14 days before plateauing, while the BCSA/WYFA-3 specimens continued to develop their strength. The volumetric CO_2 emissions of concrete made with 30% WYFA-3 was 51.3% as large as that of OPC concrete. This value holds true for any BCSA concrete with 30% SCM content, but BCSA/WYFA-3 concrete was the only concrete made in this study. Because the addition of the SCM only minimally reduced the strength of the concrete, the carbon intensity of BCSA/WYFA-3 concrete was lower than that of the control specimens for almost all specimens at almost all ages tested. Concrete specimens with higher WYFA-3 content universally had lower carbon intensity than those specimens with lower WYFA-3 content. In comparison to the carbon intensity of OPC concrete, as calculated from literature values, all BCSA concrete specimens in this study exhibited far lower carbon intensities, extending to the control BCSA concrete. The WYFA specimens exhibited superior performance due to their chemical similarity to BCSA: the SCM negligibly affected ettringite crystallization and C-S-H precipitation due to chemical similarity between the SCM and the cement allowing hydration to proceed as normal. This lack of microstructural change caused the difference in strength with increasing SCM content to be very small. Flow values improved due to the spherical microstructure of WYFA-1 itself but the effect of the SCM on length change remains unclear due to mixed behavior between WYFA samples. Set time reduction can be explained as flash-setting due to free lime content.

5.4 North Dakota Fly Ash

The North Dakota fly ash SCM (NDFA) did not meet the criteria of the ASTM C618 standard and cannot receive classification as class C or class F. Because of its unregulated status as an industrial waste product, NDFA and other unregulated fly ashes may vary in behavior as SCMs due to differences in chemical composition and crystalline and amorphous phase content. Data from XRF showed that the SCM had the highest SO_3 content of all SCMs in this study, and that the largest fraction of the SCM consisted of SO_3. Scanning the SCM via XRD revealed an abundance of crystallographic peaks corresponding to glauberite, a sodium calcium sulfate mineral. This phase was also observed under past characterization study [50]. Under the R^3 isothermal calorimetry standard, the cumulative heat release of the SCM was moderately exothermic. However, this calorimetry result does not necessarily indicate favorable reactivity in OPC, due to the high SO_3 content of NDFA. NDFA reduced workability in mortars, requiring more water to achieve constant flow in comparison to control specimens and reducing flow measurements in constant-water mortars. DTG and Rietveld refinement data both showed increases in ettringite content in pastes containing greater quantities of NDFA, but the effect was more prominent under DTG. Wollastonite appeared in NDFA pastes under DTG, increasing with SCM fraction. SEM imaging of pastes revealed normal development of ettringite, with crystals possibly somewhat thinner than those of the control specimens. Similarly to DTG and Rietveld refinement data, NDFA intensified the maximum exothermic heat flow in pastes containing 10% and 20% SCM under isothermal calorimetry. This indicates that ettringite crystallization and chemical activity between ye'elimite and the sulfates of the SCM may take place over a shorter period than in control pastes. As in all SCM pastes, the cumulative heat release decreased with increasing SCM content, but NDFA pastes more closely matched the heat release of the control

pastes than any other in this study. NDFA was the only SCM to accelerate the onset of the primary ettringite-forming peak, and this effect became more intense as more NDFA was added. The SCM generally accelerated final set in mortars while delaying initial set. Despite elevated ettringite content in NDFA pastes, which may minimize drying shrinkage, the drying shrinkage of mortars generally intensified with increasing NDFA content due to elevated water content. NDFA performed comparably to class C fly ash with regard to mortar compressive strength. In constant-water NDFA mortars, those specimens containing 20% SCM performed very closely in strength to those containing 10% SCM, but the difference was more pronounced than that between constant-flow NDFA mortars. NDFA mortars generally had a higher carbon intensity than control mortars below 28 days of age, while those NDFA mortars tested at or above 28 days matched control values or were slightly lower. As was the case with all other mortars, the addition of NDFA reduced the GWP of BCSA mortars by up to 30%, to a value as low as 0.471 kg CO_2-eq/kg cement. The behavior of NDFA in BCSA is broadly governed by its very high SO_3 content: NDFA contained more SO_3 than any other SCM in this study—almost double that of the cement itself. The clearest consequence of this was increased ettringite formation with NDFA addition: sulfate minerals in the SCM like anhydrite enabled more complete ye'elimite hydration over other SCMs. Calorimetry reflected this. Adequate sulfate content led to AH_3 production from ye'elimite hydration, in turn allowing C-S-H to precipitate from belite without the crystallization of stratlingite. Despite these microstructural and chemical factors, the early strength of NDFA mortars could not entirely match that of WYFA mortars. A large amount of water was necessary for constant flow, due to the rough microstructure of the SCM, which may have contributed to the observed magnitude of length change.

5.5 Further Study and Closing Remarks

Due to the limited available information in literature about alternative SCMs in BCSA, all SCMs used in this study should be more comprehensively characterized. Class C fly ash, paper recycling waste, and North Dakota fly ash were not used in concrete, nor did any flexural testing take place in this study. Additionally, the compressive strength of BCSA/WYFA-3 concrete cylinders at ages of 90 days or later was not measured. Finally, the use and study of SCMs in situ can provide a wealth of valuable information; such a study was performed on BCSA pavements without SCMs at the Seattle-Tacoma International Airport after 25 years [4].

Quantifying the leaching behavior of environmentally hazardous waste before and after solidification in cement should proceed in future studies. This will provide a better understanding of the potential environmental benefits of using industrial waste as SCMs in BCSA for reducing environmental harm.

Advantages of SCMs include reduced construction cost, and minimized environmental impact by way of reduced CO_2 emissions. Their disadvantages include varying loss in strength and logistical overhead due to acquisition and transport. This study quantified the chemical, microstructural, and mechanical effects of various SCMs in BCSA. The distinct chemistry of BCSA creates an environment in which an unconventional, sulfate-rich FGD material that doesn't fit the ASTM C618 standard for SCMs, primarily designed for OPC, can find utility. Wyoming FGD waste ash afforded the least detriment to strength while reducing the emissions of BCSA by up to 30%, and by nearly 50% in comparison to OPC. The employment of SCMs in BCSA can reduce the environmental harm of the cement manufacturing industry, but Caltrans regulations currently prohibit it in the state of California. The purpose of this study is to

demonstrate the utility of SCMs, including unregulated ones, in BCSA in the current, limited information landscape, and to inform their use. An example of Caltrans regulation that changed due to novel research is the length change measurement standard for RSCs: regulation originally designed for OPC used length at 28 days as a reference value, while RSCs are serviceable within hours. Research compelled change in the standard [55]. Changing SCM restrictions in RSCs like BCSA would likely entail a pilot BCSA slab using at least one of the SCMs in this study—most likely WYFA or a comparable FGD SCM—over a long period of time. This would provide necessary in situ data to enact regulatory change. All but one of 26 mortar mix designs studied maintained some degree of strength at four hours because of the early hydration of ye'elimite, which cannot take place in OPC, and continued to develop strength up to 90 days with the precipitation of C-S-H. Rapid strength development, its continued development at later ages, and low GWP make BCSA cement a viable alternative to OPC and CSA cements for the purpose of sustainable construction, and its study is instrumental in achieving that goal.

6. Appendix

6.1 XRD Scans of BCSA Pastes

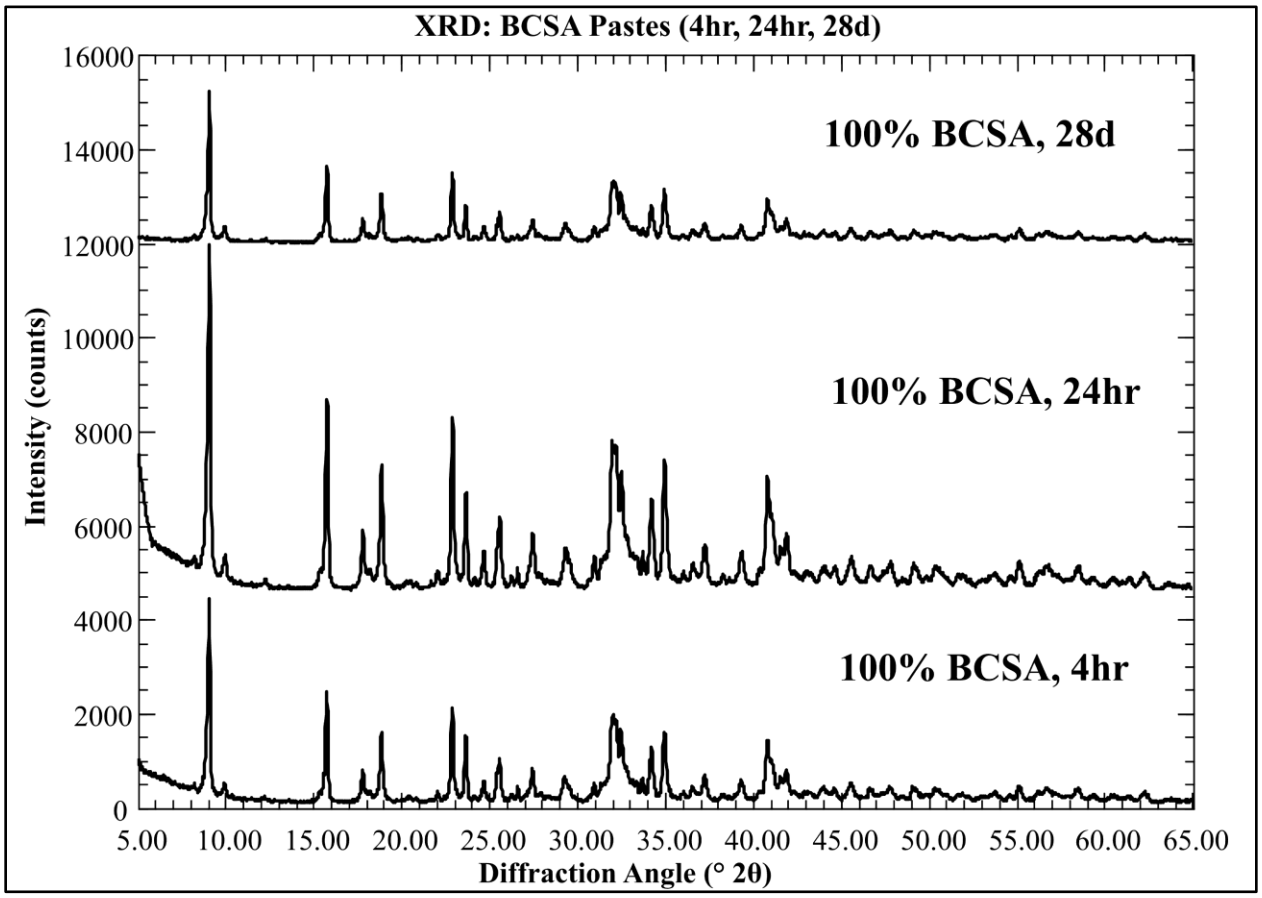

Figure 51: X-ray diffraction scans of BCSA pastes with hydration stopped at 4hr, 24hr, and 28d, used for Rietveld refinement.

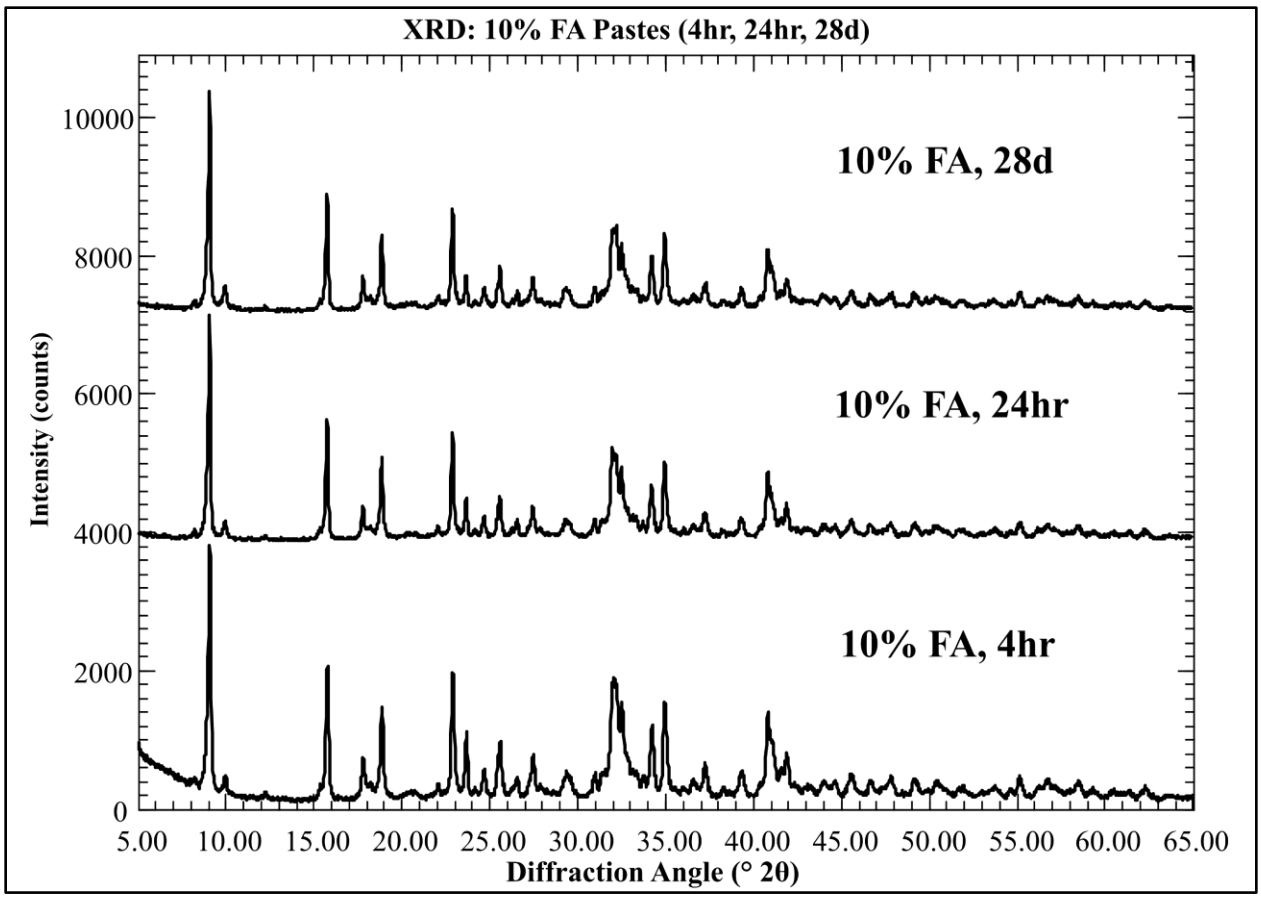

Figure 52: X-ray diffraction scans of 10% FA pastes with hydration stopped at 4hr, 24hr, and 28d, used for Rietveld refinement.

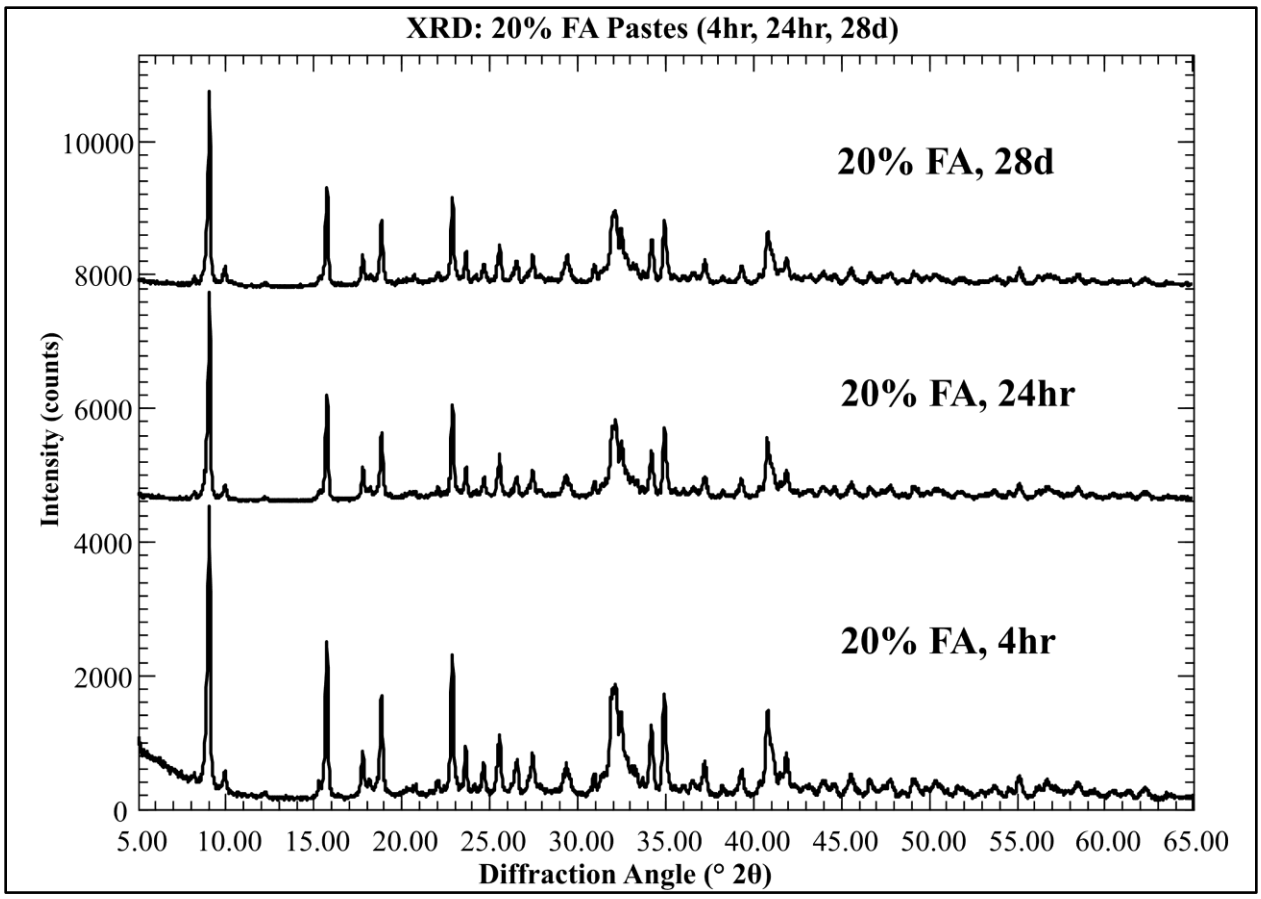

Figure 53: X-ray diffraction scans of 20% FA pastes with hydration stopped at 4hr, 24hr, and 28d, used for Rietveld refinement.

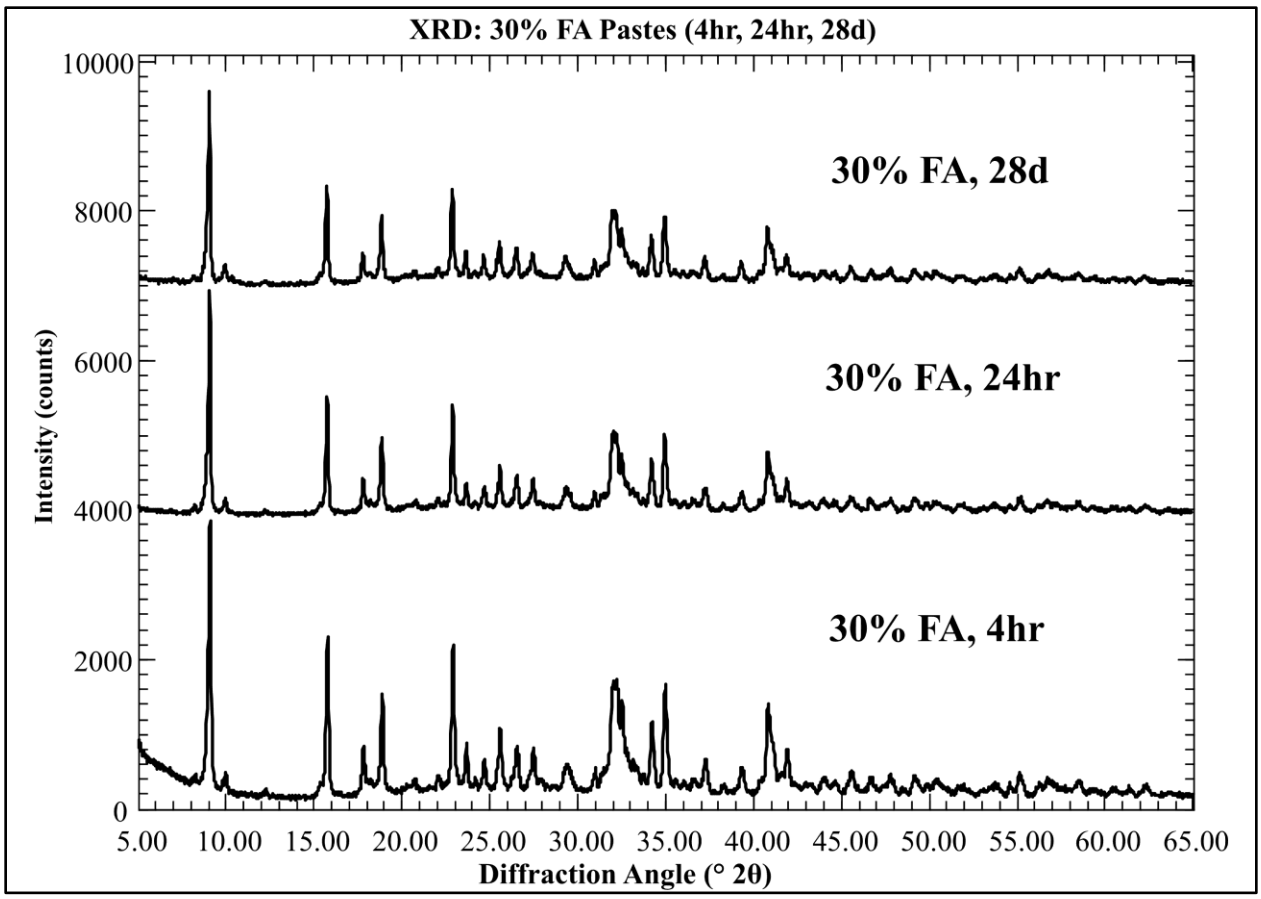

Figure 54: X-ray diffraction scans of 30% FA pastes with hydration stopped at 4hr, 24hr, and 28d, used for Rietveld refinement.

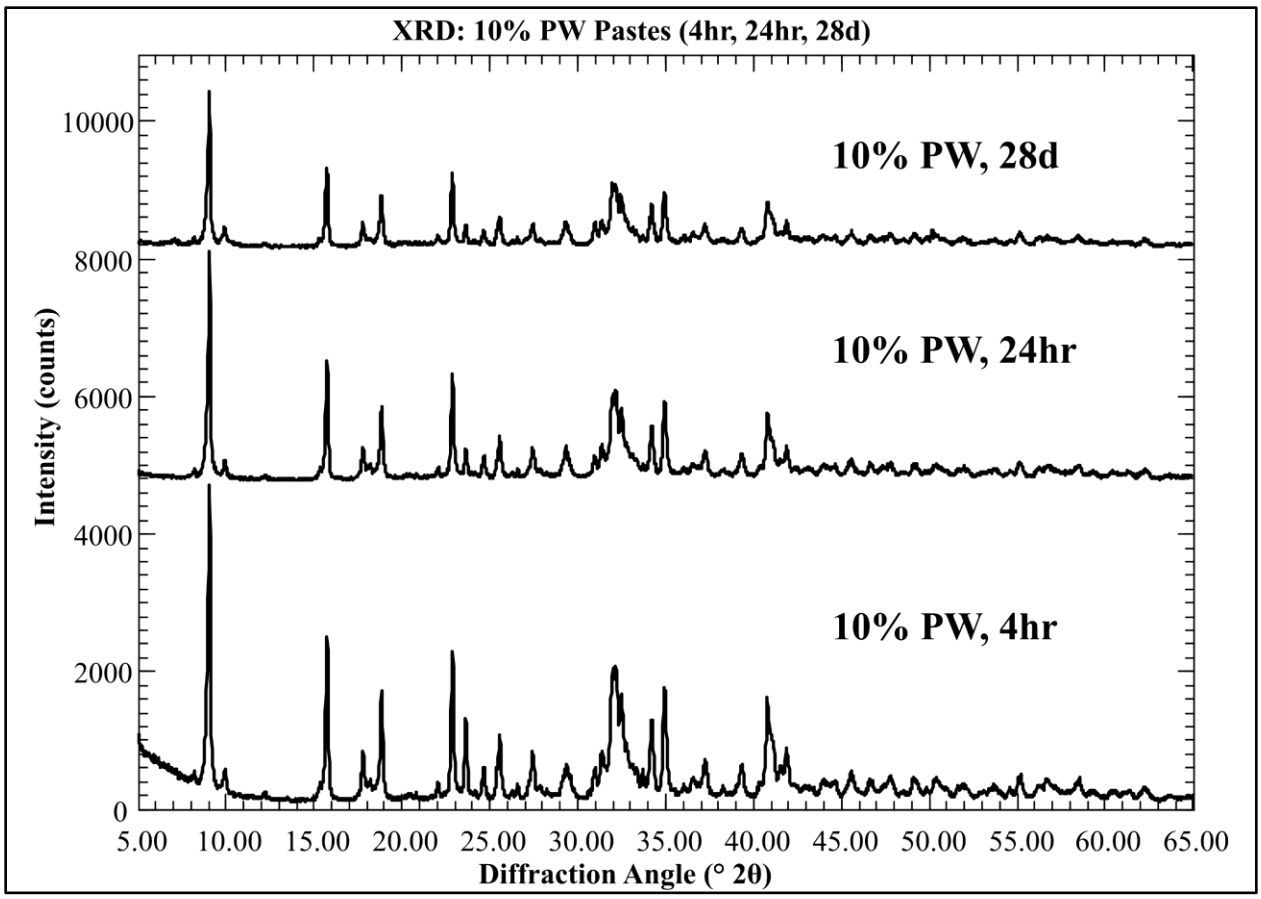

Figure 55: X-ray diffraction scans of 10% PW pastes with hydration stopped at 4hr, 24hr, and 28d, used for Rietveld refinement.

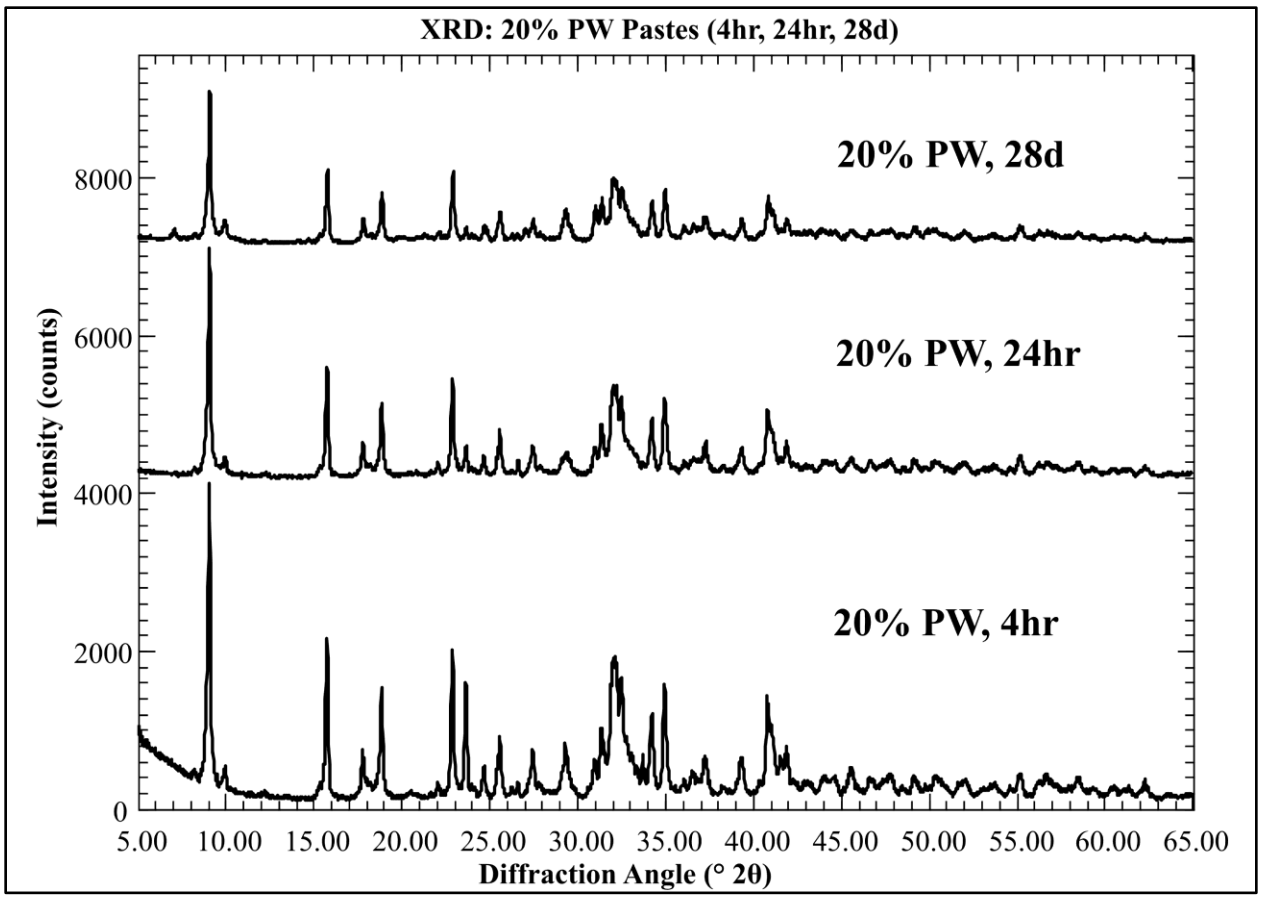

Figure 56: X-ray diffraction scans of 20% PW pastes with hydration stopped at 4hr, 24hr, and 28d, used for Rietveld refinement.

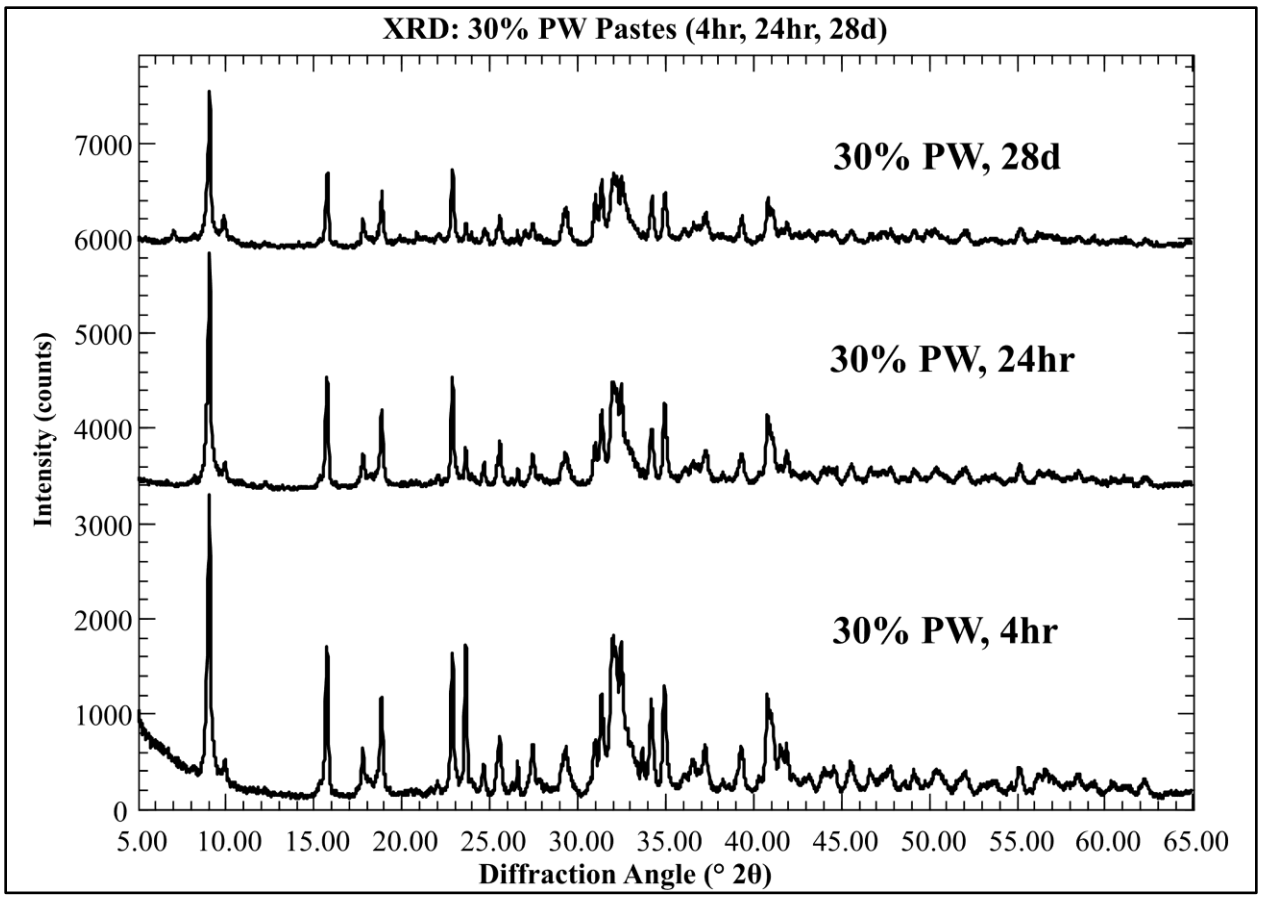

Figure 57: X-ray diffraction scans of 30% PW pastes with hydration stopped at 4hr, 24hr, and 28d, used for Rietveld refinement.

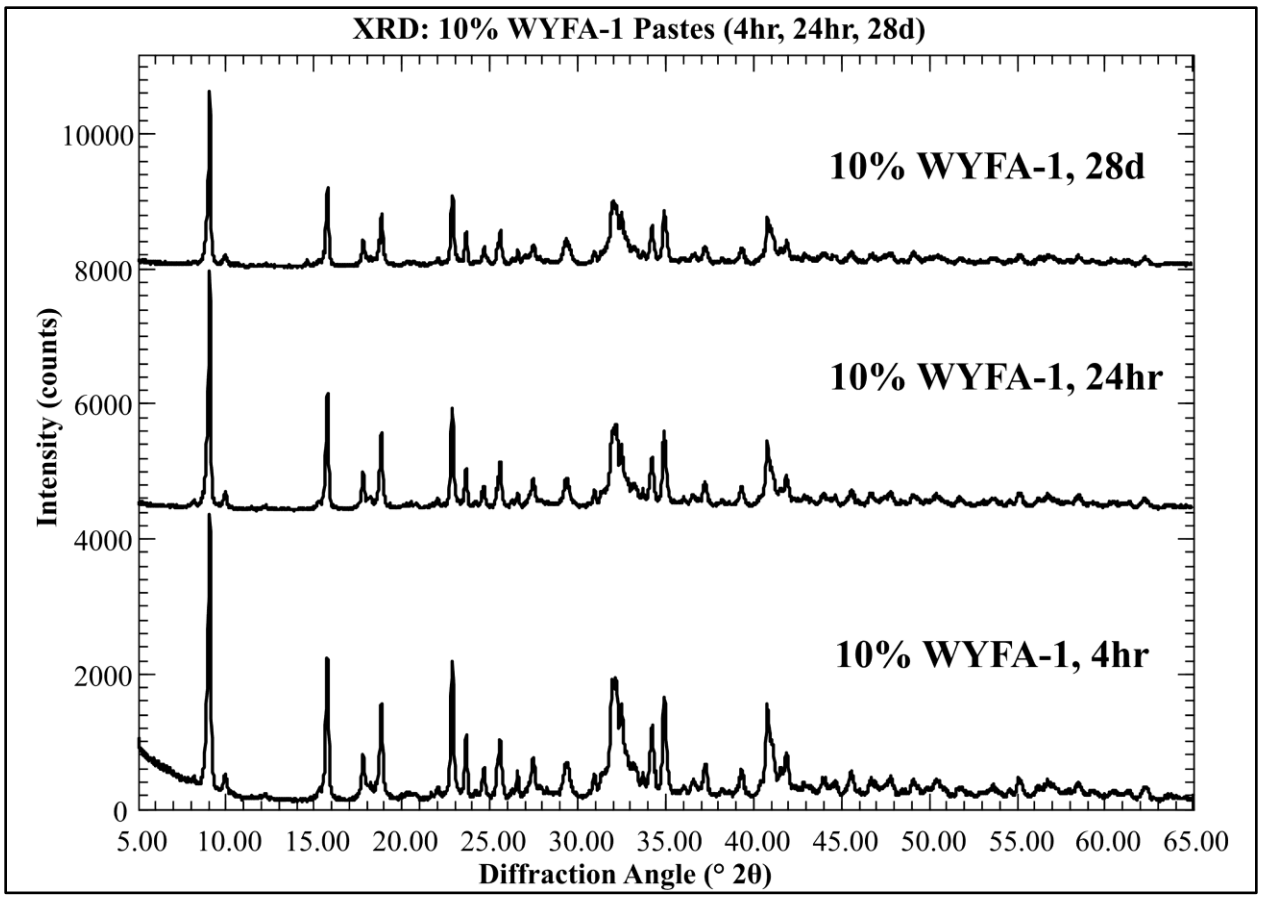

Figure 58: X-ray diffraction scans of 10% WYFA-1 pastes with hydration stopped at 4hr, 24hr, and 28d, used for Rietveld refinement.

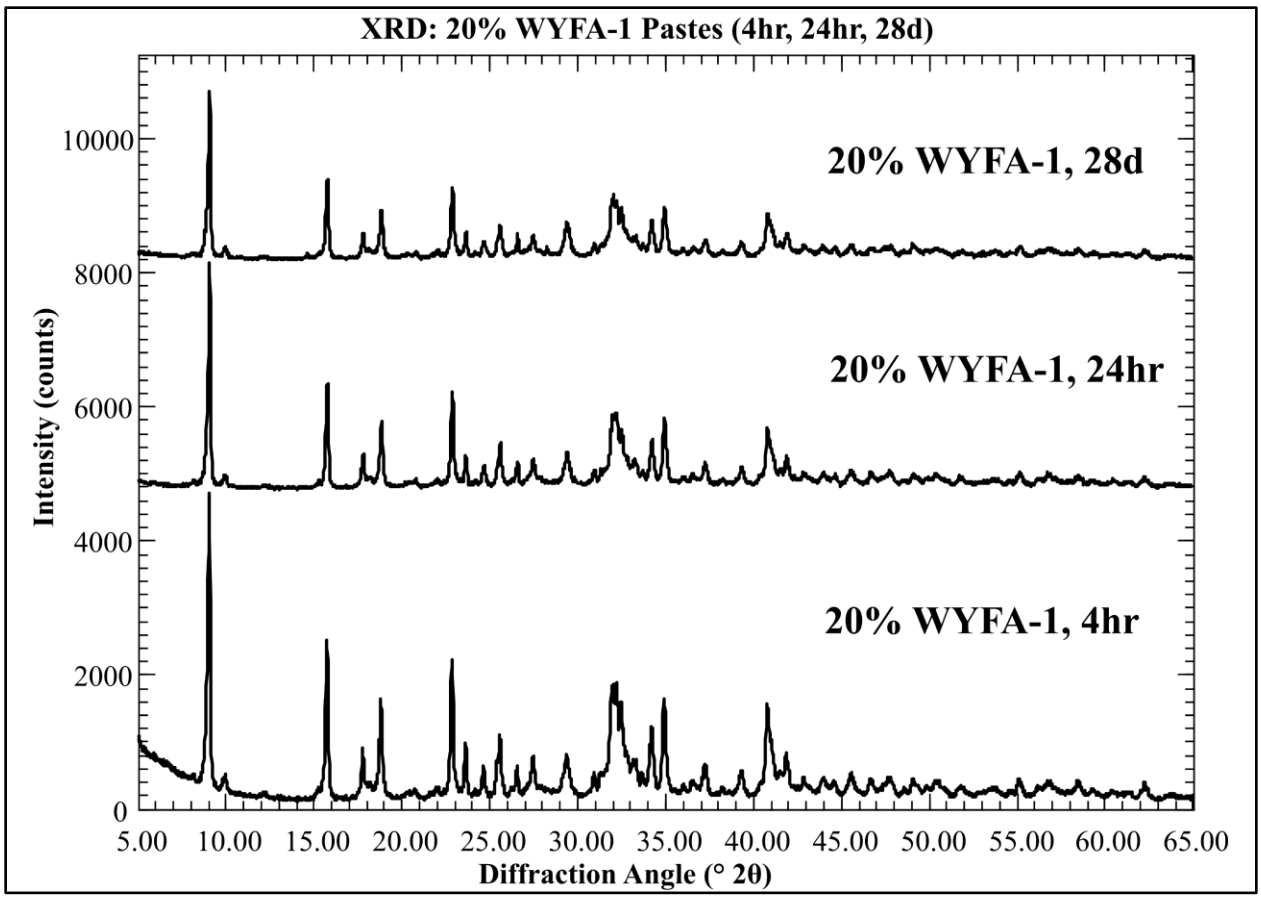

Figure 59: X-ray diffraction scans of 20% WYFA-1 pastes with hydration stopped at 4hr, 24hr, and 28d, used for Rietveld refinement.

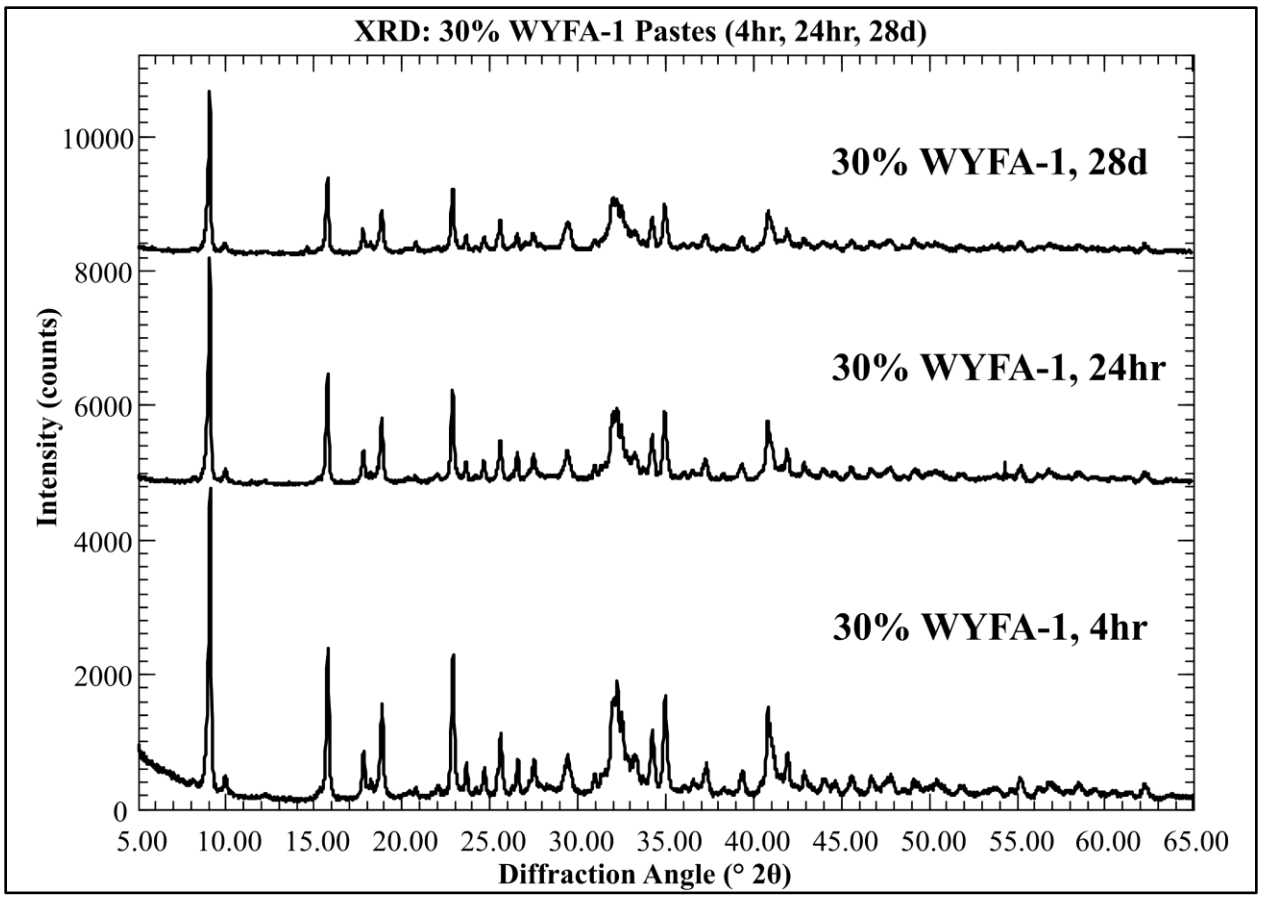

Figure 60: X-ray diffraction scans of 30% WYFA-1 pastes with hydration stopped at 4hr, 24hr, and 28d, used for Rietveld refinement.

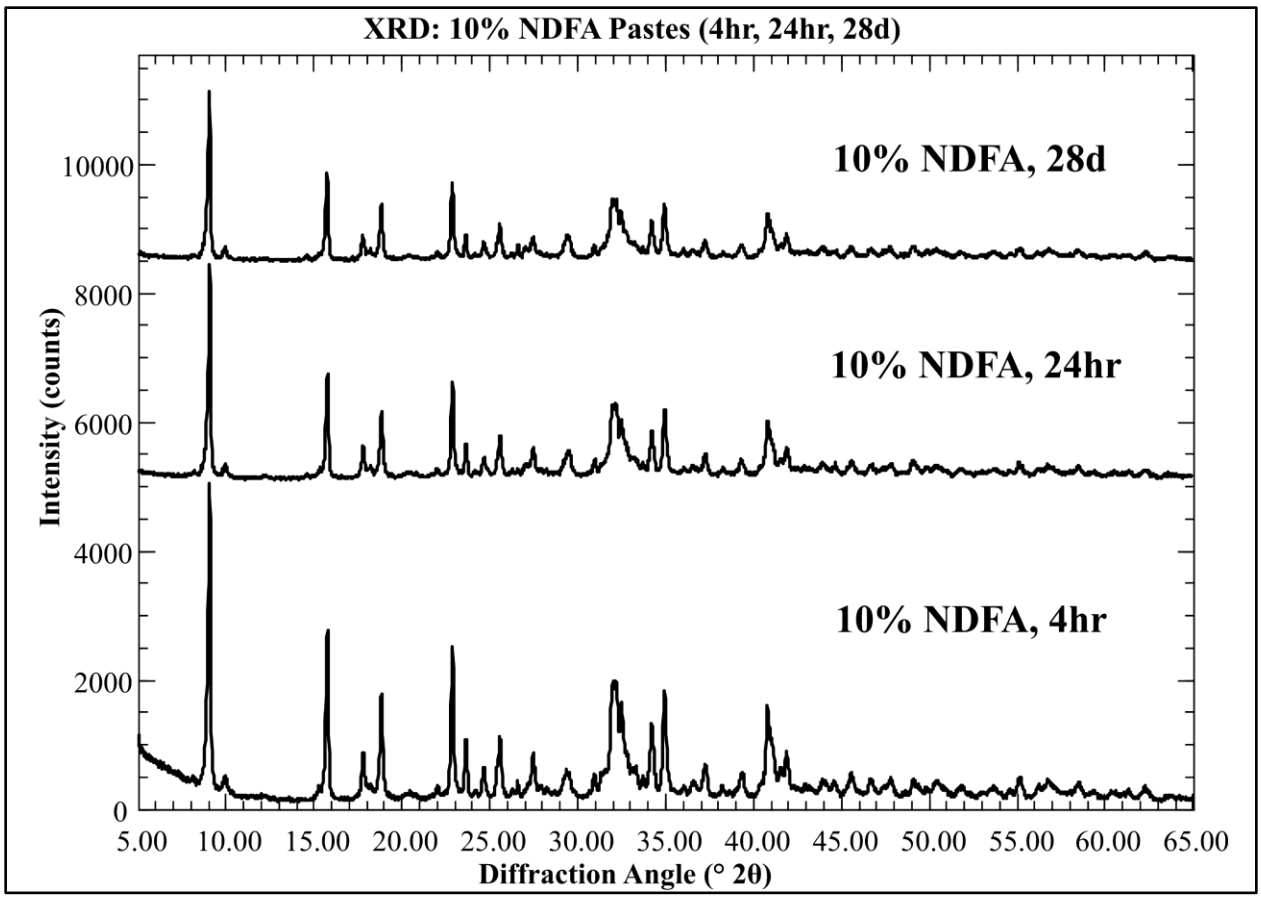

Figure 61: X-ray diffraction scans of 10% NDFA pastes with hydration stopped at 4hr, 24hr, and 28d, used for Rietveld refinement.

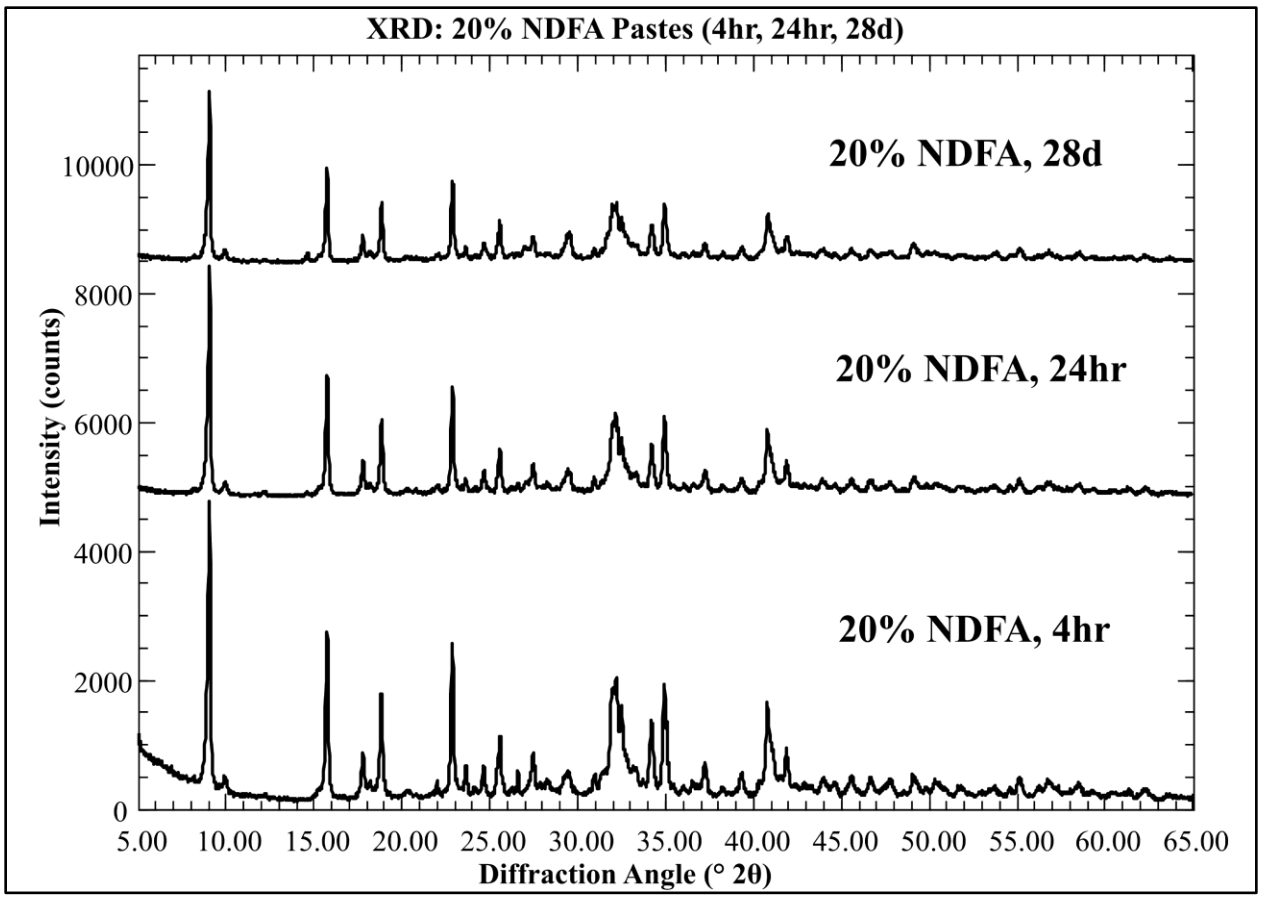

Figure 62: X-ray diffraction scans of 20% NDFA pastes with hydration stopped at 4hr, 24hr, and 28d, used for Rietveld refinement.

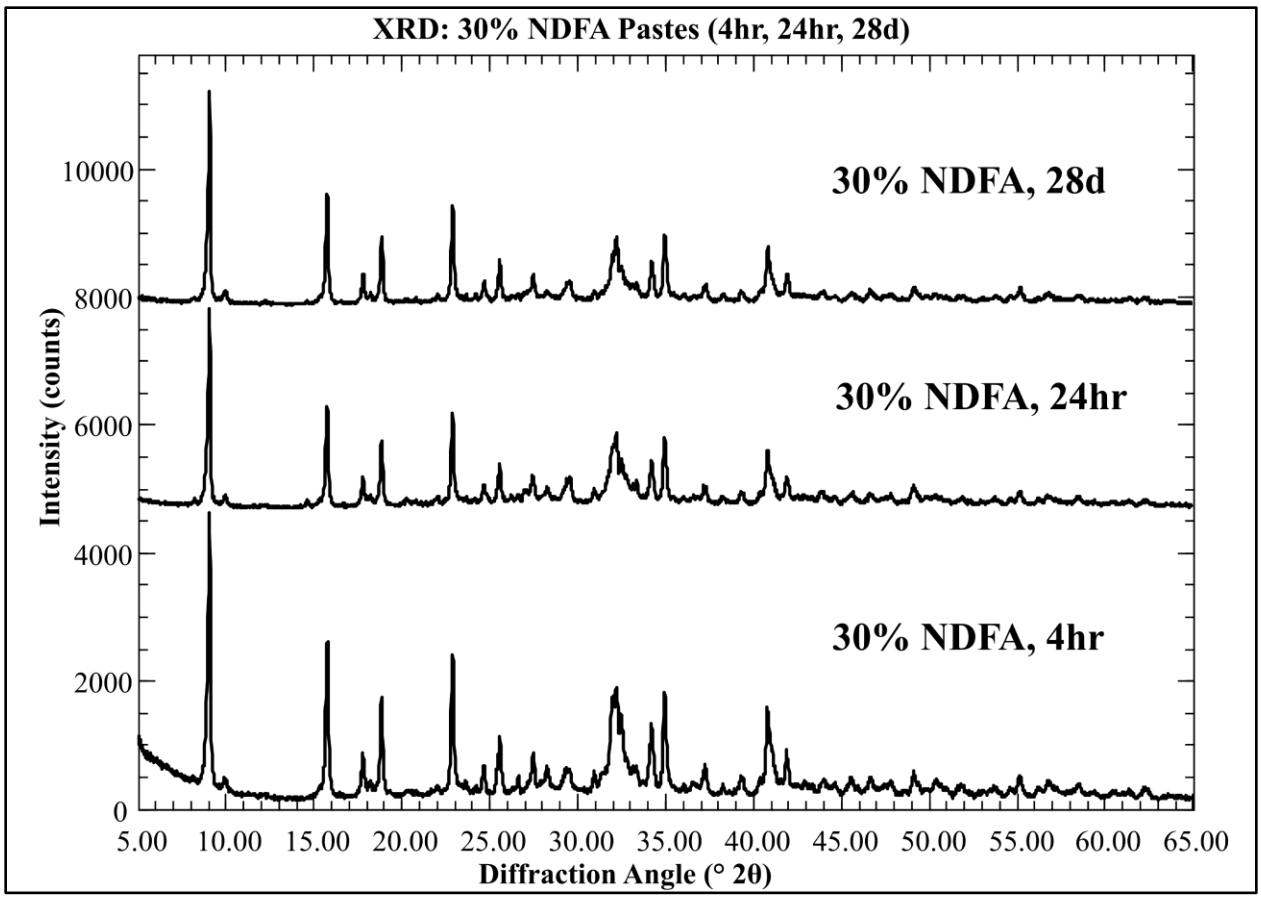

Figure 63: X-ray diffraction scans of 30% NDFA pastes with hydration stopped at 4hr, 24hr, and 28d, used for Rietveld refinement.

6.2 Rietveld Refinement Results

Table 17: Phase evolution in control BCSA pastes via Rietveld refinement of XRD

Mineral & COD ID	Fraction at 4hr	Fraction at 24hr	Fraction at 28d
Albite (9002196)	1.71%	1.66%	1.91%
Anhydrite (9017809)	1.79%	1.69%	1.30%
Brownmillerite (9016628)	0.10%	0.00%	0.00%
Calcite (9014216)	1.69%	2.79%	3.13%
Ettringite (9015084)	47.99%	49.93%	49.14%
Periclase (9006784)	0.62%	0.71%	0.64%
Perovskite (9013383)	1.43%	1.45%	1.35%
Portlandite (9006832)	0.80%	0.62%	0.65%
Vaterite (9015898)	1.04%	0.03%	1.77%
Ye'elimite (9009938)	4.69%	4.00%	3.26%
Quartz (9013321)	0.86%	2.29%	3.48%
α-Belite (1546027)	1.63%	1.00%	0.65%
β-Belite (1535815)	33.44%	31.58%	30.92%
Gypsum (9017313)	1.08%	0.93%	0.82%
Gehlenite (1000048)	1.14%	1.34%	0.98%
Sum	100%	100.01%	99.99%

Table 18: Phase evolution in 10% FA pastes via Rietveld refinement of XRD

Mineral & COD ID	Fraction at 4hr	Fraction at 24hr	Fraction at 28d
Albite (9002196)	1.79%	1.34%	1.44%
Anhydrite (9017809)	1.51%	0.96%	1.14%
Brownmillerite (9016628)	0.31%	0.08%	0.01%
Calcite (9014216)	1.97%	2.18%	2.73%
Ettringite (9015084)	48.74%	50.77%	51.24%
Periclase (9006784)	0.58%	0.70%	0.81%
Perovskite (9013383)	1.37%	1.55%	1.43%
Portlandite (9006832)	0.96%	0.61%	0.84%
Vaterite (9015898)	0.08%	0.00%	1.54%
Ye'elimite (9009938)	3.46%	2.49%	2.03%
Quartz (9013321)	1.58%	3.65%	1.29%
α-Belite (1546027)	1.53%	1.12%	0.90%
β-Belite (1535815)	33.50%	31.47%	30.88%
Gypsum (9017313)	0.91%	0.67%	0.63%
Gehlenite (1000048)	1.08%	1.86%	2.37%
Magnesioferrite (9007273)	0.22%	0.20%	0.27%
Stratlingite (9005059)	0.43%	0.34%	0.46%
Sum	100%	100%	100%

Table 19: Phase evolution in 20% FA pastes via Rietveld refinement of XRD

Mineral & COD ID	Fraction at 4hr	Fraction at 24hr	Fraction at 28d
Albite (9002196)	1.67%	1.05%	1.36%
Anhydrite (9017809)	1.17%	1.02%	1.26%
Brownmillerite (9016628)	0.42%	0.05%	0.56%
Calcite (9014216)	2.50%	2.77%	2.36%
Ettringite (9015084)	49.83%	50.50%	49.62%
Periclase (9006784)	0.85%	0.88%	0.84%
Perovskite (9013383)	1.16%	1.42%	0.99%
Portlandite (9006832)	0.77%	0.77%	0.64%
Vaterite (9015898)	0.32%	0.34%	0.79%
Ye'elimite (9009938)	2.36%	2.14%	2.30%
Quartz (9013321)	5.88%	4.89%	4.98%
α-Belite (1546027)	1.15%	0.98%	0.79%
β-Belite (1535815)	28.77%	30.20%	30.50%
Gypsum (9017313)	0.97%	0.79%	0.36%
Gehlenite (1000048)	1.33%	1.46%	1.55%
Magnesioferrite (9007273)	0.44%	0.48%	0.54%
Stratlingite (9005059)	0.42%	0.27%	0.56%
Sum	100%	100%	100%

Table 20: Phase evolution in 30% FA pastes via Rietveld refinement of XRD

Mineral & COD ID	Fraction at 4hr	Fraction at 24hr	Fraction at 28d
Albite (9002196)	1.47%	1.18%	0.80%
Anhydrite (9017809)	1.02%	0.93%	0.78%
Brownmillerite (9016628)	0.73%	0.05%	0.06%
Calcite (9014216)	2.42%	2.84%	2.96%
Ettringite (9015084)	49.36%	50.16%	49.60%
Periclase (9006784)	0.82%	0.79%	0.95%
Perovskite (9013383)	1.11%	1.45%	1.45%
Portlandite (9006832)	0.73%	0.76%	0.49%
Vaterite (9015898)	0.09%	0.40%	0.59%
Ye'elimite (9009938)	2.24%	1.74%	1.88%
Quartz (9013321)	6.02%	6.33%	6.79%
α-Belite (1546027)	1.24%	1.21%	1.36%
β-Belite (1535815)	29.41%	28.51%	27.53%
Gypsum (9017313)	0.73%	0.57%	0.30%
Gehlenite (1000048)	1.23%	1.90%	2.14%
Magnesioferrite (9007273)	0.73%	0.79%	0.92%
Stratlingite (9005059)	0.66%	0.37%	1.39%
Sum	100%	99.99%	99.99%

Table 21: Phase evolution in 10% PW pastes via Rietveld refinement of XRD

Mineral & COD ID	Fraction at 4hr	Fraction at 24hr	Fraction at 28d
Albite (9002196)	1.61%	1.46%	2.05%
Anhydrite (9017809)	1.21%	0.97%	0.80%
Brownmillerite (9016628)	0.28%	0.08%	0.09%
Calcite (9014216)	2.49%	3.03%	2.58%
Ettringite (9015084)	47.69%	50.38%	46.47%
Periclase (9006784)	0.70%	0.65%	0.87%
Perovskite (9013383)	1.10%	1.39%	1.65%
Portlandite (9006832)	1.05%	0.93%	0.50%
Vaterite (9015898)	0.00%	0.32%	2.39%
Ye'elimite (9009938)	3.88%	2.08%	2.03%
Quartz (9013321)	0.62%	0.60%	1.02%
α-Belite (1546027)	1.55%	1.78%	0.20%
β-Belite (1535815)	33.56%	32.13%	27.88%
Gypsum (9017313)	0.80%	0.55%	0.34%
Gehlenite (1000048)	2.82%	3.23%	3.78%
Bassanite (2105042)	0.27%	0.15%	0.21%
Stratlingite (9005059)	0.38%	0.29%	7.14%
Sum	100%	100.01%	100%

Table 22: Phase evolution in 20% PW pastes via Rietveld refinement of XRD

Mineral & COD ID	Fraction at 4hr	Fraction at 24hr	Fraction at 28d
Albite (9002196)	1.46%	1.73%	1.91%
Anhydrite (9017809)	0.98%	1.21%	0.48%
Brownmillerite (9016628)	0.12%	0.04%	0.43%
Calcite (9014216)	3.25%	2.41%	4.64%
Ettringite (9015084)	41.95%	47.59%	40.10%
Periclase (9006784)	0.67%	0.52%	0.70%
Perovskite (9013383)	1.92%	1.58%	2.06%
Portlandite (9006832)	0.83%	0.99%	0.33%
Vaterite (9015898)	0.12%	0.04%	4.00%
Ye'elimite (9009938)	4.84%	1.94%	0.97%
Quartz (9013321)	4.06%	0.71%	0.58%
α-Belite (1546027)	1.71%	1.93%	0.23%
β-Belite (1535815)	32.11%	31.63%	26.64%
Gypsum (9017313)	0.79%	0.60%	0.18%
Gehlenite (1000048)	4.48%	6.22%	5.42%
Bassanite (2105042)	0.18%	0.14%	1.17%
Stratlingite (9005059)	0.53%	0.72%	10.17%
Sum	100%	99.99%	100.01%

Table 23: Phase evolution in 30% PW pastes via Rietveld refinement of XRD

Mineral & COD ID	Fraction at 4hr	Fraction at 24hr	Fraction at 28d
Albite (9002196)	2.24%	1.79%	1.90%
Anhydrite (9017809)	1.24%	0.88%	0.39%
Brownmillerite (9016628)	0.05%	0.12%	0.40%
Calcite (9014216)	2.84%	3.19%	4.61%
Ettringite (9015084)	37.10%	42.08%	35.13%
Periclase (9006784)	0.61%	0.50%	0.95%
Perovskite (9013383)	2.13%	2.10%	1.87%
Portlandite (9006832)	0.79%	0.97%	0.02%
Vaterite (9015898)	0.12%	0.00%	3.90%
Ye'elimite (9009938)	5.52%	1.96%	1.31%
Quartz (9013321)	4.83%	4.92%	1.24%
α-Belite (1546027)	2.01%	2.09%	0.20%
β-Belite (1535815)	32.02%	29.25%	26.64%
Gypsum (9017313)	0.80%	0.58%	0.14%
Gehlenite (1000048)	6.61%	8.48%	8.28%
Bassanite (2105042)	0.26%	0.21%	0.95%
Stratlingite (9005059)	0.86%	0.88%	12.07%
Sum	100.01%	99.99%	100%

Table 24: Phase evolution in 10% WYFA-1 pastes via Rietveld refinement of XRD

Mineral & COD ID	Fraction at 4hr	Fraction at 24hr	Fraction at 28d
Albite (9002196)	2.12%	1.94%	1.88%
Anhydrite (9017809)	1.43%	1.39%	1.40%
Brownmillerite (9016628)	0.10%	0.08%	0.07%
Calcite (9014216)	3.43%	1.84%	2.70%
Ettringite (9015084)	48.38%	52.67%	48.44%
Periclase (9006784)	0.95%	0.92%	0.93%
Perovskite (9013383)	1.71%	1.69%	1.63%
Portlandite (9006832)	0.85%	0.93%	0.89%
Vaterite (9015898)	0.85%	0.17%	2.64%
Ye'elimite (9009938)	2.86%	2.61%	2.76%
Quartz (9013321)	1.21%	1.17%	1.43%
α-Belite (1546027)	1.68%	1.28%	1.27%
β-Belite (1535815)	31.33%	30.46%	30.12%
Gypsum (9017313)	1.15%	0.92%	0.80%
Gehlenite (1000048)	1.59%	1.64%	1.58%
Bassanite (2105042)	0.38%	0.30%	1.46%
Sum	100%	99.99%	100.01%

Table 25: Phase evolution in 20% WYFA-1 pastes via Rietveld refinement of XRD

Mineral & COD ID	Fraction at 4hr	Fraction at 24hr	Fraction at 28d
Albite (9002196)	1.39%	1.68%	2.14%
Anhydrite (9017809)	1.80%	1.28%	1.27%
Brownmillerite (9016628)	0.77%	0.21%	0.85%
Calcite (9014216)	3.29%	2.18%	2.91%
Ettringite (9015084)	48.32%	50.93%	49.26%
Periclase (9006784)	1.48%	1.22%	1.51%
Perovskite (9013383)	2.05%	2.07%	2.03%
Portlandite (9006832)	0.87%	0.89%	0.96%
Vaterite (9015898)	0.58%	0.89%	1.86%
Ye'elimite (9009938)	2.34%	2.11%	2.04%
Quartz (9013321)	2.88%	4.12%	3.79%
α-Belite (1546027)	1.15%	1.90%	0.77%
β-Belite (1535815)	30.14%	27.47%	26.79%
Gypsum (9017313)	0.91%	0.95%	0.86%
Gehlenite (1000048)	1.74%	1.90%	1.27%
Bassanite (2105042)	0.29%	0.20%	1.68%
Sum	100%	100%	99.99%

Table 26: Phase evolution in 30% WYFA-1 pastes via Rietveld refinement of XRD

Mineral & COD ID	Fraction at 4hr	Fraction at 24hr	Fraction at 28d
Albite (9002196)	2.12%	2.39%	1.80%
Anhydrite (9017809)	1.08%	0.89%	0.90%
Brownmillerite (9016628)	0.66%	0.72%	0.27%
Calcite (9014216)	1.97%	2.73%	2.55%
Ettringite (9015084)	50.80%	52.06%	47.31%
Periclase (9006784)	1.55%	1.76%	1.52%
Perovskite (9013383)	2.61%	2.59%	2.56%
Portlandite (9006832)	1.10%	1.58%	1.08%
Vaterite (9015898)	0.27%	0.27%	2.79%
Ye'elimite (9009938)	1.42%	1.27%	1.25%
Quartz (9013321)	3.55%	4.13%	5.41%
α-Belite (1546027)	2.50%	1.63%	2.28%
β-Belite (1535815)	27.43%	24.79%	24.76%
Gypsum (9017313)	1.00%	0.88%	0.95%
Gehlenite (1000048)	1.55%	2.01%	1.79%
Bassanite (2105042)	0.39%	0.30%	2.81%
Sum	99.98%	99.99%	100.03%

Table 27: Phase evolution in 10% NDFA pastes via Rietveld refinement of XRD

Mineral & COD ID	Fraction at 4hr	Fraction at 24hr	Fraction at 28d
Albite (9002196)	1.22%	1.21%	0.50%
Anhydrite (9017809)	1.90%	1.26%	1.32%
Brownmillerite (9016628)	0.53%	0.14%	0.10%
Calcite (9014216)	2.13%	2.91%	3.42%
Ettringite (9015084)	48.93%	50.58%	50.85%
Periclase (9006784)	0.92%	0.82%	1.02%
Perovskite (9013383)	1.37%	1.22%	1.48%
Portlandite (9006832)	0.70%	0.78%	0.71%
Vaterite (9015898)	1.41%	3.58%	3.57%
Ye'elimite (9009938)	2.72%	2.34%	1.96%
Quartz (9013321)	2.87%	0.68%	2.69%
α-Belite (1546027)	1.82%	1.15%	0.80%
β-Belite (1535815)	29.10%	27.21%	25.62%
Gypsum (9017313)	0.83%	0.80%	0.77%
Gehlenite (1000048)	1.12%	1.61%	1.32%
Bassanite (2105042)	0.09%	1.38%	1.66%
Glauberite (9000154)	2.35%	2.32%	2.23%
Sum	99.99%	100.01%	100.01%

Table 28: Phase evolution in 20% NDFA pastes via Rietveld refinement of XRD

Mineral & COD ID	Fraction at 4hr	Fraction at 24hr	Fraction at 28d
Albite (9002196)	2.16%	1.48%	1.22%
Anhydrite (9017809)	1.20%	0.88%	0.82%
Brownmillerite (9016628)	0.81%	0.42%	0.43%
Calcite (9014216)	2.08%	2.40%	3.24%
Ettringite (9015084)	51.28%	55.92%	53.35%
Periclase (9006784)	1.01%	0.93%	1.22%
Perovskite (9013383)	1.17%	1.17%	1.36%
Portlandite (9006832)	0.93%	0.59%	0.75%
Vaterite (9015898)	0.81%	2.74%	4.56%
Ye'elimite (9009938)	1.24%	0.90%	0.90%
Quartz (9013321)	2.52%	0.87%	0.85%
α-Belite (1546027)	1.22%	1.70%	0.54%
β-Belite (1535815)	27.71%	23.77%	22.17%
Gypsum (9017313)	0.95%	0.66%	0.65%
Gehlenite (1000048)	1.63%	1.42%	0.91%
Bassanite (2105042)	0.25%	0.67%	4.45%
Glauberite (9000154)	3.04%	3.46%	2.60%
Sum	100%	99.99%	100.01%

Table 29: Phase evolution in 30% NDFA pastes via Rietveld refinement of XRD

Mineral & COD ID	Fraction at 4hr	Fraction at 24hr	Fraction at 28d
Albite (9002196)	1.77%	1.29%	1.15%
Anhydrite (9017809)	1.01%	0.13%	0.40%
Brownmillerite (9016628)	1.02%	0.72%	0.07%
Calcite (9014216)	2.53%	3.03%	2.85%
Ettringite (9015084)	50.28%	50.69%	60.76%
Periclase (9006784)	1.41%	1.41%	1.40%
Perovskite (9013383)	1.16%	1.26%	1.42%
Portlandite (9006832)	0.89%	0.85%	0.66%
Vaterite (9015898)	0.76%	4.36%	2.66%
Ye'elimite (9009938)	0.62%	0.39%	0.28%
Quartz (9013321)	2.67%	0.99%	2.96%
α-Belite (1546027)	1.97%	1.46%	1.42%
β-Belite (1535815)	25.65%	22.29%	17.62%
Gypsum (9017313)	1.08%	0.99%	0.73%
Gehlenite (1000048)	1.99%	1.82%	1.05%
Bassanite (2105042)	0.84%	3.76%	0.91%
Glauberite (9000154)	4.34%	4.57%	3.67%
Sum	99.99%	100%	100.01%

7. References

[1] Our World in Data, "Data Page: Annual CO_2 emissions from cement," November 2025. [Online]. Available: https://ourworldindata.org/grapher/annual-co2-cement. [Accessed July 2026].

[2] D. Cheng, D. M. Reiner, F. Yang, C. Cui, J. Meng, Y. Shan, Y. Liu, S. Tao and D. Guan, "Projecting future carbon emissions from cement production in developing countries," *Nature Communications,* vol. 14, no. 8213, 11 December 2023.

[3] I. Amato, "Green cement: Concrete solutions," *Nature,* vol. 494, pp. 300-301, 2013.

[4] M. T. McNerney, S. Khilfeh and E. P. Bescher, "Rapid-Setting Belitic Calcium Sulfoaluminate Concrete Pavement at Seattle-Tacoma," in *International Conference on Transportation and Development*, 2020.

[5] CTS Cement Manufactoring Corp., "Environmental Product Declaration for cement products produced by CTS Cement Manufacturing Corporation at their CTS Cement Plant facility in Ciudad Juarez," Labeling Sustainability, 2023.

[6] Portland Cement Association, "Environmental Product Declaration: Portland Cement," Portland Cement Association, 2023.

[7] F. Paniagua, E. Essolebe, V. Isteri, J. Paniagua and E. P. Bescher, "Belitic calcium sulfoaluminate as mineral admixture in limestone-calcined clay cement and low carbon dioxide binders," *Advances in Cement Research,* pp. 1-12, 2026.

[8] S. Barbhuiya, F. Kanavaris, B. B. Das and M. Idrees, "Decarbonising cement and concrete production: Strategies, challenges and pathways for sustainable development," *Journal of Building Engineering,* vol. 86, 2024.

[9] Federal Highway Administration, "Supplementary Cementitious Materials: Best Practices for Concrete Pavements," US Department of Transportation, 2016.

[10] D. N. Huntzinger and T. D. Eatmon, "A life-cycle assessment of Portland cement manufacturing: comparing the traditional process with alternative technologies," *Journal of Cleaner Production,* vol. 17, no. 7, pp. 668-675, May 2009.

[11] Federal Highway Administration, "Fly ash - an engineering material," in *Fly Ash Facts for Highway Engineers*, 2003, pp. 1-8.

[12] T. H. Adams, "Coal Ash Recycling Rate Increased in 2024," American Coal Ash Association, 2025.

[13] S. A. Bernal, M. C. G. Juenger, X. Ke, W. Matthes, B. Lothenbach, N. D. Belie and J. L. Provis, "Characterization of supplementary cementitious materials by thermal analysis," *Materials and Structures,* vol. 50, no. 26, 10 August 2016.

[14] E. P. Bescher, J. W. Stremfel, G. M. Kao, J. T. Salkowski, W. J. Hoyle, J. K. Vallens and E. K. Rice, "Radial coal ash based micro-architectures and method of synthesis". United States of America Patent 9,115,024 B2, 25 August 2015.

[15] California DOT, *Section 40-5: Jointed Plain Concrete Pavement With Rapid Strength,* California: California DOT, 2024.

[16] Caltrans, "Concrete Technology Manual," 2013.

[17] P. Bajpai, Generation of Waste in Pulp and Paper Mills, Springer International Publishing, 2015.

[18] H. S. Jang, Y. T. Lim, J. H. Kang, S. Y. So and H. S. So, "Influence of calcination and cooling conditions on pozzolanic reactivity of paper mill sludge," *Construction and Building Materials,* vol. 166, pp. 257-270, 30 March 2018.

[19] Federal Highway Administration, "User Guidelines for Waste and Byproduct Materials in Pavement Construction," Federal Highway Administration, 2016.

[20] D. Gao, Z. Zhang, Y. Meng, J. Tang and L. Yang, "Effect of Flue Gas Desulfurization Gypsum on the Properties of Calcium Sulfoaluminate Cement Blended with Ground Granulated Blast Furnace Slag," *Materials,* vol. 14, no. 2, 14 January 2021.

[21] L. Chi, Z. Wang, S. Lu, H. Wang, K. Liu and W. Liu, "Early assessment of hydration and microstructure evolution of belite-calcium sulfoaluminate cement pastes by electrical impedance spectroscopy," *Electrochimica Acta,* vol. 389, 1 September 2021.

[22] T. A. H., A. Kienzle and R. J. Thomas, "Engineering properties and setting time of belitic calcium sulfoaluminate (BCSA) cement concrete," *Construction and Building Materials,* vol. 352, no. 2022, 17 October 2022.

[23] Global Cement and Concrete Association, "Belite calcium sulfoaluminate (BCSA)," Global Cement and Concrete Association, [Online]. Available: https://gccassociation.org/cement-and-concrete-innovation/alternative-binders/belite-calcium-sulfoaluminate-bcsa/. [Accessed June 2026].

[24] R. Trauchessec, J.-M. Mechling, A. Lecomte, A. Roux and B. L. Rolland, "Hydration of ordinary Portland cement and calcium sulfoaluminate cement blends," *Cement and Concrete Composites,* vol. 56, pp. 106-114, 2015.

[25] P. E. Stutzman, P. Feng and J. W. Bullard, "Phase Analysis of Portland Cement by Combined Quantitative X-Ray Powder Diffraction and Scanning Electron Microscopy," *Journal of Research of the National Institute of Standards and Technology,* vol. 121, no. 2016, 11 April 2016.

[26] S. Nie, Q. Zhang, M. Lan, J. Zhou, M. Xu, H. Li and J. Wang, "Fundamental design of low-carbon ordinary Portland cement-calcium sulfoaluminate clinker-anhydrite blended system," *Cement and Concrete Composites,* vol. 139, 2023.

[27] E. Bescher, K. Vallens and J. Kim, "Belitic calcium sulfoaluminate cement: Hydration chemistry, performance, and use in the United States," in *15th International Congress on the Chemistry of Cement*, Prague, Czech Republic, 2019.

[28] J. d. S. A. Neto, A. G. D. l. Torre and A. P. Kirchheim, "Effects of sulfates on the hydration of Portland cement – A review," *Construction and Building Materials,* vol. 279, no. 2021, 12 April 2021.

[29] Y. Chen, Y. Fan, Y. Huang, X. Liao, W. Xu and T. Zhang, "A comprehensive review of toxicity of coal fly ash and its leachate in the ecosystem," *Ecotoxicology and Environmental Safety,* vol. 269, no. 2024, 1 January 2024.

[30] T. Punshon, A. S. Knox, D. C. Adrian, J. C. Seaman and J. T. Weber, Eds., "Flue Gas Desulfurization (FGD) Residue," in *Biogeochemistry of Trace Elements in Coal and Coal Combustion Byproducts*, 1 ed., New York, Springer, 2011, pp. 7-28.

[31] K. Piekkari, "Solidification/stabilization of an extremely heavy metals rich industrial side stream with ettringite-rich solid binders," University of Oulu Graduate School, Oulu, Finland, 2024.

[32] E.-T. Nurmesniemi, M. Huhta, M. Derkani, V. Isteri, T. Hanein, T. Hu, P. Tanskanen and U. Lassi, "Removal of sulphate and arsenic from wastewater using calcium sulfoaluminate (ye'elimite)," *Frontiers in Materials,* vol. 9, no. 2022, 12 September 2022.

[33] Environmental Protection Agency, "Toxicity Characteristic," National Archives and Records Administration, 2026.

[34] Environmental Protection Agency, "SW-846 Test Method 1311: Toxicity Characteristic Leaching Procedure," Environmental Protection Agency, 1992.

[35] O. E. Ige, D. V. V. Kallon and D. Desai, "Carbon emissions mitigation methods for cement industry using a systems dynamics model," *Clean Technologies and Environmental Policy,* vol. 26, pp. 579-597, 9 January 2024.

[36] G. Li, C. Zhou, W. Ahmad, K. I. Usanova, M. Karelina, A. M. Mohamed and R. Khallaf, "Fly Ash Application as Supplementary Cementitious Material: A Review," *Materials,* vol. 15, no. 7, 2022.

[37] R. Snellings, J. Chwast, Ö. Cizer, N. D. Belie, Y. Dhandapani, P. Durdzinski, J. Elsen, J. Haufe, D. Hooton, C. Patapy, M. Santhanam, K. Scrivener, D. Snoeck, L. Steger, S. Tongbo and A. Vollpracht, "RILEM TC-238 SCM recommendation on hydration stoppage by solvent exchange for the study of hydrate assemblages," *Materials and Structures,* vol. 51, 2018.

[38] N. Doebelin and R. Kleeberg, "Profex: a graphical user interface for the Rietveld refinement program BGMN," *Journal of Applied Crystallography,* vol. 48, pp. 1573-1580, October 2015.

[39] A. Vaitkus, A. Merkys, T. Sander, M. Quirós, P. A. Thiessen, E. E. Bolton and S. Gražulis, "A workflow for deriving chemical entities from crystallographic data and its application to the Crystallography Open Database," *Journal of Cheminformatics,* vol. 15, 2023.

[40] A. Merkys, A. Vaitkus, A. Grybauskas, A. Konovalovas, M. Quirós and S. Gražulis, "Graph isomorphism-based algorithm for cross-checking chemical and crystallographic descriptions," *Journal of Cheminformatics,* vol. 15, 2023.

[41] A. Vaitkus, A. Merkys and S. Gražulis, "Validation of the Crystallography Open Database using the Crystallographic Information Framework," *Journal of Applied Crystallography,* vol. 54, no. 2, pp. 661-672, 2021.

[42] M. Quirós, S. Gražulis, S. Girdzijauskaitė, A. Merkys and A. Vaitkus, "Using SMILES strings for the description of chemical connectivity in the Crystallography Open Database," *Journal of Cheminformatics,* vol. 10, 2018.

[43] A. Merkys, A. Vaitkus, J. Butkus, M. Okulič-Kazarinas, V. Kairys and S. Gražulis, "COD::CIF::Parser: an error-correcting CIF parser for the Perl language," *Journal of Applied Crystallography,* vol. 49, no. 1, pp. 292-301, 2016.

[44] S. Gražulis, A. Merkys, A. Vaitkus and M. Okulič-Kazarinas, "Computing stoichiometric molecular composition from crystal structures," *Journal of Applied Crystallography,* vol. 48, no. 1, pp. 85-91, 2015.

[45] S. Gražulis, A. Daškevič, A. Merkys, D. Chateigner, L. Lutterotti, M. Quirós, N. R. Serebryanaya, P. Moeck, R. T. Downs and A. LeBail, "Crystallography Open Database (COD): an open-access collection of crystal structures and platform for world-wide collaboration," *Nucleic Acids Research,* vol. 40, pp. D420-D427, 2012.

[46] S. Gražulis, D. Chateigner, R. T. Downs, A. T. Yokochi, M. Quiros, L. Lutterotti, E. Manakova, J. Butkus, P. Moeck and A. Le Bail, "Crystallography Open Database – an open-access collection of crystal structures," *Journal of Applied Crystallography,* vol. 42, pp. 726-729, 2009.

[47] R. T. Downs and M. Hall-Wallace, "The American Mineralogist Crystal Structure Database," *American Mineralogist,* vol. 88, pp. 247-250, 2003.

[48] F. Avet, R. Snellings, A. Alujas-Diaz, M. Ben Haha and K. Scrivener, "Development of a new rapid, relevant and reliable (R3) test method to evaluate the pozzolanic reactivity of calcined kaolinitic clays," *Cement and Concrete Research,* vol. 85, no. 2016, pp. 1-11, 2016.

[49] X. Li, R. Snellings, M. Antoni, N. M. Alderete, M. B. Haha, S. Bishnoi, Ö. Cizer, M. Cyr, K. D. Weerdt, Y. Dhandapani, J. Duchesne, J. Haufe, D. Hooton and M. Juenger, "Reactivity tests for supplementary cementitious materials: RILEM TC 267-TRM phase 1," *Materials and Structures,* vol. 51, no. 6, p. 151, 2018.

[50] S. A. Benson, D. K. Rindt, G. G. Montgomery and D. R. Sears, "Microanalytical Characterization of North Dakota Fly Ash," *Industrial & Engineering Chemistry Product Research and Development,* vol. 23, no. 2, pp. 252-256, 1984.

[51] K. Scrivener, R. Snellings and B. Lothenbach, Eds., A Practical Guide to Microstructural Analysis of Cementitious Materials, Boca Raton, FL: CRC Press, 2016.

[52] M. Borštnar, N. Daneu and S. Dolenec, "Phase development and hydration kinetics of belite-calcium sulfoaluminate cements at different curing temperatures," *Ceramics International,* vol. 46, no. 18, pp. 29421-29428, 2020.

[53] I. Koufany, J. Fernandez-Sanchez, A. Cuesta, I. Santacruz, E. P. Bescher, M. A. Aranda and A. G. D. l. Torre, "Understanding early hydration in belite calcium sulfoaluminate cements: Impacts of minor elements and citric acid," *Cement and Concrete Research,* vol. 198, 2025.

[54] B. J. Lee, S. H. Kee, T. Oh and Y. Y. Kim, "Effect of Cylinder Size on the Modulus of Elasticity and Compressive Strength of Concrete from Static and Dynamic Tests," *Advances in Materials Science and Engineering,* vol. 2015, no. 1, 2015.

[55] E. P. Bescher, J. Kim and M. McNerney, "On the Differences in Chemistry and Performance Between Types of Rapid Strength Concretes (RSCs)," in *International Conference on Concrete Pavements*, 2021.